CHARACTERIZING AND QUANTIFYING LOCAL AND REGIONAL PARTICULATE MATTER EMISSIONS FROM DEPARTMENT OF DEFENSE INSTALLATIONS

Dr. J.A. Gillies, Dr. W.P. Arnott, Dr. V. Etyemezian, Dr. H. Kuhns, Dr. H. Moosmüller, Dr. D. DuBois, Dr. M. Abu-Allaban

Mr. Geary Schwemmer **Dr. D.A. Gillette**

Dr. W.G. Nickling **Dr. T. Wilkerson**

Dr. R. Varma

Final Report for SERDP Project CP-1191

Prepared for:

SERDP

March 2005

Report Documentation Page

Form Approved
OMB No. 0704-0188

1. REPORT DATE	2. REPORT TYPE	3. DATES COVERED
05 MAR 2005	**Final**	**-**

4. TITLE AND SUBTITLE	5a. CONTRACT NUMBER
Characterizing and Quantifying Local and Regional Particulate Matter Emissions from DoD Installations	5b. GRANT NUMBER
	5c. PROGRAM ELEMENT NUMBER
6. AUTHOR(S) **Dr. John A. Gillies**	5d. PROJECT NUMBER **CP 1191**
	5e. TASK NUMBER
	5f. WORK UNIT NUMBER
7. PERFORMING ORGANIZATION NAME(S) AND ADDRESS(ES) **Desert Research Institute Division of Atmospheric Sciences 2215 Raggio Parkway Reno, NV 89512**	8. PERFORMING ORGANIZATION REPORT NUMBER
9. SPONSORING/MONITORING AGENCY NAME(S) AND ADDRESS(ES) **Strategic Environmental Research & Development Program 901 N Stuart Street, Suite 303 Arlington, VA 22203**	10. SPONSOR/MONITOR'S ACRONYM(S) **SERDP**
	11. SPONSOR/MONITOR'S REPORT NUMBER(S)

12. DISTRIBUTION/AVAILABILITY STATEMENT
Approved for public release, distribution unlimited

13. SUPPLEMENTARY NOTES
The original document contains color images.

14. ABSTRACT

15. SUBJECT TERMS

16. SECURITY CLASSIFICATION OF:			17. LIMITATION OF ABSTRACT	18. NUMBER OF PAGES	19a. NAME OF RESPONSIBLE PERSON
a. REPORT **unclassified**	b. ABSTRACT **unclassified**	c. THIS PAGE **unclassified**	**SAR**	**111**	

TABLE OF CONTENTS

LIST OF FIGURES Page No.

LIST OF FIGURES (cont.) Page No.

LIST OF FIGURES (cont.) Page No.

LIST OF TABLES Page No.

ACKNOWLEDGEMENTS

Our research team would like to acknowledge the support of Ft. Bliss for supplying military vehicles to this project and providing a secure area in which to carry out the testing. We are grateful to the personnel of the M88 for accommodating our schedule and providing exceptional service to our project. The support of the Directorate of the Environment at Ft. Bliss has been invaluable and the work of Mr. Clyde Durham (formerly of the DoE) on our behalf was instrumental in our success. Ms. Elza Cushing and Mr. Hector Moldanado, also of the Directorate of the Environment, helped us out in numerous ways. The personnel of the Ft. Bliss Range Patrol contributed to the project by helping to maintain the sampling schedule during the air quality measurement component of the research.

We also gratefully acknowledge El Paso Water and Power for allowing us to set up an air quality monitor in a secure location on their property and for providing electricity at their own expense to run the sampler.

We would also like to thank the students and technicians who contributed to this effort. From the University of Guelph, Guelph, Ontario, Canada: Laura Brown, James King, John Coursaut, Igor Hoogendorn, Andrew Torcolletti, and Torin Macpherson who aided in the wind tunnel measurement campaigns. From the Desert Research Institute: Ravi Varma, John Walker, and Kurt Cupp for their exceptional help in the field during the vehicle dust emission measurement campaigns, and Mahmoud Abu-Allaban and Julide Koracin for their contributions to data analysis.

This research project was supported wholly by the U.S. Department of Defense, through the Strategic Environmental Research and Development Program (SERDP). Dr. Robert Holst is the SERDP Compliance Program Manager and Mr. Bradley Smith is the Executive Director of SERDP.

EXECUTIVE SUMMARY

CP-1191 had six primary objectives: 1) Determine contributions from dust and other sources at Ft. Bliss, TX, to assess the regional impacts of these emissions on ambient particulate matter levels, 2) Develop a dust emission factor database for military vehicles traveling on unpaved surfaces that reflects the influence of the surface over which the travel takes place and the speed of the vehicles, 3) Develop and test a dust emission transport model that can effectively determine the potential of these emissions for long-range transport, 4) Evaluate military vehicle disturbance effects on soil and surface properties and quantify the effects of disturbance on dust emission potential from impacted surfaces, 5) Assess the potential visibility degradation off-post by the emitted PM, and 6) Develop emission components that will be integrated with a GIS-based

emission model to estimate dust emission contributions from testing and training activities. To meet the objectives listed above several field studies and one modeling exercise were carried out.

The field work was done at Ft. Bliss, TX, and our appreciation of the support of this facility and associated personal are gratefully acknowledged. The air quality component of this research indicated that contributions of particulate matter emissions from Ft. Bliss were principally mineral dust. This contribution reached a measurable quantity only during periods when high wind events mobilized the soil surfaces within Ft. Bliss creating dust emissions on the regional scale. Emissions that could be attributed to testing and training activities could not be discerned outside of the boundaries of Ft. Bliss with the instruments used in this study. The samplers used are recognized as being acceptable by the U.S. EPA to determine compliance with Federal air quality standards.

Fugitive dust emission factors for military vehicles were developed using a multiple tower system that measured dust concentrations in vehicle-emitted plumes in real time. The results clearly indicated that the strength of the emission was linked most closely with an individual vehicle's speed and weight. Emissions for multiples of vehicles traveling in convoy, based on the available data are additive not multiplicative. In comparison to emission estimates derived using U.S. EPA AP-42 (U.S. EPA, 1996, 1999) methods the measured emission factors indicate larger than estimated contributions for speeds generally > 10-20 km hr^{-1} and for vehicle weights > 3,000 kg. The spatial variability of dust emissions from the unpaved roadways within Ft. Bliss was measured using the TRAKER vehicle. This technology was further developed as part of CP-1191. TRAKER is an effective method to map dust emission potential for paved and unpaved surfaces and can be used as a transfer standard to estimate dust emission potential for other wheeled-vehicles using the relationship developed as part of this project to convert TRAKER measurements to emission flux and the developed emission relationship between vehicle speed and weight. From the collected data it was determined that for the condition present at Ft. Bliss during the emissions testing there was very little deposition of the emitted particles within 100 m of the source. It was observed that only particles >20 μm deposited in measurable quantities indicating that this particulate matter was capable of being carried longer distances by the wind.

Military disturbance of the soil surface was observed to exacerbate wind erosion and dust emissions. The degree of increase was linked to how much loose and erodible sand was created by the impact. The strength of the dust emissions was found to scale with the amount of sand that was carried by the wind. The effect of the impacts was reduced by an order of magnitude with the passage of three years time. This was attributed to the soil crusts that developed as well as the establishment of a significant cover of vegetation. This was facilitated by locally significant rainfall events that promoted plant growth and soil crusting.

The visibility degrading potential of the dust emissions from the vehicles was evaluated with three new instruments: 1) the DRI Integrating Sphere Integrating Nephelometer, 2) the DRI Photoacoustic Instrument, and 3) the DRI Extinction meter. These instruments measure light scattering, light absorption, and light extinction, respectively. This project provided the first opportunity to test two of these instruments (DRI ISIN and Extinction

meter) in the field, and for the Photoacoustic instrument to measure absorption for a predominantly mineral phase aerosol. Data from these instruments showed that the freshly emitted dust primarily contributes to visibility degradation through light scattering. Emission factors based on the light scattering efficiency were developed as part of this project to quantify the visibility degrading potential of the emitted dust.

The emission factor data has been integrated into the Dust Emission and Transport (DUSTRAN) model developed by a research team led by Dr. Jerry Allwine of Pacific Northwest National Laboratory as part his SERDP project "Development of a GIS-Based Complex Terrain Model for Atmospheric Dust Dispersion, CP-1195. Data from CP-1191 provides the model with the ability to predict contributions of fugitive dust from wheeled vehicle activity and predict local and region dust concentration levels. The model is also being further developed to utilize TRAKER-derived data to map the spatial and temporal variability in dust emissions from paved and unpaved surfaces.

1. PROJECT OBJECTIVES

The objectives of this project can be stated as follows:

- Determine contributions from dust and other sources at Ft. Bliss, TX, to assess the regional impacts of these emissions on ambient particulate matter levels.
- Develop a dust emission factor database for military vehicles traveling on unpaved surfaces that reflects the influence of the surface over which the travel takes place and the speed of the vehicles.
- Develop and test a dust emission transport model that can effectively determine the potential of these emissions for long-range transport.
- Evaluate military vehicle disturbance effects on soil and surface properties and quantify the effects of disturbance on dust emission potential from impacted surfaces.
- Assess the potential visibility degradation off-post by the emitted PM.
- Develop emission components that will be integrated with a GIS-based emission model to estimate dust emission contributions from testing and training activities.

2. PROJECT BACKGROUND

Military activities on Department of Defense (DoD) installations in the southwest U.S. are potentially large contributors of mineral dust to the atmosphere. These contributions can arise from wind erosion processes acting upon the large expanses of fragile desert soils found within military installations and via testing and training activities. Testing and training activities inject dust particles into the air through various mechanisms including vehicle traffic and troop movements. Particulate matter (PM) emitted by these activities threatens the health and safety of military personnel due to inhalation of PM, impacts vehicle performance, and through loss of visibility. It impacts the performance of electro-optical systems and compromises flight operations. Potential off-post effects include regional visibility and air quality degradation that These latter impacts may result

in DoD facing external pressures from regulatory agencies.

Developing cost-effective strategies to deal with these problems requires identification of the main on-post PM source contributions, their characterization (e.g., particulate chemistry, light-scattering and -extinction properties, and potential for transport), and the environmental conditions that control the emissions. Following identification it will be critical to define the relative contributions of these sources to ambient PM concentrations both within and external to DoD installations. By accurately identifying the major sources of on-post PM, resources can be targeted to reduce contributions more effectively.

3. TECHNICAL APPROACH: MATERIALS AND METHODS

The general approach of this project was an empirically based field study with multiple components to meet the stated objectives. The components of this program and their links are shown in Fig. 3.1.

The specifics of the technical approaches for obtaining our research goals are detailed below.

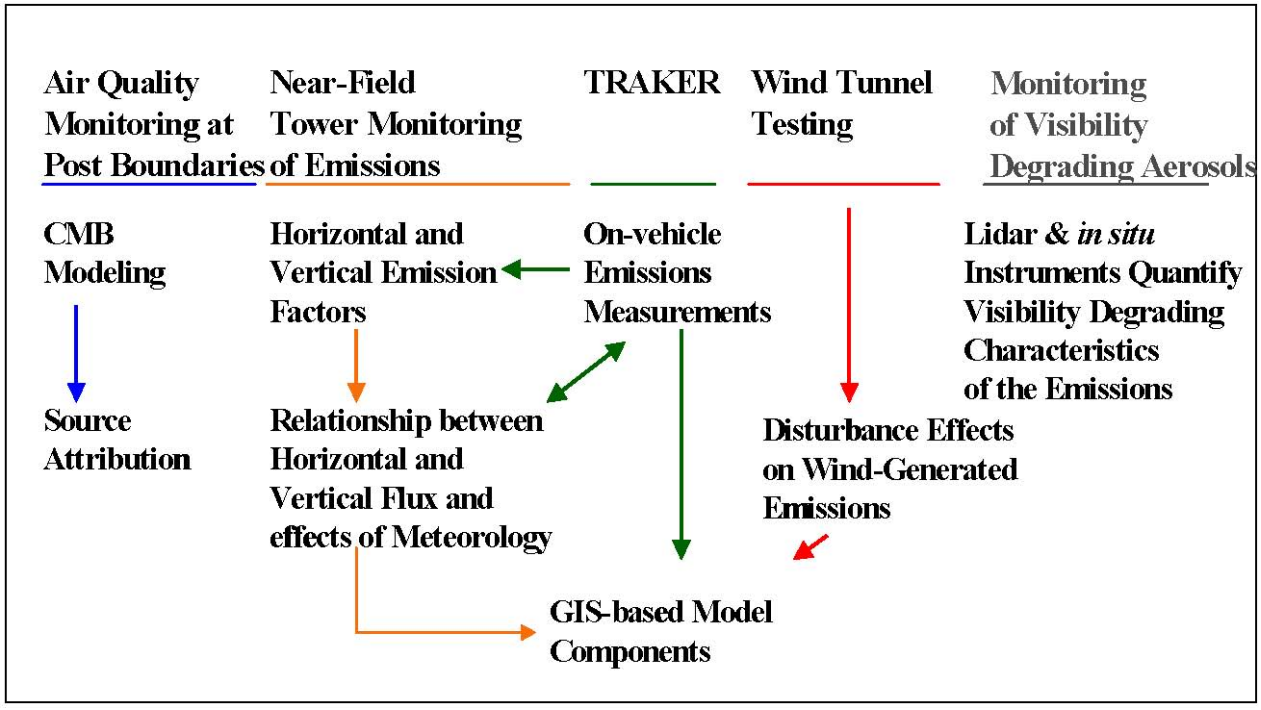

Figure 3.1. Schematic diagram of the structure and links between components of the empirically-based field study.

3.1 Air Quality Monitoring/CMB Receptor Modeling

The goal of this task was to assess the contributions of PM_{10} from Ft. Bliss that could be discerned to contribute to regional levels. This was accomplished with an air quality

measurement campaign in which four monitoring sites were established where 24 hour sampling of PM_{10} was carried out for three months on an every six day schedule with an additional 14 consecutive days of intensive monitoring, during the large training exercise code named Roving Sands in June 2001.

Particulate matter samples were collected on EPA-approved PM_{10} medium-volume (MedVol) samplers following established measurement protocols (Gertler et al., 1993). Particles less than 10 μm aerodynamic diameter are collected simultaneously on two types of filters. Teflon-membrane filters are used to collect samples for gravimetric and chemical speciation by x-ray fluorescence (XRF). Quartz-fiber filters are used for determination of the amount of organic and elemental carbon by thermal optical reflectance (TOR), and ionic species (chloride, sulfate, and nitrate anions, ammonium, soluble potassium and sodium) by ion chromatography (IC), automated colorimetry (AC) and atomic absorption spectroscopy (AAS). Dynamic field blanks (10% of the total number of ambient samples) are taken and used to evaluate measurement precision.

To define sources (e.g., wind-blown dust, mobile sources, forest fires, industry, secondary species, and others) and their relative contributions to ambient PM levels the Chemical Mass Balance (CMB) receptor model (Watson et al., 1990) was applied to the speciated PM_{10} database. The CMB estimates the relative contributions of different emission sources with known precision and accuracy to the loading of atmospheric PM. In order to ensure reasonable model estimates the CMB applications and validation protocols described by Watson et al. (1991) were be applied. Individual CMB model runs were carried out for selected pairs (upwind and downwind on the same sampling date) of the valid 24-hour samples for which the full chemical analyses had been carried out. The differences in the downwind versus upwind apportionment for similar sources were used to define the in-post contributions of the identified source types.

3.2 Vehicle Generated Emission Factor Measurements, Horizontal/Vertical Flux Relationships.

Unpaved road emissions flux experiments were conducted at Ft. Bliss, TX, using an upwind/downwind technique that has been used by other investigators. Three towers were set up collinearly and perpendicular to a 1000 m section of unpaved road on the open range of Ft. Bliss, TX, which was oriented in a north-south direction (Fig. 3.2). Historical meteorological data indicated that winds at this time of year in this area were predominantly from the west. The three towers were all downwind of the road at distances of 7 m, 50 m, and 100 m. The towers were instrumented to measure vertical profiles of dust concentration mass and particle size. Meteorological measurements were also taken. These data were combined to estimate the mass flux of dust (grams of PM_{10} produced per vehicle kilometer traveled) traveling downwind from the source area created by the tested vehicles. The emissions from a mix of civilian and military vehicles covering a substantial range of weights, length and width dimensions, and number of wheels were measured to understand how these properties relate to emissions of dust, specifically the PM_{10} component.

A second aspect of this component of the project was to evaluate the potential for the

measured emissions to be transported longer distances and contribute to regional particulate matter levels. This was examined by assessing the near-source removal of PM_{10} dust emitted from the unpaved test road at Ft. Bliss. This assessment was accomplished by comparing measured results with predictions from a simple dispersion model. From this comparison an estimate of the fraction of PM_{10} fugitive dust emissions from unpaved roads that is regionally transportable, for the conditions observed at Ft. Bliss was calculated.

3.3 TRAKER

In order to develop a greater understanding of how emissions of dust change as a function of surface type a complimentary measurement procedure that utilized the TRAKER (Testing Re-entrained Aerosol Kinetic Emissions from Roads) (Kuhns et al., 2001; Etyemezian et al., 2003a; Etyemezian et al., 2003b) approach was also utilized in this project (Fig. 3.3). The TRAKER is a vehicle designed to measure the dust emissions potential of a roadway (paved and unpaved) or any off-road surface over which vehicles traverse. The principle of operation of the TRAKER is fairly simple. The TRAKER instrumentation is designed to measure the concentration of

Figure 3.2. The three-tower system used to characterize and quantify the dust emissions from the test vehicles.

Figure 3.3. The TRAKER vehicle measuring road dust emissions at Ft. Bliss, TX.

airborne particles in a specific size range in the dust plume generated behind the front tires of a vehicle. A background measurement of particle concentrations is obtained simultaneously at a location on the vehicle far away from the tires. The difference in the signals between the influence monitors and the background monitor is related to the amount of dust generated from the surface by the vehicle moving over it. The TRAKER measurement is related to the emission of dust from the surface over which the vehicle is traveling. The strength of the signal is influenced by such factors as vehicle speed, weight, and also the surface characteristics.

3.4 Wind Tunnel Testing to Assess Surface Disturbance Effects on Dust Emissions

Portable wind tunnel tests were conducted on a test surface (within the M88 Driver Training Area, Ft. Bliss) with different levels of disturbance created by three different military vehicle types (HUMVEE, 5-ton truck, and Bradley Fighting Vehicle) (Fig. 3-4). A control surface with no disturbance was used for comparison purposes. Horizontal saltation and vertical dust fluxes were measured in the wind tunnel and surface characteristics monitored directly following disturbance and again two years after disturbance. These measurements were used to assess the effect of disturbance levels on the absolute and relative amount of dust emissions. The post-disturbance recovery process was also evaluated by taking repeated measurements of the surface characteristics (e.g., degree of crusting, plant cover) in conjunction with the wind tunnel tests.

Figure 3.4. The University of Guelph portable wind tunnel deployed at the vehicle disturbance test site, Ft. Bliss, TX

3.5 Contributions to Regional Visibility Degradation

Visibility and its degradation due to aerosol can be quantified by aerosol light extinction (NRC, 1993). To quantify the flux of visibility degrading aerosol (VDA) originating

from emissions measured as a function of vehicle activity, light extinction and wind velocity vectors need to be measured over a three-dimensional surface enclosing the emission zone. To characterize the visibility degrading potential of the emitted particulates and estimate the particle flux, *in situ* light extinction and its scattering and absorption components will be measured at one location in the downwind flux plane. Semi-quantitative lidar (light detection and ranging) measurements of light extinction covering the whole downwind flux plane were made in an attempt to correlate backscatter with the *in situ* measurements resulting in a quantitative determination of VDA concentrations for the downwind flux plane. A sun photometer that measures the slant-path integrated light extinction in this flux plane was also deployed to assess possibility of using these much simpler instruments for the routine monitoring of VDA flux from DoD installations.

3.6 GIS-based emission model Components

The emission factors and TRAKER results were developed to be specific components for the Pacific Northwest Laboratory DUSTRAN (DUST TRANsport; SERDP CP-1195) model. This dust dispersion modeling system requires GIS input files (e.g., roads, political boundaries, terrain elevations, soil types, surface cover) and meteorological data from National Weather Service or local meteorological networks. DUSTRAN includes the dust-emission factors for wheeled military vehicles developed in project CP-1191.

4. PROJECT ACCOMPLISHMENTS

This section provides details on the accomplishments for the Tasks identified above.

4.1 Air Quality Monitoring/CMB Receptor Modeling

Military activity on the open range of Ft. Bliss, TX, produces PM_{10} (particulate matter $\leq$10 μm aerodynamic diameter) fugitive dust from driving on paved and unpaved roads as well as during periods of off-road travel and activities as troops carry out testing and training maneuvers (Gillies et al., 2002). Exhaust emissions from military vehicles operating in the range area are another source. PM_{10} from dust emissions from Ft. Bliss range areas during periods of elevated wind speed is another potential source. In response to concerns that Ft. Bliss may contribute significantly to regional fugitive dust PM_{10} levels through its testing and training activities and from wind-generated dust emissions a study was carried out to estimate source contributions in relation to regional levels under certain meteorological conditions and testing and training activities.

To characterize contributions of PM_{10} that could be attributable to Ft. Bliss an air quality monitoring program was carried out using U.S. EPA equivalent samplers (DRI medium volume samplers, Gertler et al., 1993) to measure 24-hour average PM_{10} mass concentrations in four locations near eastern and western boundary points of the Ft. Bliss open range. Sampling was carried out on the U.S. EPA every-sixth-day schedule for the periods May through August 2001, and January through April 2002. These two periods were chosen because they cover times during which there is an increased probability of high wind speed events with predictable wind directions (February through April),

periods of calm (winter inversions and summer high pressure), as well as a period in which the highest intensity testing and training activity occurs on the post. This is a two-week period code named Roving Sands, which is a large joint training exercise in the in which large numbers of vehicles, equipment, and troops travel throughout the open range of Ft. Bliss. During this period (June 12-25, 2001) 24-hour average PM_{10} samples were collected each day at the four monitoring sites.

This section of the document reports on the observed ambient levels of PM_{10} through the monitoring periods, its chemical composition, and provides source attribution information as well as estimates of the contributions from Ft. Bliss to the ambient levels. Source attribution was accomplished through comparison of mass concentration differences in upwind and downwind sampling locations near Ft. Bliss boundaries and using chemical mass balance (CMB) receptor modeling (Watson et al., 1991) on selected samples. The samples chosen for full analysis were representative of periods of time in which there were different meteorological and military activity conditions.

4.1.1 Air Quality Sampling Sites

Ft. Bliss, a ~4.5×10^{5} ha military post near the city of El Paso, TX, lies within the Chihuahuan desert region (Fig. 4.1). A summary of the annual and seasonal average temperature, precipitation, and wind conditions for El Paso is presented in Table 4.1.

Ft. Bliss is a U.S. Army post that operates under the Training and Doctrine Command (TRADOC) mission and is in large part dedicated to training military personnel with a focus on Air Defense Artillery. In support of this mission personnel are trained to use military vehicles and equipment, which involves large areas of the Ft. Bliss range. These activities can raise dust clouds as well as creating conditions on the range that make the soils there susceptible to wind erosion and dust emissions.

Four sampling sites were established in total, three on the Ft. Bliss range and one within the city of El Paso, TX (Fig. 4.1) to monitor air quality in the vicinity of the boundaries of Ft. Bliss. Samplers were all placed on 2.0 m high platforms at each of the sites. Site one (SW Castner), which represents a location near the southwest boundary of Ft. Bliss, in El Paso, was located on El Paso Water Company property on the western edge of the El Paso suburb of North Hills. The sampler was placed in an open area adjacent to a water tank in an elevated location above the surrounding urban area that lies to the east with undeveloped land to the west extending up the slopes of the Franklin Mountains State Park and Castner Range area. The second western boundary site (NW Doña Ana) was located at the Doña Ana Range Camp. The sampler was placed on the west side of the camp near a large water tower and away from camp activity. This site was located within the open range of the Ft. Bliss Doña Ana

Table 4.1. Summary of average climatic conditions[1], El Paso, TX.

Period	**Average Temperature (°C)**[2]	**Average Precipitation (cm)**[2]	**Average Wind Speed**[2] **(km/hr)**	**Prevailing Wind Direction**[2] (degrees)

Annual	17.3	22.4	14.2	360
Winter (Dec.-Feb.)	7.2	1.2	13.6	333
Spring (March-May)	17.4	0.6	17.3	267
Summer (June-August)	27.2	3.2	13.6	183
Fall (Sept. Nov.)	17.6	2.5	12.4	243

[1] Source: National Climatic Data Center, Ashville, NC.

[2] 30-year average.

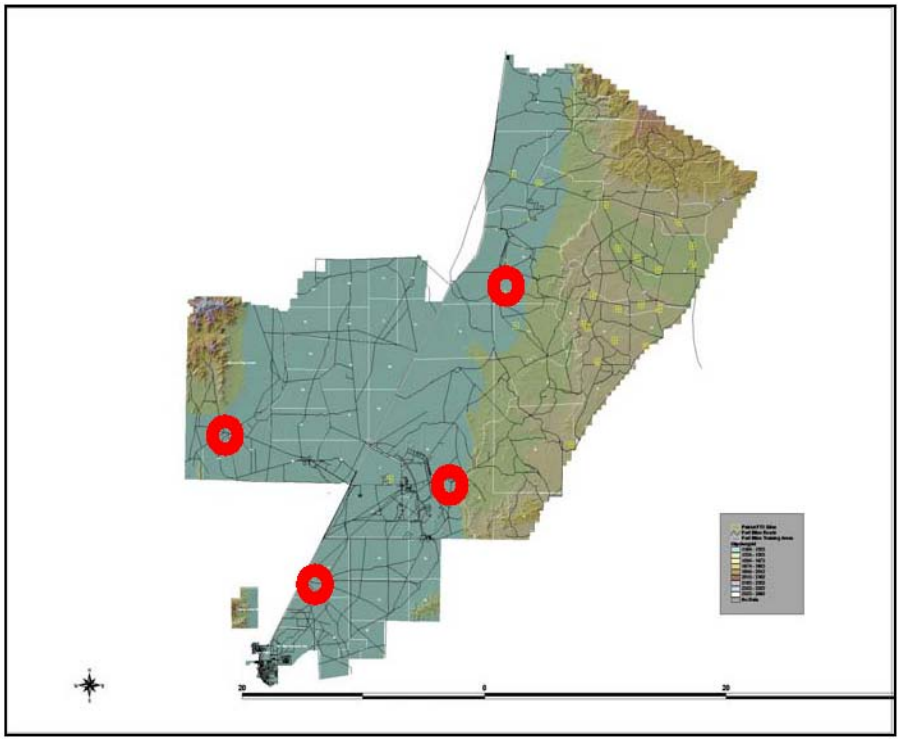

Figure 4.1. Ft. Bliss and the locations of the four ambient air quality monitoring sites.

Orogrande complex. The eastern locations were located within Ft. Bliss at the Short Range Air Defense installation (NE SHORAD) near Orogrande, NM, and at the western side of the McGregor Camp (SE McGregor), an installation to the south of Orogrande, NM. These sites were chosen because of their openness and lack of intense local PM-generating activities that could have influenced the samples. In addition they represent locations for sampling PM_{10} that is entering, traversing, and exiting Ft. Bliss under certain wind conditions providing the opportunity to observe contributions (or losses) of PM_{10} from (or within) the installation.

4.1.2 Ambient Measurement Methods

PM_{10} samples were collected on a twenty-four hour basis at the four locations using the sampling protocol described by (Watson and Chow, 1994). At each location a medium-volume sampler designed to collect samples for chemical analyses was utilized (Gertler et al., 1993). This type of sampler employs a Sierra-Andersen 254 PM_{10} inlet to determine the size fractions collected. The ambient air is transmitted through the size-selective inlet and into a plenum. Maintaining a constant pressure across a valve with a differential pressure regulator controls the flow rate in the sampler. For the size-selective inlet to work properly, a flow rate of 113 lpm must be maintained through the sampler. Flow

rates of 20 lpm through each Savillex filter holders were used to collect adequate samples for gravimetric and chemical analyses. This flow rate was drawn simultaneously through two parallel filter packs, one with a ringed 47 mm Teflon-membrane filter (Gelman Scientific, Ann Arbor, MI) and one with a 47 mm quartz-fiber filter (Pallflex Corp., Putnam, CT). The remaining 33 lpm was drawn through a makeup air port. The flow rates were each set with a calibrated rotameter and were monitored with the same rotameter at each sample change.

4.1.3 Ambient PM_{10} Sample Analysis

As the same chemical analysis was performed on the source and the ambient samples the procedures are presented herein for completeness. The analysis methods are similar to those used in recent source characterization and apportionment studies (e.g., Chow et al., 1992; Watson and Chow, 2001; Chow et al., 2003). The Teflon-membrane filters were analyzed for mass by gravimetry using a Cahn 31 Electro-microbalance and for 40 elements (Na through U) by x-ray fluorescence (XRF) (Watson et al., 1999). One half of each quartz-fiber filter was extracted and analyzed for ions () by ion chromatography (Chow and Watson, 1999); for ammonium () by automated colorimetry; and for soluble sodium (Na^{+}) and soluble potassium (K^{+}) by atomic absorption spectrophotometry. A 0.5 cm^2 punch from the remaining half of each quartz fiber filter was analyzed for eight carbon fractions following the IMPROVE thermal/optical reflectance (TOR) protocol (Chow et al., 1993; Chow et al., 2001; Fung et al., 2002).

4.1.4 Sample Selection and Analysis

In total 149, 24-hour PM_{10} samples were collected during the monitoring period for all sites combined. Gravimetric measurements were carried out on all the collected samples, however resources were not available to perform chemical analysis on all the samples. A subset of samples was chosen based on several criteria including: mass loading, season of collection, days with different meteorological conditions (e.g., high wind days), and days with high activity on the Ft. Bliss range. The final selection included three days for which valid mass and chemical speciation data were available for only two of the four sites. The PM_{10} concentrations with associated uncertainties for each site in temporal sequence for all the gravimetric measurements are shown in Fig. 4.2 for 2001 and Fig. 4.3 for 2002. In 2001 and 2002 the average percent uncertainty of the mass concentration measurements was 6.4% (±11.0%) and 6.8 (±4.2%), respectively. These low uncertainty values make it difficult to see the error bars on the figures (Fig. 4.2 and 4.3). In Fig. 4.3 the PM_{10} measurements taken by Texas Natural Resource Conservation Commission monitors in two locations in El Paso (UTEP and Ascarte Park) for the same sampling days in 2001 are shown for comparison purposes. In general the sites closer to El Paso have higher PM_{10} levels than those observed at the Ft. Bliss monitors.

A subset of 38 filters representing 11 different days was selected for full chemical analysis. Brief descriptions of the meteorology associated with the selected samples and information on past precipitation events are provided in Table 4.2. The data presented in Table 4.2 show that inmost cases the wind directions had a predominantly eastern or western component and very small amounts of precipitation had fallen during the

sampling periods.

Comparisons between the observed mass concentrations and chemical speciation of the samples among the four sites as a function of the prevailing meteorological conditions or military activity levels are described below. The samples are grouped under the following categories: 1) winds with a westerly direction, 2) winds with an easterly direction, and 3) samples from during Roving Sands (i.e., high on-post activity).

Westerly Winds

Five of the selected sample days have resultant wind directions with a predominantly westerly component (Table 4.2). Of these selected days there are two in which a significant net gain in PM_{10} concentration is observed at the downwind boundary monitoring locations. On 13-06-01

Figure 4.2. PM_{10} mass concentrations measured for the 2001 air quality sampling days.

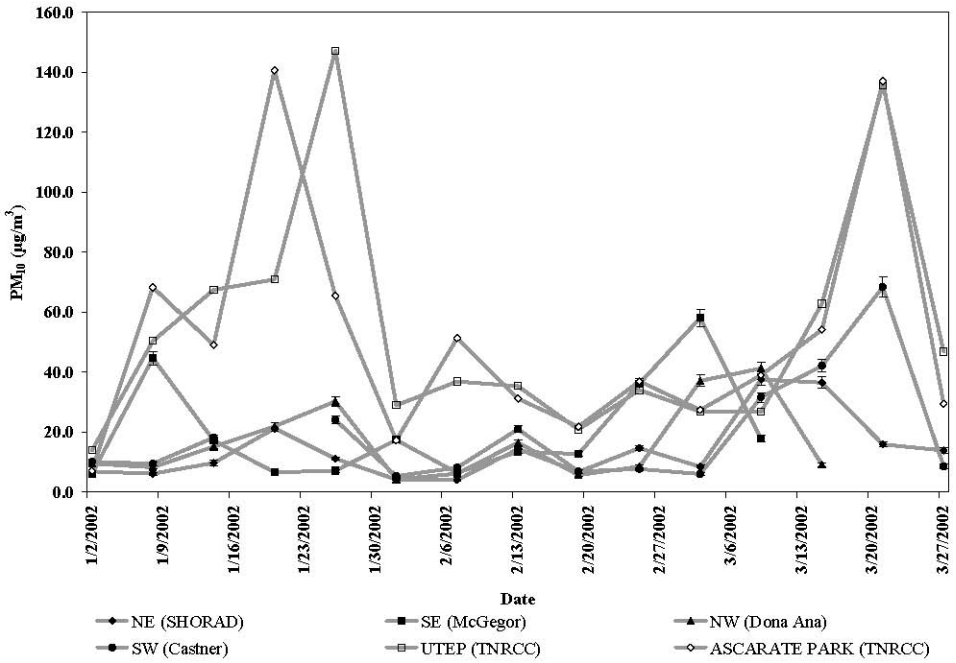

Figure 4.3. PM_{10} mass concentrations measured for the 2002 air quality sampling days, including TNRCC data from UTEP and Ascarate Park.

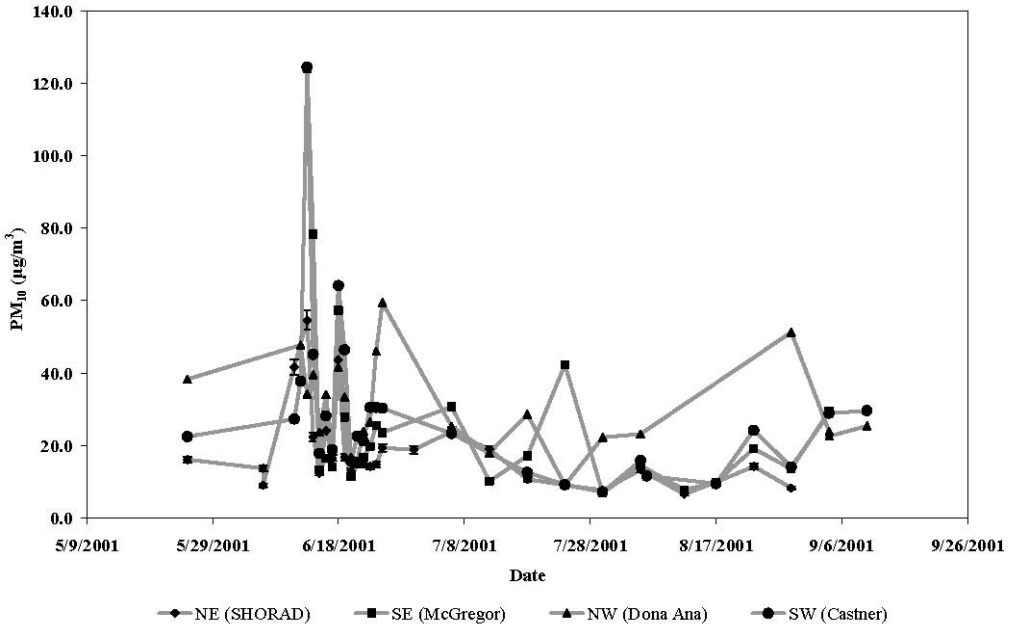

Table 4.2. Selected sampling days and associated climate data.

	Temperature (C)			Pressure (kPa)		Wind		Days from Last	Precipitation
Date	Max	Min.	Avg.	Avg. Station	Avg. Sea Level	Avg. Speed (km/h)	Resultant Direction	Precipitation Event	from Event (mm)
13/06/2001	35.0	23.9	31.1	87.1	105.0	37.8	240	6	2.8
17/06/2001	34.4	22.2	27.8	88.2	101.3	12.7	120	9	2.8
21/06/2001	35.0	20.6	27.8	88.2	101.3	14.0	80	2	0.5
22/06/2001	35.0	21.7	28.3	88.2	101.3	11.6	40	3	0.5
06/07/2001	33.3	21.1	27.2	88.1	101.3	13.7	200	1	0.3
30/07/2001	37.2	23.3	30.6	87.9	100.9	13.0	230	2	0.3
26/01/2002	15.0	-5.6	5.0	88.2	102.0	7.4	40	26	2.0
13/02/2002	11.1	0.0	5.6	88.7	102.4	11.9	80	8	7.9
15/03/2002	17.2	8.3	12.8	87.4	100.7	14.8	290	38	7.9
21/03/2002	24.4	2.2	13.3	88.7	102.2	15.3	80	44	7.9
27/03/2002	27.2	5.6	16.7	87.8	101.5	15.9	250	50	7.9

Data are from El Paso Airport

winds from the west reached speeds of 30-39 km/hr at the El Paso Airport and the Dona Aña-SHORAD pair shows an increase in PM_{10} from 34.2 (±1.7) µg/m^3 at Dona Aña to 54.6 (±2.7) µg/m^3 at SHORAD, a gain of 20.4 µg/m^3 or an increase of approximately 30%. Individual species that show a significant increase in mass concentration included Si, Ca, and Fe (Fig. 4.4). A significant change in mass is defined when the difference in mass concentration between sites is greater than the propagated uncertainty (i.e., the square root of the sum of the squared uncertainty of the individual species concentration measurement). For the southern boundary pair (Castner-McGregor) no difference was observed in the measured mass concentrations. However, these speciated data show net gains at the downwind site (McGregor) in total Carbon, Al, Ca, and Fe (Fig. 4.4).

The second day with an observed increase at the downwind border monitoring site was 27-03-02. On this day average wind speed and resultant wind direction measured at El Paso airport were 15.9 km/hr and 250°, respectively. Available wind data (Fig. 4.5) also indicate winds from the W to SW reached speeds between ~19-30 km/hr for a significant portion of the day (~43%). There was a net gain in PM_{10} mass concentration at

SHORAD of 4.7 µg/m^3 representing a 51% gain. At the southern monitoring site PM_{10} levels increased from 8.5 (±0.8) µg/m^3 at Castner to 17.8 (±1.0) µg/m^3 at McGregor on the east side, an increase of 110%. Species showing significant increase in mass concentration include S, K, CA, Mn, and Fe at SHORAD (Fig. 4.5), and the additional species Mg, Al, and Si at the McGregor site (Fig. 4.5).

The other selected days with westerly winds exhibit a different pattern that shows either no difference in total mass concentration between sites or a net loss of mass concentration between the upwind and downwind site. Examples of the neutral case were observed between certain pairs of stations on 06-07-01, 30-07-01, and 15-03-02. On 06-07-01 average wind speed at El Paso airport was 13.7 km/hr for a resultant direction of 200°. Winds did reach speeds in excess of 30 km/hr (Fig. 4.6) for brief periods (~5% of the day) from the WSW. Comparing between SHORAD with an average PM_{10} of 23.8 (±1.2) µg/m^3 in the NE and Castner with an average PM_{10} of 23.3 (±1.2) µg/m^3 in the SW no significant difference in mass concentration of PM_{10} was observed. Even though no difference in the PM_{10} mass concentration was observed several individual species did show positive increases including the ionic species Na^{+}, NH_4^{+}, $SO_4^{=}$, NO_3^{-}, as well as Mg, S, and Ca (Fig. 4.6).

Figure 4.4. Differences in PM_{10} observed during westerly winds for the north (top) and south monitoring sites, 13-06-01.

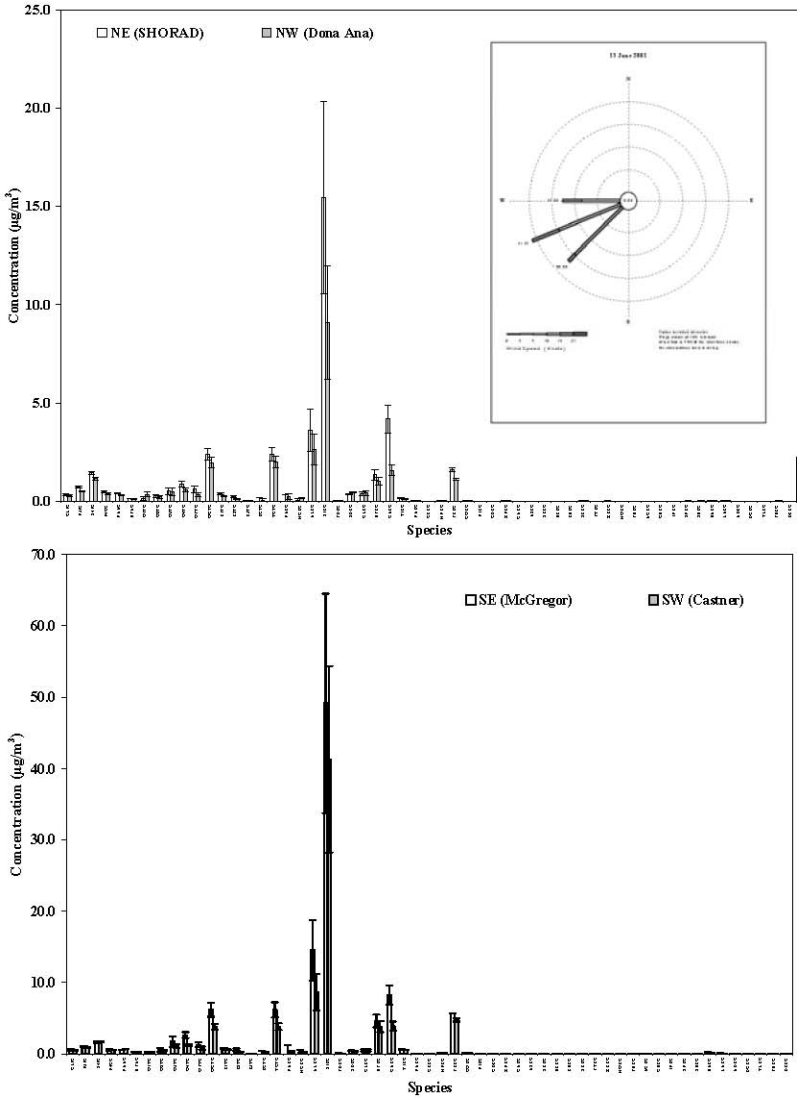

F

monitoring sites, 27-03-02.

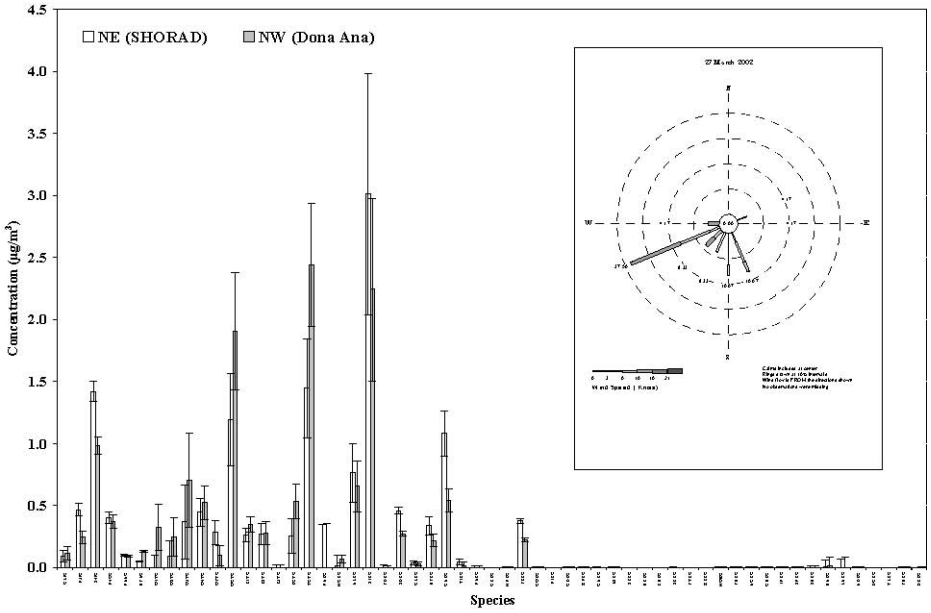
NE (SHORAD)
NW (Dona Ana)
Concentration (µg/m³)
Species

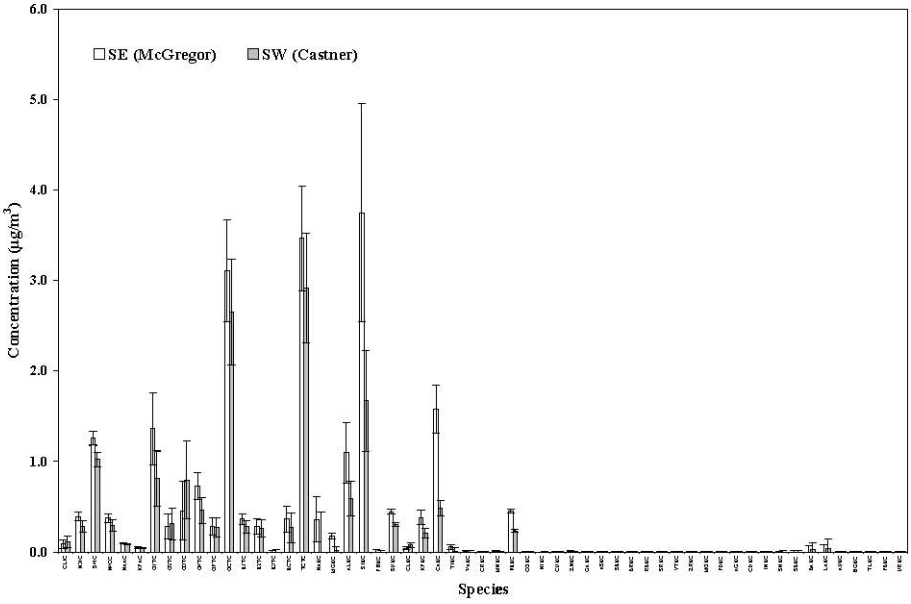
SE (McGregor)
SW (Castner)
Concentration (µg/m³)
Species

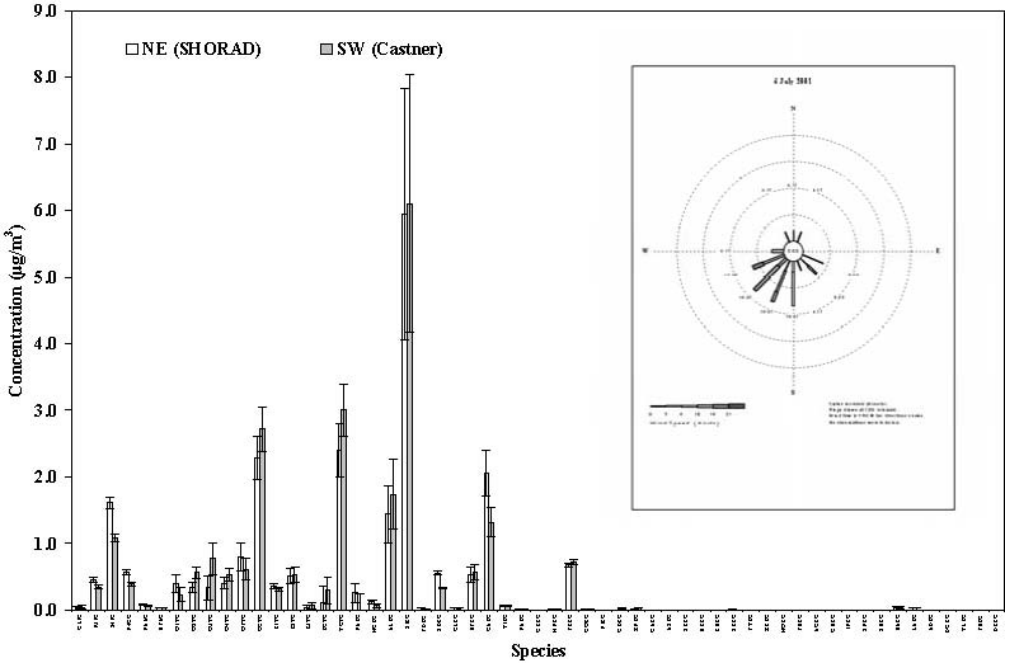

F

westerly winds for the NE SHORAD and SW Castner monitoring sites, 06-07-01.

Other neutral cases occurred on 30-07-01 for the southern McGregor and Castner pair and on 15-03-02 for the SHORAD and Dona Aña pair in the north. For the 30-07-01 case winds averaged 13.0 km/hr at the El Paso airport along a resultant wind direction of 230°. During a portion of the day however (~10% of the time), the wind speed exceeded 40 km/hr from the W and WSW. On 15-03-02, average wind speed was 14.8 km/hr for the resultant direction of 290° with winds reaching speeds between ~19 – 30 km/hr for 25% of the day from the WNW to NW.

Several comparisons between upwind and downwind boundary monitors also show that in certain instances a net loss of mass concentration can occur at the downwind site. On 30-07-01 (Fig. 4.7) while the southern site pair (McGregor and Castner) showed no change in mass concentration (Fig. 4.7), the northern pair showed a downwind decrease in mass concentration of 14.6 µg/m^3 or a change of 65%. Species in which a significant loss of mass was observed were Na^+, Al, Si, S, K, Ca, Mn, and Fe (Fig. 4.7). A similar situation occurred for the McGregor-Castner pair on 15-03-02 where a net loss of 5.9 µg/m^3 was observed on the predominantly downwind site, which represents a 14% loss. In this case the speciated data did not show that the loss occurred in a few specific species.

Easterly Winds

For five sampling days with easterly winds only the positive downwind addition (17-06-

01, 21-06-01, 26-01-02, 21-03-02) or neutral cases (21-06-01, 13-02-02) were observed in the mass concentration data. On 17-06-01 average wind speed was 12.7 km/hr for the resultant wind direction of 120°. For ~16% of the day wind from the SE to ESE reached speeds of between 11 and 30 km/hr (Fig. 4.8). The PM_{10} concentration difference between the upwind McGregor and the downwind Dona Aña sites was a modest 3.1 $\mu g/m^3$, which represented a 22% increase. The speciated data show a decrease in carbonaceous PM_{10} and a significant increase in Fe. These data suggest there are also increases in Al, Si, and Ca (Fig. 4.8), however the difference in the mass concentration for these species is less than the propagated uncertainty so the significance is questionable.

For the sampling day 21-06-01 the average wind speed at El Paso airport was 14.0 km/hr for a resultant wind direction of 80°. For ~25% of the day the wind were ESE to SE in the range of ~12-19 km/hr (Fig. 4.9). In the south PM_{10} mass concentration increased from 14.9 (±1.1) $\mu g/m^3$ to 22.6 (±1.2) $\mu g/m^3$), a change of 52%, from upwind to downwind. The gain in mass was mainly attributable to inputs of S, Ca, and Fe (Fig. 4.9).

26-01-02 was also a day in which net gains in PM_{10} were observed on the downwind monitoring site for both the north and south sampling pairs (Fig. 4.10). The wind speed on this day averaged 7.4 km/hr for a resultant direction of 40°. Easterly component winds blew for ~66% of the day ranging in speed between ~6-19 km/hr (Fig. 4.10). Average PM_{10} mass concentration at SHORAD was 11.1 (±0.6) $\mu g/m^3$ and 30.2 (±1.5) $\mu g/m^3$ for the downwind Don Aña site, a difference of 19.1 $\mu g/m^3$ representing a 172% increase. Major contributing species were Al, Si, Ca, Fe as well as carbonaceous material (Fig. 4.10). In the south the average PM_{10} at McGregor

Figure 4.7. Example of the case where a net loss of PM_{10} is observed on the downwind sampling location during predominantly westerly winds for the NW Dona Aña and NE SHORAD monitoring sites, 30-07-01.

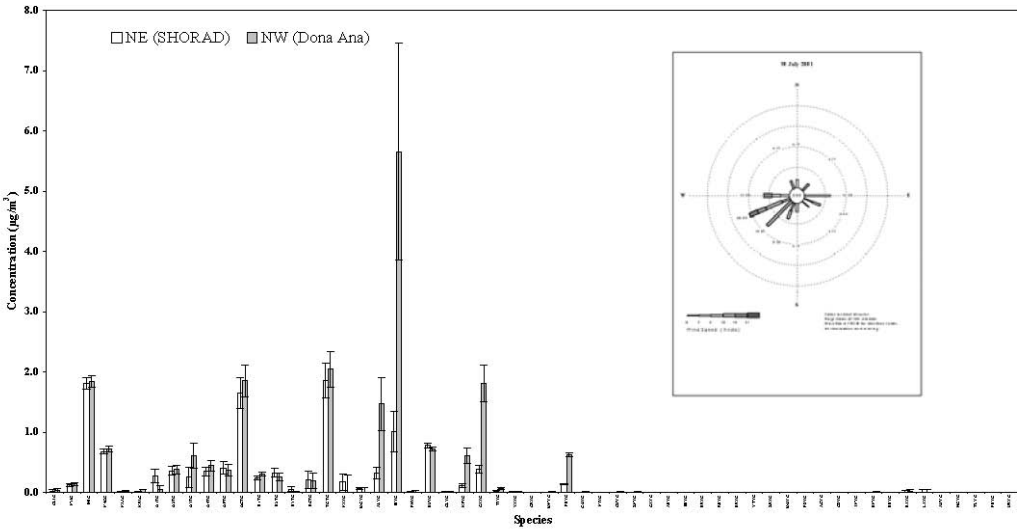
NE (SHORAD)
NW (Dona Ana)
Concentration (µg/m3)
Species

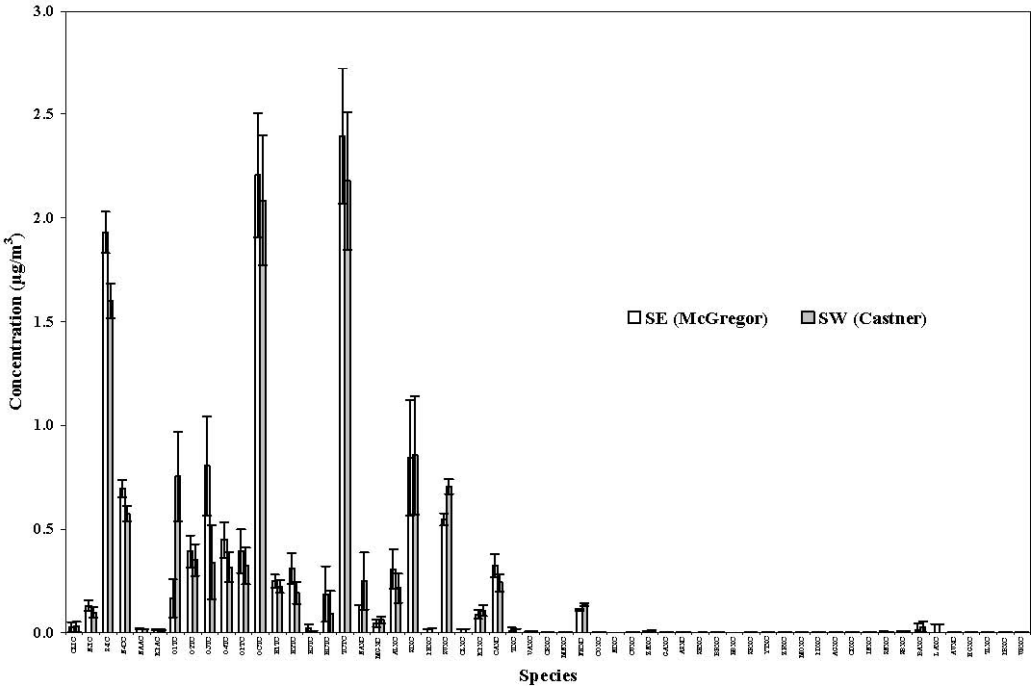
SE (McGregor)
SW (Castner)
Concentration (µg/m3)
Species

Figure 4.8. Differences in PM_{10} observed during easterly winds for the NW Dona Aña and SE McGregor monitoring sites, 17-06-01, showing a net downwind increase.

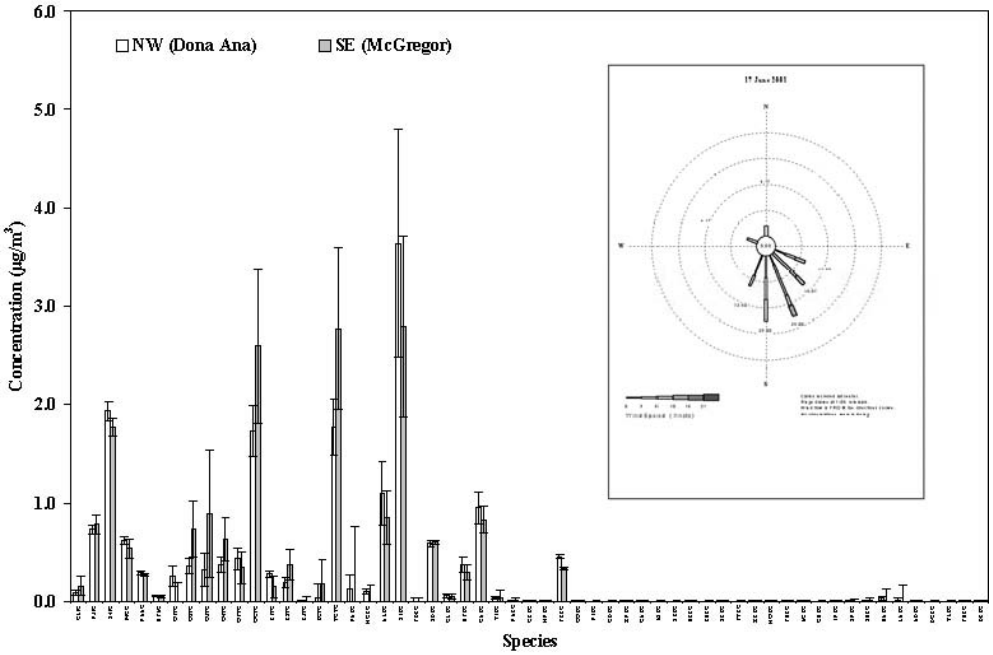

Figure 4.9. Differences in PM_{10} observed during easterly winds for the NE SHORAD and NW Dona Aña and SE McGregor and SW Castner monitoring sites, 21-06-01, showing a net downwind increase.

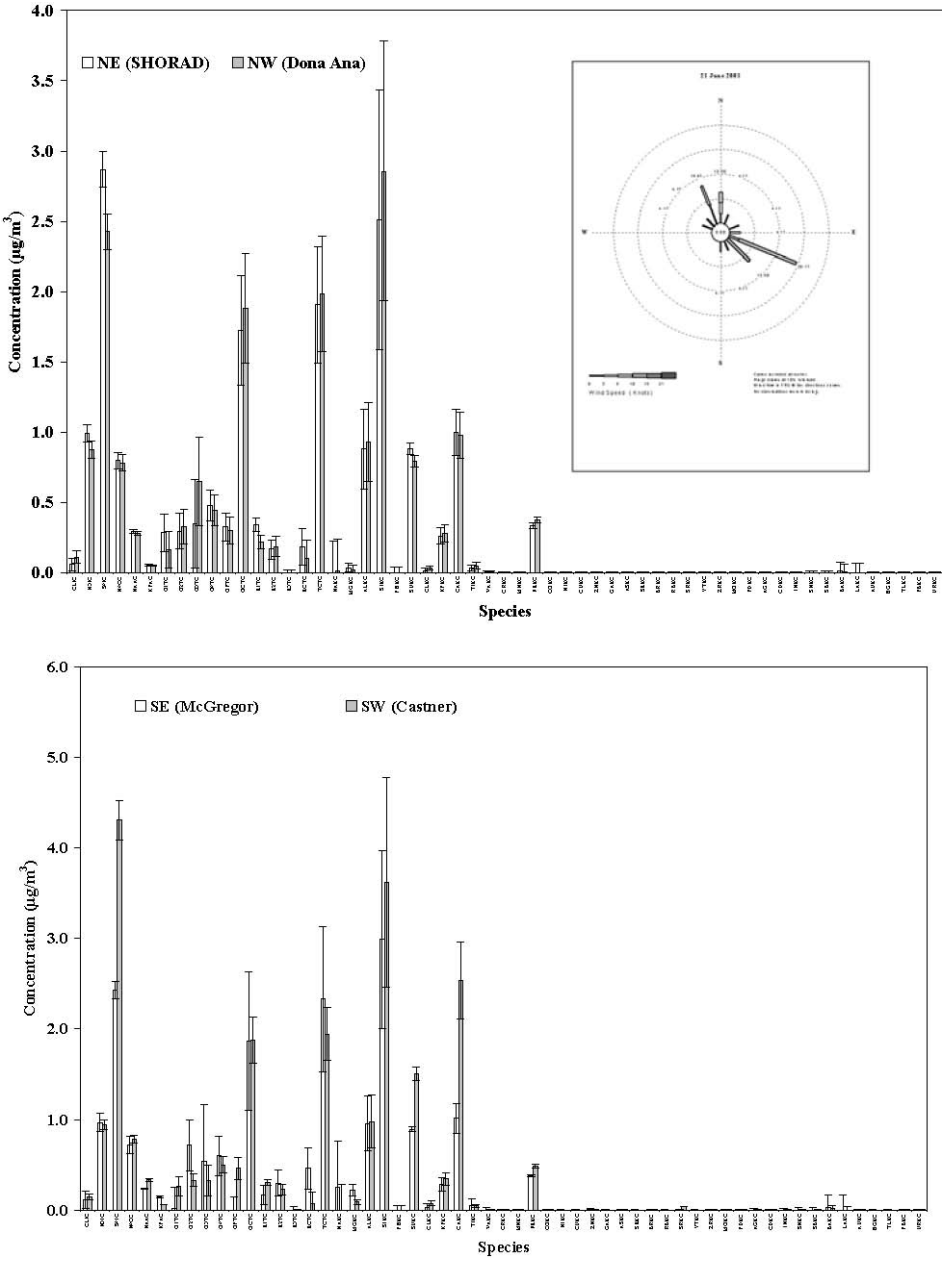

Figure 4.10. Differences in PM_{10} observed during easterly winds for the NE SHORAD and NW Dona Aña and SE McGregor and SW Castner monitoring sites, 26-01-02, showing a net downwind increase.

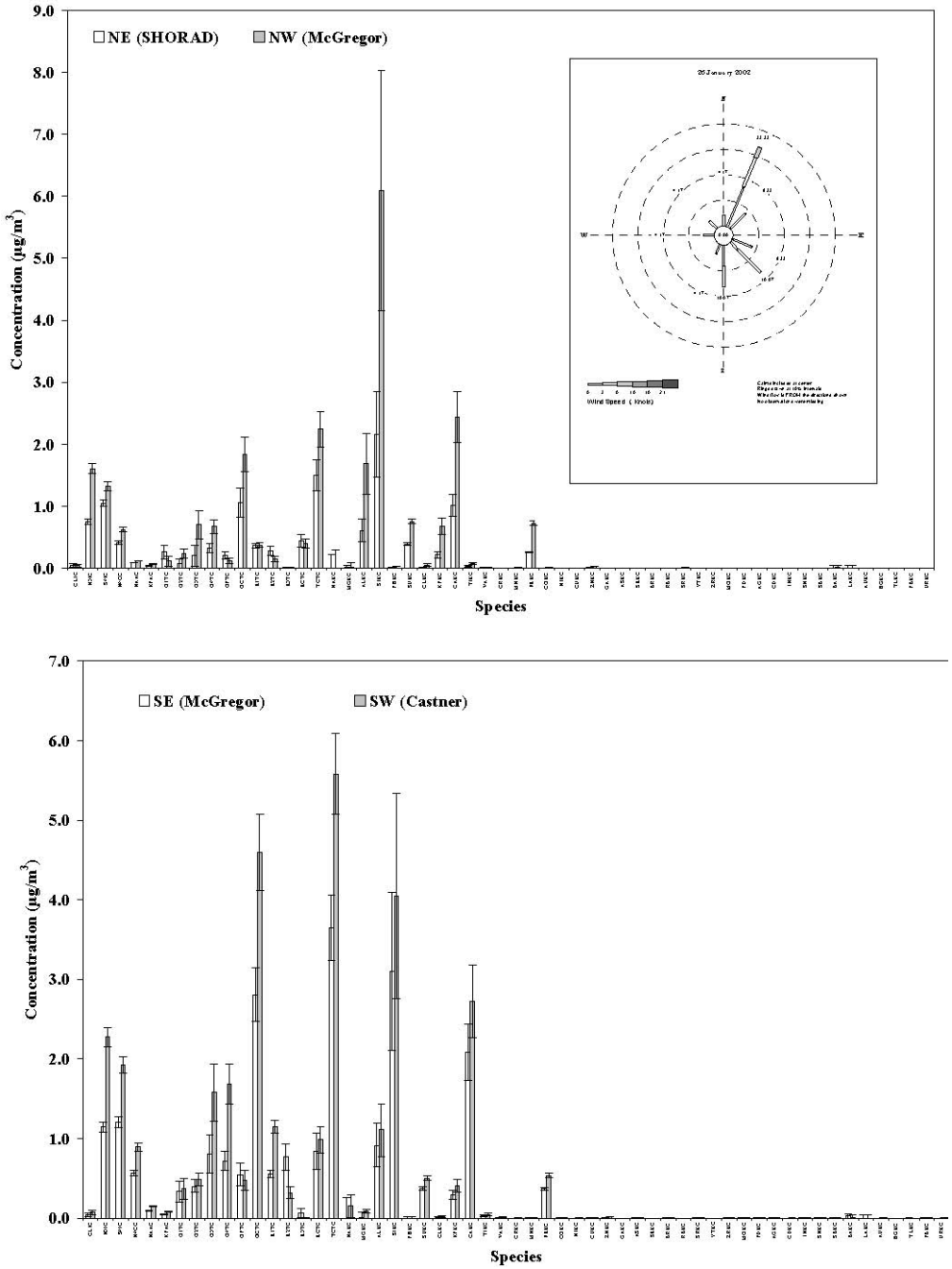

was 17.2 (±0.9) µg/m^3 and downwind at Castner 24.0 (±1.2) µg/m^3, a change of 40%. The increase in contributions from specific species was similar to the northern case (Fig. 4.10).

The last sampling day, 21-03-02, with easterly winds also showed net increases in PM_{10} for the downwind sites for both the north and south monitoring stations. Wind speed on this day averaged 15.3 km/hr for a resultant direction of 80°, but winds from the E

through SE blew for ~66% of the day ranging in speed between ~6-30 km/hr. In the north at SHORAD, PM_{10} averaged 15.9 (±0.8) µg/m^3 while downwind at Don Aña it was 41.3 (±2.1) µg/m^3, a gain of 25.3 µg/m^3 or an increase of 159%. The major species contributors to the gain were Al, Si, Ca, and Fe along with organic carbon. In the south, Castner had a higher PM_{10} average as compared to McGregor, gaining 10.3 µg/m^3 that represented an increase of 18%. The species that contributed to this increase are not as well defined as in the north, but the data suggests that Al, Si, and Fe are among the more important ones.A neutral event was observed on 13-02-02, a day in which wind speed averaged 11.9 km/hr in El Paso for a resultant wind direction of 110° (Fig. 4.11). A significant portion of the day, 36%, had winds from the E to SSE between 6 and 19 km/hr. Comparing between McGregor in the southeast with an average PM_{10} concentration of 17.4 (±0.9) µg/m^3 and Dona Aña in the northwest with an average of 16.4 (±0.9) µg/m^3, no significant difference in concentration was observed. There is a lower contribution of carbonaceous material in the northwest PM_{10}, but for most other species the values are similar (Fig. 4.11).

Roving Sands

Air quality sampling during the military exercise Roving Sands took place from 13-06-01 through 25-06-01. A synopsis of the daily meteorological conditions for each of the Roving Sands sampling days is presented in Table 4.3. The average PM_{10} mass concentrations measured at the four monitoring sites on the days are shown in Fig. 4.12. It should be noted that four of the sampling days described previously also occurred during this exercise period.

The variability in the wind direction during most of these sampling days makes it more difficult to define a definitive upwind and downwind site than in the previously described samples. Using the resultant wind direction data from Table 4.3 as a guide for defining upwind and downwind sites, it is observed that in general, increases in the ostensibly downwind monitors are observed in 19 of the 26 samples. This represents eight out of the 14 sampling days during the Roving Sands monitoring period. The downwind addition of mass concentration ranged from ~4 to 40 µg/m^3 on days with apparently positive additions from within Ft. Bliss (Fig. 4.13). In comparison to only non-Roving Sands sampling days for which three out of seven (43%) days showed significant downwind additions of mass there seems to be a very slight increase in the likelihood of additional mass inputs of PM_{10} during Roving Sands (57% of days) can be observed. The meteorological conditions, especially the range of wind speeds is not greatly different between the sampling days suggesting that it is not the driving mechanism behind the observed differences, but it could be related to increased military activity.

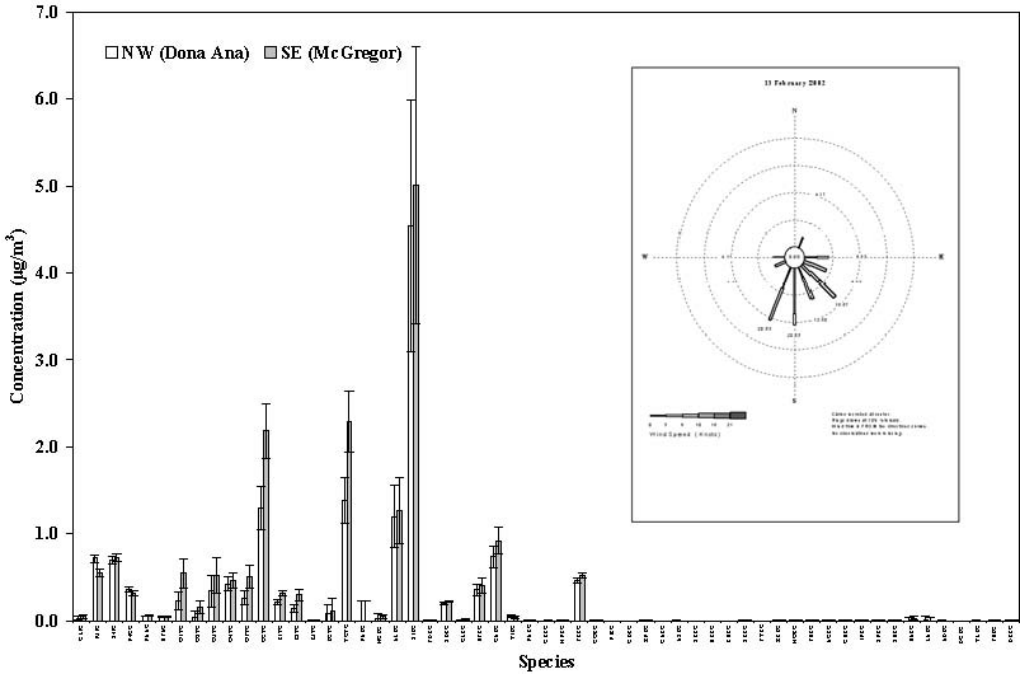

Figure 4.11. A neutral event showing no change in PM_{10} between NW Dona Aña and SE McGregor for south-easterly winds, 13-02-02.

Date	Temperature (C)			Pressure (kPa)		Wind		Precipitation
	Max	Min.	Avg.	Avg. Station	Avg. Sea Level	Avg. Speed (km/h)	Resultant Direction	(mm)
6/13/2001	35.0	23.9	29.4	87.1	105.0	37.8	240	0.00
6/14/2001	31.7	19.4	25.6	87.6	100.7	15.5	320	0.00
6/15/2001	35.6	16.7	26.1	88.1	101.2	11.6	60	0.00
6/16/2001	36.1	22.2	29.4	88.2	101.2	14.7	120	0.00
6/17/2001	34.4	21.1	27.8	88.2	101.3	12.7	120	0.00
6/18/2001	35.6	22.2	28.9	87.9	101.0	14.3	140	0.00
6/19/2001	37.2	22.2	30.0	88.2	102.0	7.4	40	0.01
6/20/2001	36.1	20.6	28.3	88.1	101.2	10.5	30	0.00
6/21/2001	35.0	20.6	27.8	88.2	101.3	14.0	80	0.00
6/22/2001	35.0	21.7	28.3	88.2	101.3	11.6	40	0.00
6/23/2001	37.8	22.8	30.6	87.9	101.0	13.4	310	trace
6/24/2001	37.8	23.9	31.1	88.0	100.9	15.5	160	0.00
6/25/2001	36.1	19.4	27.8	88.0	101.0	14.7	150	0.04

Table 4.3. Daily meteorological conditions for each of the Roving Sands sampling days.

Figure 4.12. PM_{10} concentrations observed at the air quality monitoring sites during the Roving Sands exercise, June 13-25, 2001.

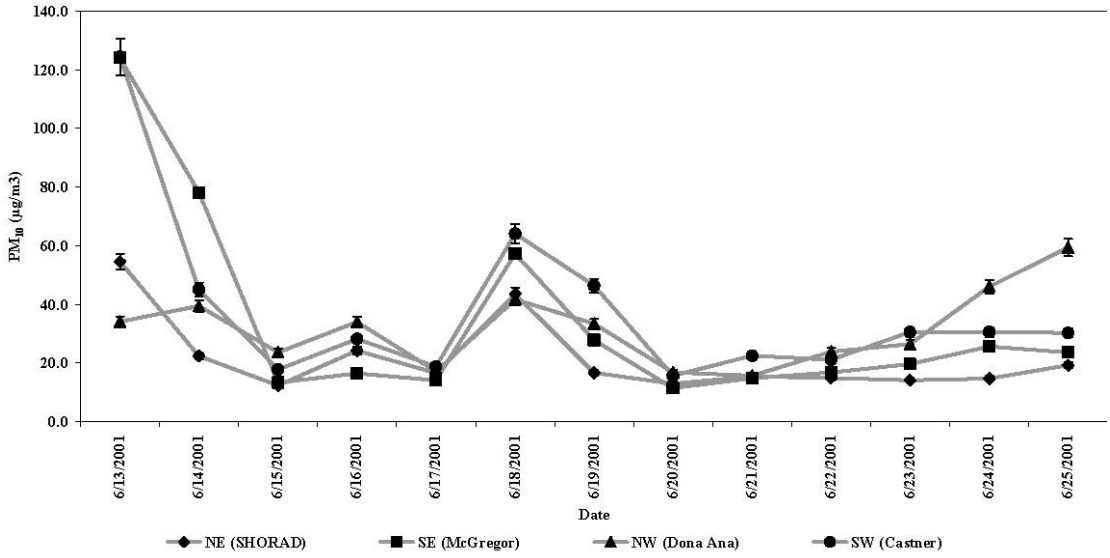

Figure 4.13. Observed differences in PM_{10} between the northern and southern air quality sites during Roving Sands.

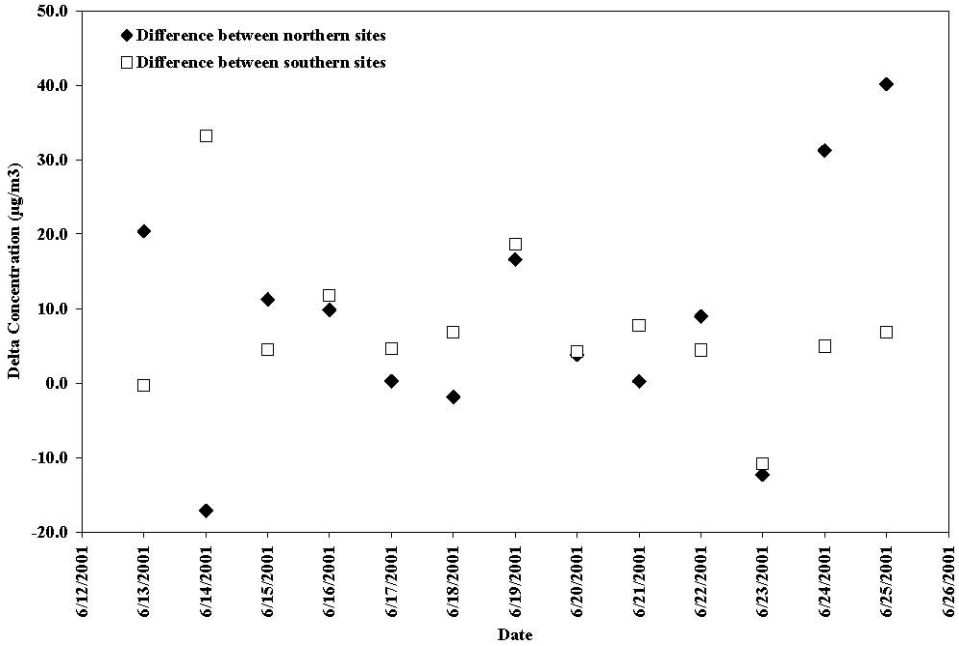

4.1.5 Chemical Mass Balance Receptor Modeling Application and Validation

The CMB receptor modeling was used to apportion PM and its chemical constituents to their sources (Watson et al., 1984). The CMB consists of a set of linear equations, which express the ambient concentrations of a chemical species as the sum of products of source contributions and source composition profiles. The CMB applications and validation protocol consists of six major steps (Pace and Watson, 1987). The activities carried out for each of these steps are described in the following sections.

For the chemical mass balance receptor modeling component of the study combustion profiles (vegetative burning and motor vehicles) from previous studies (Fujita et al., 1988) were used. Twenty two new fugitive dust source profiles from areas within New Mexico (Doña Ana CO.), west Texas (Ft. Bliss), Utah (Tooele Co., Grand Co., Garfield Co., and Dugway Proving Ground), and California (Ft. Irwin) were available to use in the CMB analysis for source attribution (Labban et al., 2003) (Table 4.4). The details of the fugitive dust sample locations, sampling procedures, sample preparation, and chemical characterization of the PM_{10} and $PM_{2.5}$ components are provided in (Labban et al., 2003). Briefly, ~5 kg of loose surface sediment was swept from unpaved roads and non-maintained vehicle trails at the sampling locations. These samples were subsequently air dried (~15% relative humidity, and 18° C) in the laboratory. Subsequent to drying the samples were mechanically dry-sieved to separate out the <38 µm fraction. A laboratory resuspension procedure (Chow et al., 1994) was then used to acquire PM_{10} and $PM_{2.5}$ particles from this size fraction. These samples were collected on Teflon-membrane, and quartz-fiber filters for chemical analysis.

CMB Model Applicability

The requirements for CMB model applicability are: 1) a sufficient number of receptor samples are taken with an accepted method to evaluate compliance with standards; 2) samples are analyzed for chemical species that are also present in source emissions; 3) potential source contributors have been identified and chemically characterized; and 4)

the number of non-collinear source types is less than the number of measured species. All of these criteria were met for the present study. Combinations of representative source profiles were used (Table 4.4). The profiles of the sulfate, nitrate, and sodium chloride were constructed based on their chemical formulas. The number of non-collinear source profiles is less than the number of measured species. Examination of the chemical profiles shows significant differences among profiles for major source types such as primary geological material, primary motor vehicle exhaust, and vegetative burning.

CMB Model Outputs and Performance Measures

Pace and Watson (1987) defined several performance measures that are examined with each CMB modeling run to eliminate source profile and species combinations from further consideration. The most important of these measures are: 1) the source contributions estimates and their uncertainties; 2) "CHI SQUARE," the weighted sum of the squares of the differences between calculated and measured species concentrations. Values between one and two indicate acceptable fits; values less than one indicate very good fit to the data; 3) "R SQUARE," the fraction of the variance in the measured concentrations accounted for by the variance in the calculated species concentrations. Values of "R SQUARE" greater than 0.9 indicate a good fit to the measured data; and 4) "PERCENT MASS," or the percent of total mass accounted for by the source contribution estimates. Values between 80% and 120% are considered to be acceptable.

Table 4.4. Source profiles and descriptions[1] used in the CMB modeling.

Mnemonic	Size Fraction	Description
AMBSUL	$PM_{2.5}$	Secondary ammonium bisulfate
AMNIT	$PM_{2.5}$	Secondary ammonium nitrate
NACL	$PM_{2.5}$	Sodium chloride
NWS	$PM_{2.5}$	Light-duty gasoline (Fujita et al., 1998)
NWHDc	$PM_{2.5}$	Heavy-duty diesel (Fujita et al., 1998)
NWSHc2	$PM_{2.5}$	Wood stove burning hardwood (Fujita et al., 1998)
FTBW01	PM_{10}	Ft. Bliss, TX, west fence area in the pass between two mountain ranges on the base boundary with urban areas to the west.
FTBM01	PM_{10}	Ft. Bliss, TX, main supply road used during training exercises
FTBR01	PM_{10}	Ft. Bliss, TX, higher elevation area in the foothills.
NMST01	PM_{10}	New Mexico samples west of Ft Bliss. Composite of unpaved parking lot and unpaved road material.
FTBD01	PM_{10}	Ft. Bliss, TX, driving training range, similar to main supply road (i.e., RS611)
FTBTS02	PM_{10}	Ft. Bliss, TX, unpaved road used for dust emissions testing, prior to testing (Gillies et al., 2002)
FTBTE02	PM_{10}	Ft. Bliss, TX, unpaved road used for dust emissions testing, post testing (Gillies et al., 2002).
FTBM02	PM_{10}	Same as FTBM01 sampled one year later.
FTBW02	PM_{10}	Same as FTBW01 sampled one year later.

FTBR02	PM_{10}	Same as FTBR01 sampled one year later.
NMWM02	PM_{10}	NM, West Mesa composite, unpaved road.
NMAC02	PM_{10}	NM-Achenbach, native soil, test road
UTWD02	PM_{10}	Dugway, UT West Desert -Pony Express route, sand and gravel soil in foothill area.
UTMC02	PM_{10}	Canyonlands, UT, Mancos Clay, shale soil that erodes to form large areas of clay hills north of Arches, UT.
FILZ02	PM_{10}	Ft. Irwin, CA, Langord Impact Zone, active training site with loamy sand with gravel soils.
FIWV02	PM_{10}	Ft. Irwin, CA, John Wayne Hill -V.Heavy, active training site with loamy sand with gravel soils.
FIWH02	PM_{10}	Ft. Irwin, CA, John Wayne Hill - Heavy, active training site with loamy sand with gravel soils.
UTFL02	PM_{10}	Auora, UT, feed lot, roadside material from a valley bottom agricultural area adjacent to animal feed lots.
UTDG02	PM_{10}	Dugway Proving Grounds UT, Dugway Test Road, fine silty soil collected from soft areas in the road.

[1] Complete descriptions of all the fugitive dust profiles (indicated by shading) are presented in Labban et al. (2003).

Initial Source Contribution Estimates

Initial tests with different combinations of PM_{10} source profiles were done to determine which profiles best explain the ambient data and the robustness of the results with respect to the choice of source profiles. Examples of the results of the source apportionment sensitivity test for the averages of the four locations are presented as a series of trials representing different combinations of source profiles in Table 4.5. Determining which profile combination represents realistic apportionment is based on R^2, Chi^2, and percent calculated mass.

Deviations from Model Assumptions

One of the most important assumptions of the CMB model is that the source profiles are linearly independent (i.e., they are statistically different) (Watson et al., 1984). The degree to which this assumption can be met in practice depends to a large extent on the types and quality of chemical measurements made at the sources and receptor. Source profiles that are not statistically different are called collinear. The collinearity tends to inflate the variances of the source contribution estimates (Lowenthal et al., 1992). The sensitivity analysis did not indicate any significant collinearity problem.

4.1.6 Source Apportionment Results

Based on the initial CMB test results, the profile combination that fit the ambient $PM_{2.5}$ data best at a specific certain location was used to PM_{10} at all locations. The CMB results are summarized in Table 4.6. The CMB model diagnostics are quite good. R^2 was between 0.85 and 0.95 for all samples. On average, the calculated mass was within 10% of the measured mass. Chi-square varied from 0.57 to 2.76.

Major PM_{10} sources were road dust (a%), vegetative burning (b%), ammonium sulfate (or bisulfate) (c%), ammonium nitrate (d%), and sodium chloride (e%). Vehicle exhaust particles were not observed at any location. This could be due to the fact that three out of four locations were very far from any mobile sources activities. Another reason for not identifying motor vehicles contribution is that the elemental carbon (a tracer for combustion sources) uncertain, as a result the CMB failed to account for motor vehicles. The vegetative burning sources have another important tracer (soluble potassium) in addition to the carbon that is why it was identified.

Comparison with other studies

The sixth step of the CMB application and validation protocol according to Pace and Watson (1987) is evaluation of the results of the CMB analysis with respect to other source attribution methods. For this purpose we determined the mass contribution from the major categories using the Material Balance (MB) method (Solomon et al., 1989). The results are shown in Table 4.7. An examination of the results from Tables 4.6 and 4.7 shows there is an excellent agreement between the two approaches. The MB method does not split the combustion sources into motor vehicles and vegetative burning because it depends only on the concentration of the carbon, which comes from the two sources.

4.1.7 Ambient Monitoring, Source Apportionment Conclusions

The ambient air quality and source apportionment study undertaken at Ft. Bliss indicated

that this methodological approach could be used to identify particulate matter that was being contributed to regional levels by emissions from within the post. In the case of Ft. Bliss, when

Table 4.5. Example of the CMB source profiles sensitivity test results for the averages of all locations.

	NE Average				NW Average				
Source	TRIAL 1	TRIAL 2	TRIAL 3	TRIAL 4	TRIAL 1	TRIAL 2	TRIAL 3	TRIAL 4	TRIAL 5
AMBSUL	2.2	2.2	2.2	2.2	2.1	2.1	2.1	2.1	2.2
AMNIT	0.9	0.9	0.9	0.9	1	1	1	1	1
NACL	0.4	0.4	0.4	0.4	0.5	0.5	0.5	0.5	0.5
NWHDc	-----	-----	-----	-----	-----	-----	-----	0.3*	
NWS	-----	1.8	1.7	1.4	-----	2	-----	-----	1.9
NWSHc2	1.5	-----	-----	-----	-----	-----	1.5	-----	-----
FTBW01	18.6	18.1	-----	-----	25.4	23.7	24.7	25.2	
FTBD01	-----	-----	18.9	-----	-----	-----	-----	-----	24.2
FTBTS02	-----	-----	-----	19.8	-----	-----	-----	-----	-----
R^2	0.94	0.94	0.89	0.93	0.89	0.91	0.9	0.89	0.85
CHI^2	0.88	0.81	1.93	1.28	1.65	1.24	1.55	1.67	2.66
M%	109	108	112	114	117	118	120	118	120
	SE Average				SW Average				
Source	TRIAL 1	TRIAL 2	TRIAL 3	TRIAL 4	TRIAL 1	TRIAL 2	TRIAL 3	TRIAL 4	TRIAL 5
AMBSUL	1.9	1.8	1.8	1.9	2.2	2.2	2.2	2.3	2.2
AMNIT	1	1	1	1	1.1	1.1	1.1	1.1	1.1
NACL	0.4	0.4	0.4	0.4	0.5	0.5	0.5	0.6	0.6
NWHDC	-----	-----	-----	-----	-----	-----	-----	-----	-----
NWS	-----	2.9	-----	2.8	2.4	-----	-----	2.7	1.8
NWSHc2	-----	-----	2.6	-----	-----	-----	2	-----	-----
FTBW01	32.3	30.1	31.4	-----	38.4	42.4	41.4	-----	-----
FTBD01	-----	-----	-----	33.1	-----	-----	-----	40.8	-----
FTBTS02	-----	-----	-----	-----	-----	-----	-----	-----	42.7
R^2	0.94	0.96	0.96	0.94	0.95	0.92	0.93	0.84	0.9
CHI^2	0.66	0.47	0.49	0.77	0.64	1.1	0.98	2.87	1.94
M%	110	115	115	121	118	122	125	125	128

Table 4.6. Source apportionment results and associated uncertainties for ambient samples ($\mu g/m^3$) using the chemical mass balance receptor modeling approach.

Site	Date	Sulfate	Nitrate	Sodium Chloride	Vegetative	Geological
NE	6/13/2001	1.33 ± 0.11	0.92 ± 0.11	0.91 ± 0.12	0.96 ± 1.02	44.21 ± 2.96
NW	6/13/2001	1.39 ± 0.11	0.59 ± 0.08	0.81 ± 0.11	1.39 ± 0.78	30.68 ± 2.06
SE	6/13/2001	1.19 ± 0.17	1.25 ± 0.24	1.06 ± 0.22	0.65 ± 3.07	##### ± 8.35
SW	6/13/2001	1.09 ± 0.15	1.12 ± 0.20	1.29 ± 0.22	0.00 ± 0.00	##### ± 7.62
NW	6/17/2001	2.18 ± 0.15	0.86 ± 0.10	0.72 ± 0.09	1.86 ± 0.55	12.47 ± 0.95
SE	6/17/2001	2.06 ± 0.16	0.98 ± 0.15	0.44 ± 0.04	2.80 ± 1.16	10.60 ± 1.03
NE	6/21/2001	3.19 ± 0.23	1.25 ± 0.14	0.02 ± 0.05	2.04 ± 0.55	10.25 ± 0.80
NW	6/21/2001	2.86 ± 0.20	1.03 ± 0.13	0.69 ± 0.08	2.12 ± 0.69	10.86 ± 0.93
SE	6/21/2001	2.97 ± 0.21	1.21 ± 0.16	0.45 ± 0.04	1.74 ± 1.04	10.51 ± 0.78
SW	6/21/2001	4.58 ± 0.32	1.11 ± 0.13	0.84 ± 0.10	1.99 ± 0.58	13.77 ± 1.15
NE	6/22/2001	2.95 ± 0.21	0.77 ± 0.09	0.05 ± 0.03	2.45 ± 0.60	10.37 ± 0.83
NW	6/22/2001	4.48 ± 0.31	0.86 ± 0.10	0.81 ± 0.09	2.66 ± 0.68	13.81 ± 1.10
SE	6/22/2001	2.47 ± 0.18	0.91 ± 0.15	0.26 ± 0.03	3.97 ± 1.37	10.91 ± 1.12
SW	6/22/2001	3.44 ± 0.24	0.94 ± 0.11	0.31 ± 0.04	2.80 ± 0.68	12.91 ± 1.09
NE	7/6/2001	1.94 ± 0.14	0.62 ± 0.08	0.11 ± 0.03	2.06 ± 0.73	20.92 ± 1.46
SW	7/6/2001	1.18 ± 0.09	0.46 ± 0.06	0.08 ± 0.03	2.90 ± 0.80	19.67 ± 1.42
NE	7/30/2001	2.66 ± 0.18	0.15 ± 0.04	0.04 ± 0.01	2.13 ± 0.52	4.08 ± 0.42
NW	7/30/2001	2.61 ± 0.17	0.18 ± 0.04	0.04 ± 0.02	1.56 ± 0.51	20.81 ± 1.38
SE	7/30/2001	2.41 ± 0.16	0.16 ± 0.04	0.05 ± 0.01	2.94 ± 0.66	2.40 ± 0.31
SW	7/30/2001	2.32 ± 0.16	0.12 ± 0.04	0.04 ± 0.01	1.88 ± 0.37	3.75 ± 0.41
NE	1/26/2002	1.31 ± 0.10	0.84 ± 0.10	0.22 ± 0.03	1.42 ± 0.44	7.90 ± 0.65
NW	1/26/2002	1.46 ± 0.16	1.88 ± 0.18	0.22 ± 0.03	1.49 ± 0.53	24.94 ± 1.57
SE	1/26/2002	1.42 ± 0.11	1.32 ± 0.14	0.14 ± 0.02	3.77 ± 0.85	11.07 ± 0.94
SW	1/26/2002	2.06 ± 0.16	2.53 ± 0.26	0.02 ± 0.03	6.51 ± 1.36	15.98 ± 1.34
NW	2/13/2002	0.74 ± 0.06	0.94 ± 0.09	0.09 ± 0.01	1.06 ± 0.40	13.28 ± 0.93
SE	2/13/2002	0.81 ± 0.07	0.65 ± 0.08	0.07 ± 0.02	2.41 ± 0.67	13.91 ± 1.05
NE	3/15/2002	2.16 ± 0.16	1.52 ± 0.17	1.40 ± 0.17	0.00 ± 0.00	33.91 ± 1.67
NW	3/15/2002	1.86 ± 0.15	1.43 ± 0.16	1.29 ± 0.14	1.65 ± 0.95	38.15 ± 2.56
SE	3/15/2002	1.88 ± 0.15	1.39 ± 0.15	1.10 ± 0.12	0.00 ± 0.00	33.76 ± 1.83
SW	3/15/2002	1.98 ± 0.16	1.62 ± 0.18	1.77 ± 0.21	3.10 ± 1.12	39.45 ± 2.94
NE	3/21/2002	2.43 ± 0.17	0.90 ± 0.11	0.14 ± 0.03	1.50 ± 0.49	11.43 ± 0.88
NW	3/21/2002	2.07 ± 0.17	1.51 ± 0.16	0.17 ± 0.06	1.86 ± 1.04	41.48 ± 2.68
SE	3/21/2002	2.05 ± 0.17	1.36 ± 0.16	0.17 ± 0.07	2.70 ± 1.37	54.69 ± 3.61
SW	3/21/2002	1.98 ± 0.17	1.30 ± 0.16	0.58 ± 0.11	2.22 ± 1.42	59.78 ± 4.36
NE	3/27/2002	1.65 ± 0.12	0.54 ± 0.08	0.25 ± 0.04	1.36 ± 0.60	11.85 ± 0.99
NW	3/27/2002	1.07 ± 0.09	0.35 ± 0.07	0.16 ± 0.02	2.19 ± 0.75	7.02 ± 0.56
SE	3/27/2002	1.46 ± 0.12	0.49 ± 0.08	0.15 ± 0.03	3.71 ± 1.05	14.50 ± 1.23

Table 4.7. Source apportionment results uncertainties for ambient samples ($\mu g/m^3$) using Material Balance method.

SITE	DATE	Sulfate	Nitrate	Combustion	Geological
NE	6/13/2001	2.00 ± 0.10	0.94 ± 0.06	3.33 ± 0.26	48.00 ± 5.36
NW	6/13/2001	1.59 ± 0.09	0.67 ± 0.05	2.78 ± 0.23	28.15 ± 3.18
SE	6/13/2001	2.22 ± 0.13	1.30 ± 0.12	8.62 ± 0.82	152.19 ± 16.98
SW	6/13/2001	2.32 ± 0.12	1.15 ± 0.07	5.31 ± 0.35	116.94 ± 14.22
NW	6/17/2001	2.67 ± 0.14	0.94 ± 0.06	2.46 ± 0.22	11.84 ± 1.29
SE	6/17/2001	2.44 ± 0.13	1.01 ± 0.12	3.80 ± 0.65	9.22 ± 1.02
NE	6/21/2001	3.96 ± 0.20	1.28 ± 0.07	2.59 ± 0.22	8.92 ± 0.90
NW	6/21/2001	3.35 ± 0.18	1.13 ± 0.08	2.74 ± 0.32	9.77 ± 1.03
SE	6/21/2001	3.36 ± 0.13	1.25 ± 0.12	3.08 ± 0.63	10.15 ± 1.10
SW	6/21/2001	5.95 ± 0.30	1.22 ± 0.07	2.69 ± 0.22	13.84 ± 1.30
NE	6/22/2001	3.41 ± 0.17	0.78 ± 0.05	2.88 ± 0.23	8.31 ± 0.83
NW	6/22/2001	5.82 ± 0.29	0.94 ± 0.06	3.48 ± 0.28	13.78 ± 1.31
SE	6/22/2001	2.93 ± 0.14	0.93 ± 0.13	5.08 ± 0.71	10.50 ± 1.06
SW	6/22/2001	4.08 ± 0.21	1.00 ± 0.06	3.37 ± 0.24	12.48 ± 1.21
NE	7/6/2001	2.22 ± 0.12	0.59 ± 0.04	3.31 ± 0.30	19.28 ± 2.08
SW	7/6/2001	1.49 ± 0.08	0.45 ± 0.04	4.09 ± 0.29	19.24 ± 2.14
NE	7/30/2001	2.49 ± 0.13	0.16 ± 0.03	2.52 ± 0.22	3.50 ± 0.37
NW	7/30/2001	2.54 ± 0.13	0.19 ± 0.03	2.79 ± 0.23	18.29 ± 1.98
SE	7/30/2001	2.66 ± 0.14	0.17 ± 0.03	3.27 ± 0.25	2.99 ± 0.31
SW	7/30/2001	2.21 ± 0.12	0.13 ± 0.03	3.01 ± 0.26	2.77 ± 0.31
NE	1/26/2002	1.45 ± 0.08	0.96 ± 0.06	1.92 ± 0.20	7.55 ± 0.77
NW	1/26/2002	1.82 ± 0.10	2.08 ± 0.11	2.98 ± 0.23	20.67 ± 2.15
SE	1/26/2002	1.67 ± 0.09	1.48 ± 0.08	4.77 ± 0.30	11.82 ± 1.12
SW	1/26/2002	2.66 ± 0.14	2.94 ± 0.16	7.42 ± 0.40	15.34 ± 1.45
NW	2/13/2002	0.96 ± 0.06	0.92 ± 0.06	1.90 ± 0.21	13.67 ± 1.59
SE	2/13/2002	1.00 ± 0.06	0.71 ± 0.05	3.17 ± 0.27	15.14 ± 1.75
NE	3/15/2002	2.90 ± 0.15	1.83 ± 0.10	3.36 ± 0.26	28.25 ± 3.11
NW	3/15/2002	2.80 ± 0.14	1.78 ± 0.10	3.61 ± 0.26	27.86 ± 2.99
SE	3/15/2002	2.71 ± 0.14	1.71 ± 0.09	4.39 ± 0.30	29.25 ± 3.20
SW	3/15/2002	3.06 ± 0.16	2.07 ± 0.11	5.08 ± 0.31	31.46 ± 3.34
NE	3/21/2002	2.72 ± 0.14	0.98 ± 0.06	2.13 ± 0.20	9.64 ± 0.99
NW	3/21/2002	2.69 ± 0.14	1.48 ± 0.08	4.01 ± 0.31	35.66 ± 3.76
SE	3/21/2002	2.86 ± 0.15	1.48 ± 0.08	5.80 ± 0.36	44.84 ± 4.43
SW	3/21/2002	2.82 ± 0.15	1.41 ± 0.08	5.45 ± 0.35	53.25 ± 5.50
NE	3/27/2002	1.96 ± 0.12	0.60 ± 0.06	1.92 ± 0.31	9.94 ± 1.07
NW	3/27/2002	1.36 ± 0.10	0.32 ± 0.07	3.20 ± 0.39	7.13 ± 0.81
SE	3/27/2002	1.73 ± 0.11	0.51 ± 0.07	4.71 ± 0.46	12.94 ± 1.34
SW	3/27/2002	1.41 ± 0.11	0.36 ± 0.08	3.97 ± 0.48	5.70 ± 0.62

in-post generated PM_{10} could be distinguished it was in all cases fugitive dust. No emissions from combustion sources originating from within Ft. Bliss could be resolved by the CMB analysis. This component of the study indicated however, that in-post contributions to regional levels were only observed to occur under a limited range of environmental conditions, specifically elevated wind events that caused regional scale

emissions due to wind erosion and the associated emissions of dust. Fugitive emissions attributable to military activity were not observed to contribute at measurable levels. These types of emissions may result in high local levels, as was measured during vehicle emission tests, but they could not be resolved as contributions on a regional level.

4.2 Vehicle Generated Emission Factor Measurements, Horizontal/Vertical Flux Relationships.

The results of this experiment are detailed in several publications (Gillies et al., in press; Gillies et al., 2003) and are briefly re-iterated here.

Most unpaved roads consist of a graded and compacted roadbed usually created from the parent soil-material. The rolling wheels of the vehicles impart a force to the surface that pulverizes the roadbed material and ejects particles from the shearing force as well as by the turbulent vehicle wakes (Nicholson et al., 1989). Studies have found that dust emission rates depend on the fine particle content of the road (Cowherd, 1999; MRI, 2001), soil moisture content, vehicle speed (Nicholson et al., 1989), and vehicle weight (U.S. EPA, 1996; MRI, 2001).

Part of this study was to understand the contributions of military testing and training activities to regional particulate matter in the western U.S. (Gillies et al., 2001, 2002, 2003b). As a component of this part of the study unpaved road dust emissions from wheeled vehicles were measured and their wakes and dust injection heights were characterized. These tests were carried out at Ft. Bliss, TX. A mix of civilian and military vehicles covering a substantial range of weights, length and width dimensions, and number of wheels were used to understand how these properties relate to emissions of dust, specifically the PM_{10} component.

As part of CP-1191 PM_{10} fugitive dust emission factors for a range of vehicles types were developed and the influence of vehicle and wake characteristics on the strength of emissions from an unpaved road were examined. Vertical profile measurements of mass concentration of the passing plumes were carried out using a series of 3 instrumented towers (Fig. 3.2). PM_{10} emission fluxes at each tower were calculated from knowledge of the vertical mass concentration profile, the ambient wind speed and direction, and the time the plume took to pass the towers. The emission factors showed a strong linear dependence on speed and vehicle weight. Emission factors (EF=grams of PM_{10} emitted per vehicle kilometer traveled) ranged from approximately $EF=0.8\times(km\ hr^{-1})$ for a light (~1,200 kg) passenger car to $EF=48\times(km\ hr^{-1})$ for large military vehicles (~18,000 kg) (Figures 4.14 and 4.15). This suggests that emissions are linearly dependent on a vehicle's momentum (Fig. 4.16). Other physical characteristics of the vehicles (e.g., # wheels, undercarriage, area, height) did not appear to heavily influence the emissions. In comparison to emission estimates derived using U.S. EPA AP-42 (U.S. EPA, 1996, 1999) methods the measured emission factors indicate larger than estimated contributions for speeds generally > 10-20 km hr^{-1} and for vehicle weights > 3,000 kg. The size of a wake created by a vehicle was observed to be dependent on the size of the vehicle, increasing

roughly linearly with vehicle height. Injection height of the dust plume is least important to long-range transport of PM_{10} under unstable conditions and most important under stable atmospheric conditions.

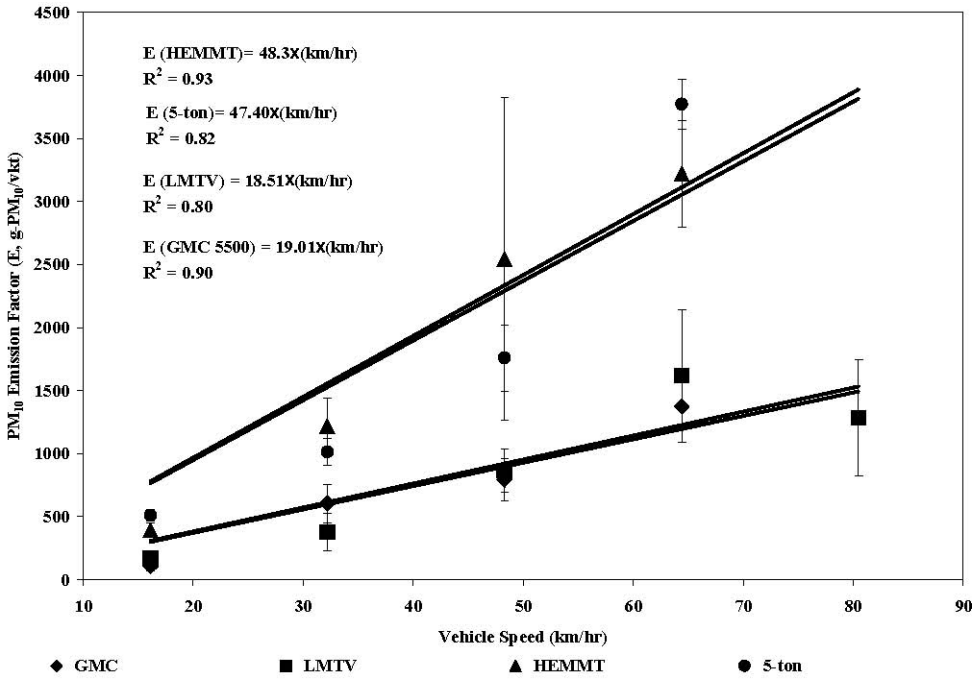

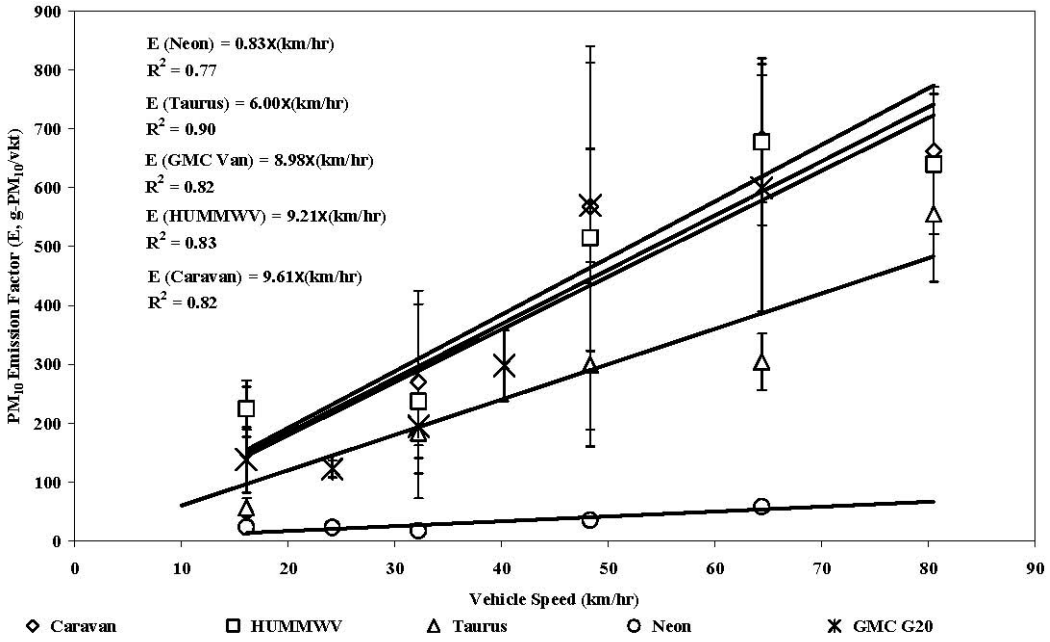

Figure 4.14. Emission factors as a function of speed for vehicles <4,000 kg. Error bars represent the standard deviation of the mean value for that speed based on multiple vehicle passes, and for all three towers combined.

Figure 4.15. Emission factors as a function of speed for vehicles >4,000 kg. Error bars represent the standard deviation of the mean value for that speed based on multiple vehicle passes, and for all three towers combined. i(i()i()i(

Figure 4.16. Vehicle emissions of dust characterized as a function of the product of vehicle speed and mass.

4.3 The Transportable Fraction of Emitted Dust

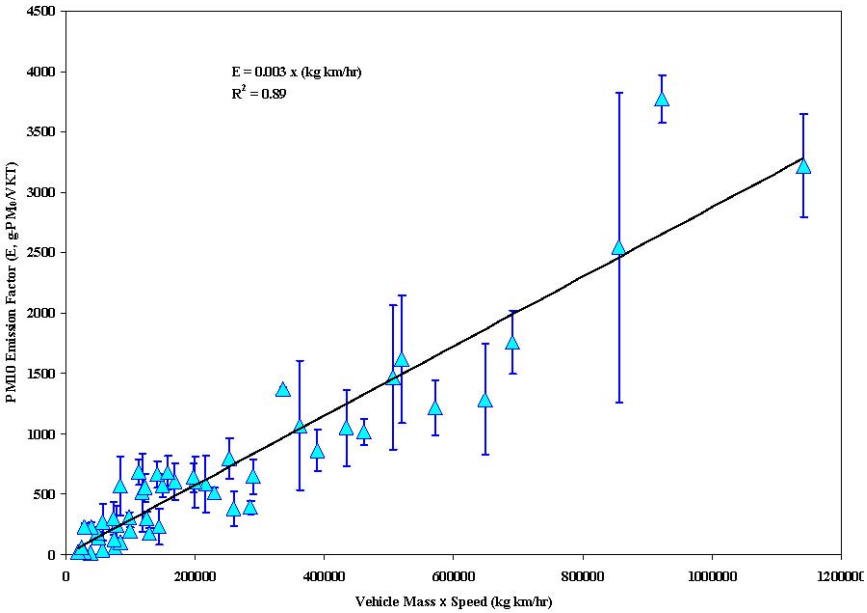

The results of this experiment are detailed in several publications (Etyemezian et al.,

2003c, Etyemezian et al., 2003d; Etyemezian et al., 2004) and are briefly re-iterated here.

Fugitive dust is emitted from an unpaved road when a vehicle passes and disturbs the surface, raising a cloud of dust that begins to travel downwind. Initially, the cloud is dense but with travel downwind, the cloud is dispersed by turbulent eddies in the atmosphere. Particles suspended in the cloud can be removed by interaction with the ground surface, terrain anomalies (i.e., buildings, boulders, etc.), or vegetative cover in the downwind fetch of the unpaved road.

Watson and Chow (2000) documented the discrepancy between emission inventories for PM_{10} fugitive dust and the source attribution of ambient filter samples. Their analysis indicated that the amount of geologically-derived PM_{10} found in the air is smaller than would be expected based on the emission inventories and dispersion models. Countess (2001) summarized eleven shortcomings in the current treatment of fugitive dust emissions. One of the recommendations made by Countess (2001) was to upgrade existing models with "sub-models" to account for the removal of particles near the source. Based on the analysis of PM_{10} concentrations downwind of an unpaved road Watson and Chow (2000) hypothesized that coarse particles in the PM_{10} range deposit rapidly within the first several hundred meters downwind of the road. That analysis did not consider the vertical dispersion of PM with distance downwind, resulting in a great overestimate of the effect of near-source deposition.

This work was motivated by the need to better reconcile emission factors for fugitive dust with the amount of geologic material found on ambient filter samples. The deposition of PM_{10} (particulate matter with aerodynamic diameter less than or equal to 10 μm), generated by travel over an unpaved road, over the first 100 m of transport downwind of the road was examined at Ft Bliss, near El Paso, TX. The field conditions, typical for warm days in the arid southwestern United States, represented sparsely-vegetated terrain under neutral-unstable atmospheric conditions. Emission fluxes of PM_{10} dust were obtained using towers downwind of the unpaved road at 7, 50, and 100 m. The horizontal flux measurements at the 7 m and 100 m tower indicated that PM_{10} deposition to the vegetation and ground was too small to measure. These data indicated, with 95% confidence, that the loss of PM_{10} between the source of emission at the unpaved road, represented by the 7 m tower, and a point 100 m downwind was less than 9.5%.

A Gaussian model was used to simulate the plume. Values of the vertical standard deviation σ_z and the deposition velocity V_d were similar to the U.S. EPA (1995) ISC3 model. For the field conditions, the model predicted that removal of PM_{10} unpaved road dust by deposition over the distance between the point of emission and 100 m downwind would be less than 5 percent. However, the model results also indicated that particles larger than 10 microns (aerodynamic diameter) would deposit more appreciably. The model was consistent with changes observed in size distributions between 7 m and 100 m downwind that were measured with optical particle counters.

The Gaussian model predictions were also compared to another study conducted over

rough terrain and stable atmospheric conditions (Veranth et al., 2003). Under such conditions measured PM_{10} removal rates over 95 m of downwind transport were reported to be between 86% and 89%, while the Gaussian model predicted only a 30% removal. One explanation for the large discrepancy between measurements and model results was the possibility that under the conditions of the study, the dust plume was comparable in vertical extent to the roughness elements, thereby violating one of the model assumptions.

Results of the field study reported here and the previous work over rough terrain bound the extent of particle deposition expected to occur under most unpaved road emission scenarios.

4.4 TRAKER

The results of this component of CP-1191 are detailed in several publications (Etyemezian et al., 2003b, Etyemezian et al., 2003c; Kuhns et al., 2005) and are briefly re-iterated here.

4.4.1 TRAKER: Methods and Calibration

Testing re-entrained aerosol kinetic emissions from roads (TRAKER) is a vehicle-based method for measuring road dust emissions. Particulate matter is sampled in front and behind a vehicle's tire and the difference in PM concentration is related to emissions (Fig. 4.17). In the calibration phase of TRAKER and its particulate sampling system it was observed that the losses of particles to the walls in the inlet lines were similar for the left and right inlets and were less than the inter-instrument precision for particles between 0.56 and 7.3 mm in diameter. Indicating these losses are relatively small and do not compromise the measurement quality. When summed over the PM_{10} size range, losses were less than 20%. Line losses were also characterized when a dilution system was used to sample emissions from unpaved roads. Two independent tests indicated that the TRAKER signal increases as the cube of the speed for a given road dust loading. Simultaneous measurement of PM_{10} dust emitted behind the tires by TRAKER with PM_{10} flux measured using upwind/downwind towers suggested that the emission factor for road dust was proportional to the cube root of the TRAKER signal (Fig. 4.18). The results also showed a linear relationship between unpaved road dust PM_{10} emissions and vehicle speed. The TRAKER has been calibrated over a small range of conditions—unpaved road, 5–20 km/h, neutral to slightly unstable conditions, and open desert topography. Further development of the measurement

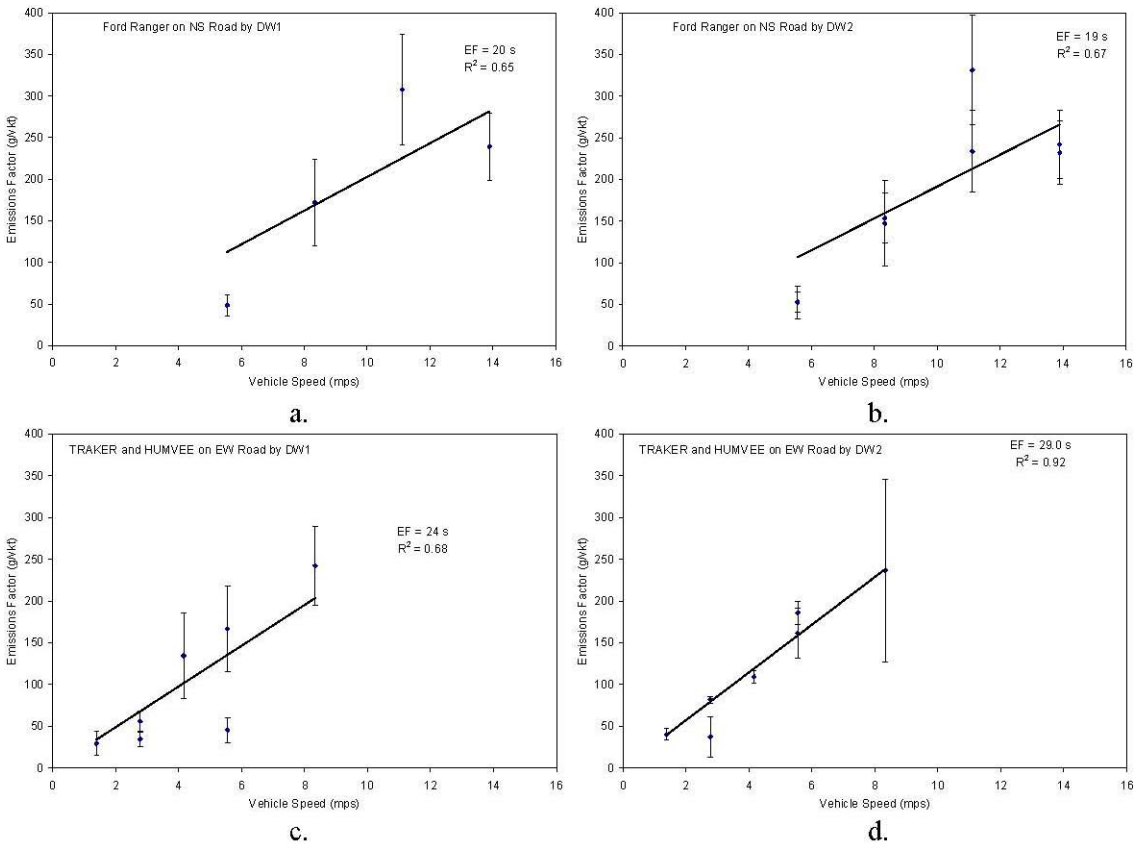

classes of vehicles. The Ford Ranger weighs ~1.5 Mg while the TRAKER and HUMVEE weigh ~3.5 Mg. The vertical bars are standard errors. Data from the 5/18/01 TRAKER runs are not shown due to a limited range of speeds; a. Ford Ranger on North-South road vs. DT_1; b. Ford Ranger on North-South road vs. DT_2; c. TRAKER and HUMVEE on East-West road vs. DT_1; d. TRAKER and HUMVEE on East-West road vs. DT_2.

Figure 4.18. Relationship between unpaved road dust PM_{10} emission factors and the TRAKER signal from Ft. Bliss. The error bars on the figure are the standard errors of the mean of each measurement.

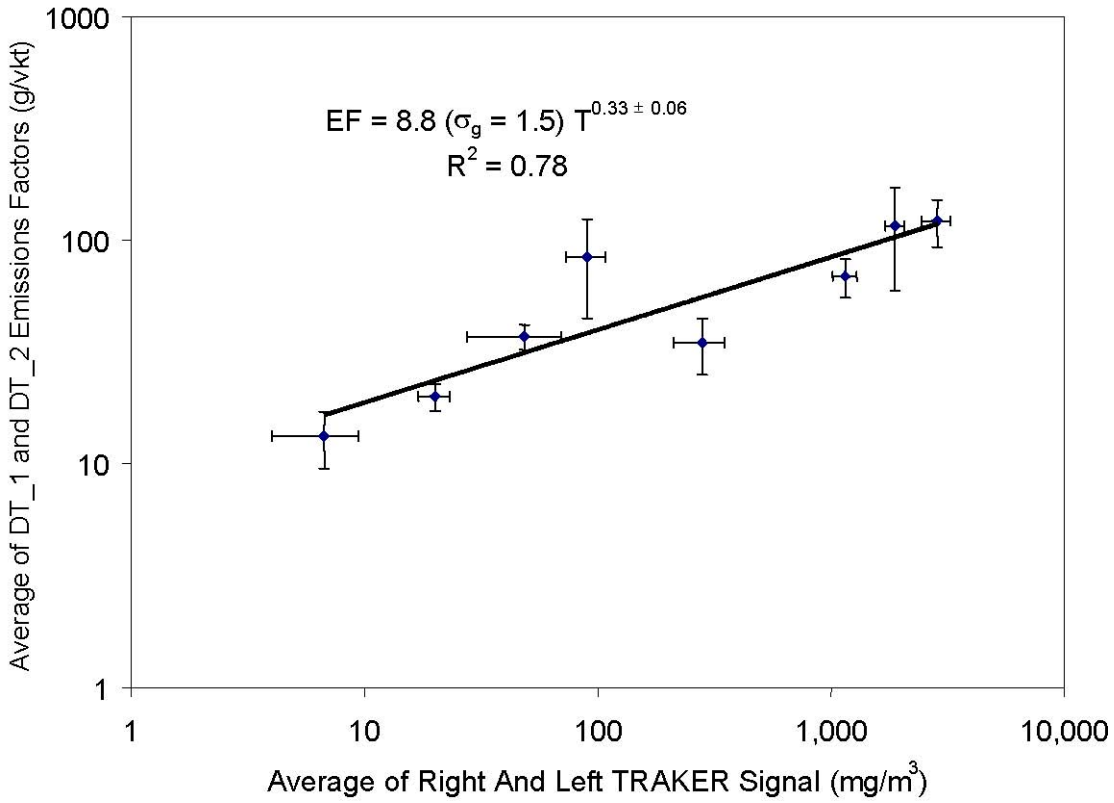

method also requires a better understanding of how ambient winds affect the concentration of PM_{10} dust behind the tires.

4.4.2 TRAKER-Evaluated Spatial Variability of Unpaved Road Dust PM_{10} Emission Factors near El Paso, TX

The TRAKER system was used to measure the emission potential of unpaved roads on the Ft. Bliss military base. Measurements from this vehicle were calibrated with the downwind flux of PM_{10} measured on instrumented towers. The calibration was used to infer the emission potential on 72 km of unpaved roads near El Paso, TX. When measured emission potential was compared with visual attributes of the road, roads surfaced with gravel had only slightly lower emission potentials than roads that were predominantly sand.

Some spatial patterns were observed in the unpaved emission potentials; however the range of emission potentials across the base was generally narrow (Fig. 4.19). Sixty percent of all measurements fell between 6.7 [g/VKT]/[m/sec] and 9.6 [g/VKT]/[m/sec]. Five different soil types were sampled with the TRAKER vehicle at Ft. Bliss. When the emission potentials were compared with the soil survey database, unpaved roads surfaces with the highest wind erodibility index also had the highest road dust emission potentials. Additional TRAKER survey datasets spanning a more diverse range of soils are needed to definitively link road dust emission potentials to surface soil composition and derived wind erodibility indices.

4.4.3 TRAKER Spatial Variability Data for Reno, NV

A second set of TRAKER emission potential data was collected near Reno, NV, in August 2004, for purposes of comparison with the Ft. Bliss data set. The objective of the comparison was to evaluate how the measured emission potential may change between disparate geographic locations with different soil types. The emission potential of the unpaved roads as a function of location in the Reno TRAKER data is shown in Fig. 4.20. The range of the emission potential for all the unpaved roads in the Reno survey is 0.3 to 28.4 [g/VKT]/[m/sec] with an average value of 8.3 (±4.8) [g/VKT]/[m/sec]. A frequency distribution of the percent occurrence of emission potential in 5 unit increments is shown in Fig. 4.21. Approximately 50% of the emission potential values lie within 0.3 and 5 [g/VKT]/[m/sec], with 54% between 10 and 15 [g/VKT]/[m/sec]. Approximately 90% of the values are ≤20 [g/VKT]/[m/sec].

The average Reno unpaved road emission potential value (8.3 [g/VKT]/[m/sec]) and the range within most emissions occur (10-15 [g/VKT]/[m/sec]) are very similar to the values observed for the general Ft. Bliss data (8 [g/VKT]/[m/sec]) as well as the Ft. Bliss test road (~14 [g/VKT]/[m/sec]). These average values suggest that it is not unreasonable to treat unpaved roads as having similar dust emission potential regardless of their location and the parent material that underlies them. The data comparing emission potential as function of Wind Erodibility Group does suggest however, that a more refined relationship can be used to increase the accuracy of the emission potential attributable to an unpaved road. As was done for the Ft. Bliss data set the emission potential of the Reno data set was compared to the Wind Erodibility Index to examine if the relationship observed in the Ft. Bliss data held for the Reno data. Both the Reno and Ft. Bliss data are shown together in Fig. 4.22. Although there is more scatter in the Reno than Ft. Bliss data, the trend is consistent. This suggests that the WEI of the soil type on which a road is found could be used to assign an emission potential to that road.

Figure 4.19. Map of unpaved roads survedy by TRAKER at the Ft. Bliss Military Base near El Paso Texas. The multishaded line represents the TRAKER emission potentials (g/VKT)/(m/sec). The irregular shapes represent regions of different soil types on the military base. The data intervals of emission potentiles correspond to the quintile ranges of the 72 km dataset.

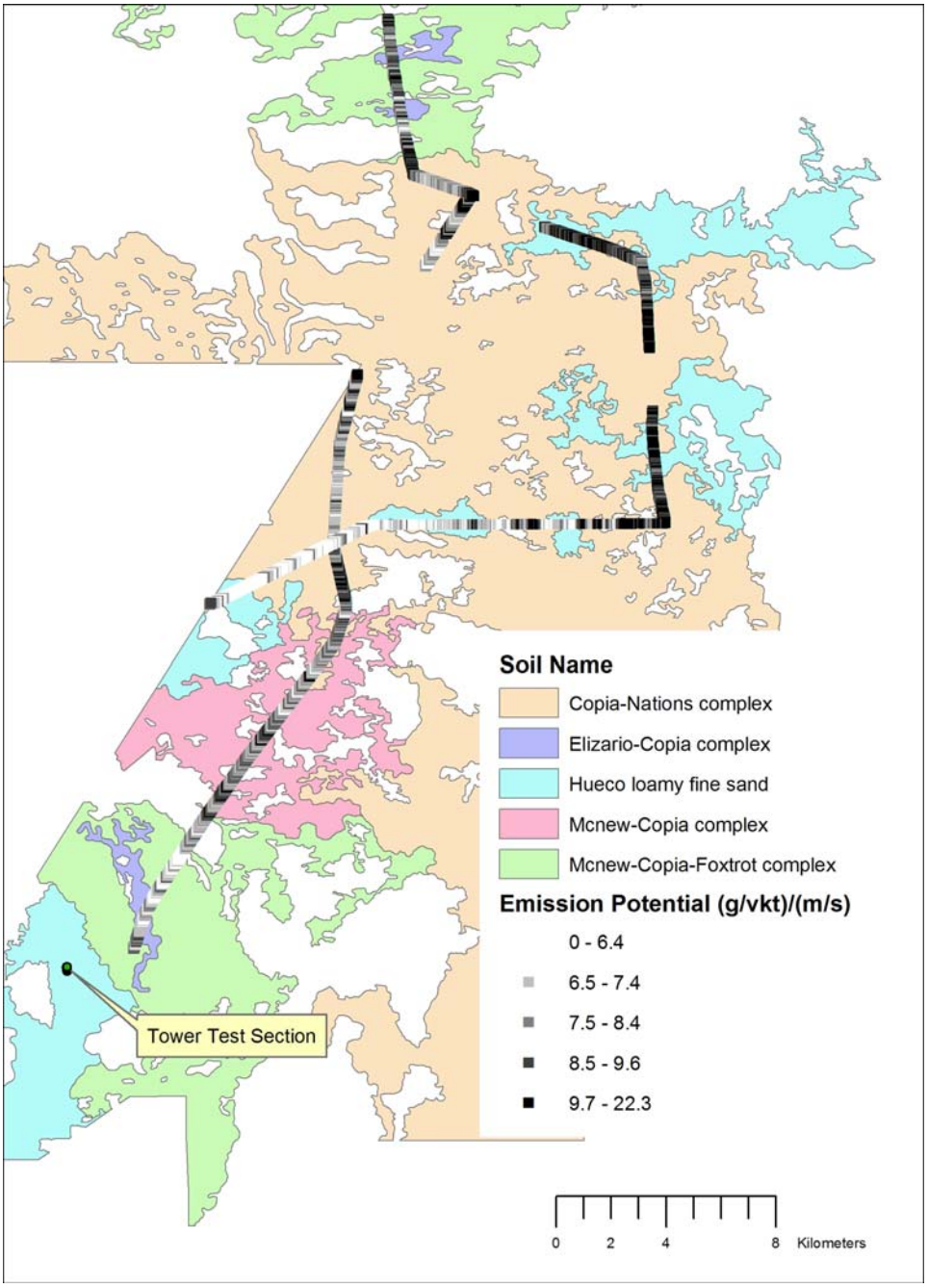
Soil Name
Copia-Nations complex
Elizario-Copia complex
Hueco loamy fine sand
Mcnew-Copia complex
Mcnew-Copia-Foxtrot complex
Emission Potential (g/vkt)/(m/s)
0 - 6.4
6.5 - 7.4
7.5 - 8.4
8.5 - 9.6
9.7 - 22.3
Tower Test Section
0
2
4
8
Kilometers

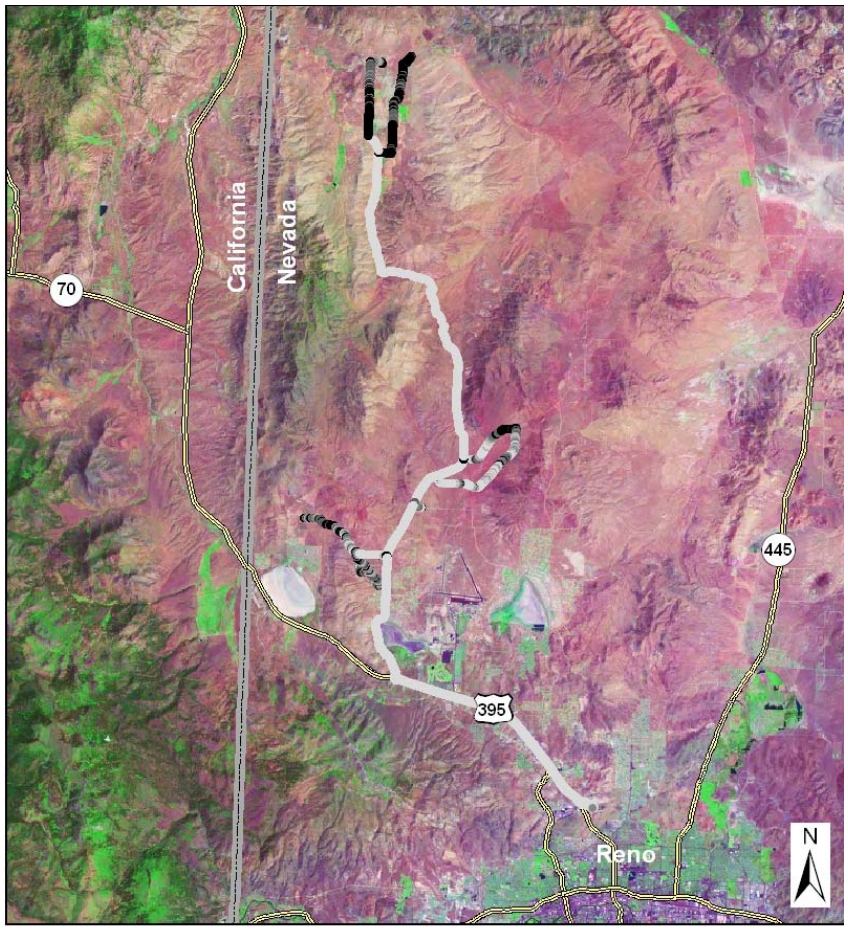

Legend

Major roads

State boundary

Emission Potential (g/vkt)/(m/s)

- 0.0 - 6.4
- 6.4 - 7.4
- 7.4 - 8.4
- 8.4 - 9.6
- 9.6 - 29.71

0 3 6 12 Kilometers

Data Sources:
Landsat TM Red (band 7), Green (band 4), Blue (band 2) circa 1990 +/- 3 years from GeoCover Landsat Mosaics
Roads and state boundary from 2000 Census TIGER

Figure 4.20. Map of the TRAKER-measured emission potential [g/VKT]/[m/sec] for unpaved roads near Reno, NV.

Figure 4.21. Frequency distribution of emission potential measured for the Reno TRAKER survey of unpaved roads.

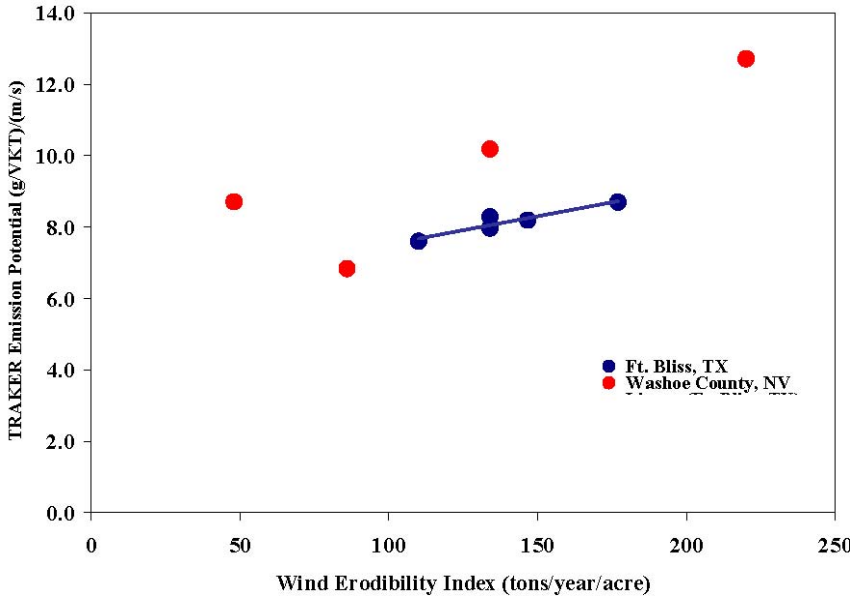

Figure 4.22. The TRAKER emission potential as a function of the U.S. Dept. of Agriculture's Wind Erodibility Index.

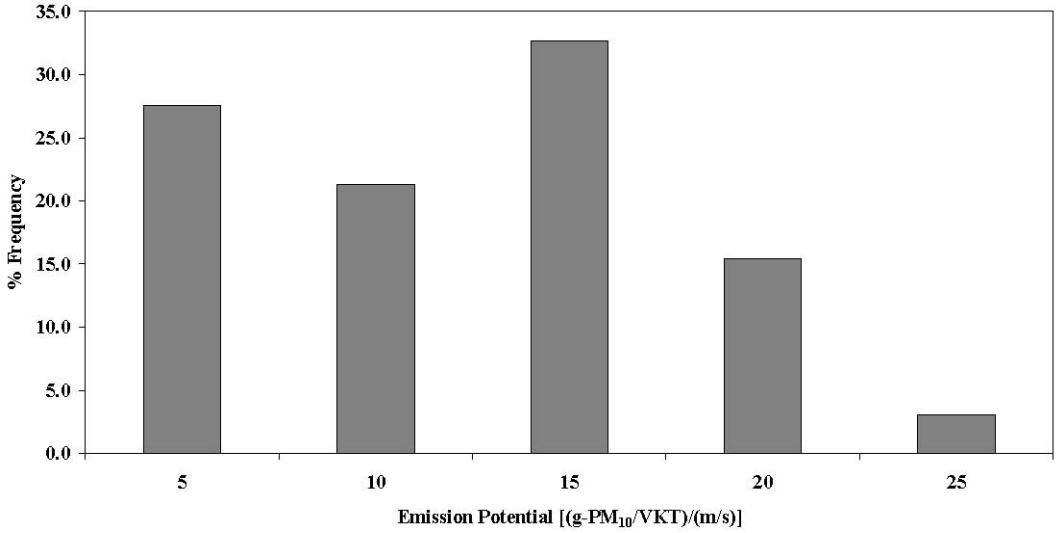

It should be noted that there are cases in which the general unpaved road dust emission potential should not be applied. For example, Gillies et al. (1999) clearly demonstrated that an unpaved road that had been treated with different dust suppressants or palliatives had very different dust emissions for the different treated sections. In the case of treated unpaved roads the strength of the emissions were controlled mainly by the amount of silt size particles (g/m^2) in the loose surface material and the moisture content of the material.

Some spatial patterns were observed in the unpaved road emission potentials measured by TRAKER, however the range of emission potentials across the base and on the roads near Reno, NV, was generally narrow. Sixty percent of all measurements at Ft. Bliss fell between 6.7 [g/VKT]/[m/sec] and 9.6 [g/VKT]/[m/sec], while in Reno 54% of the measurements ranged between 10-15 [g/VKT]/[m/sec]. Unpaved roads in five different soil types were sampled with the TRAKER vehicle at Ft. Bliss, and eight different types were sampled near Reno. When the emission potentials were compared with the soil survey database, unpaved roads surfaces in areas with the highest soil wind erodibility index also had the highest road dust emission potentials.

This component of CP-1191 demonstrated that the TRAKER technology can effectively map dust emission potential for unpaved surfaces. In addition the measurements demonstrated that for untreated unpaved roads there appears to be a limited range of emission potentials and an average emission potential for most unpaved roads may be adequate for inventory purposes. It should be noted however that this is not a definitive statement and it will become increasingly evident whether it is a reliable way to treat unpaved road emission potential as the database of unpaved road dust emission potential is increased substantively. Evidence does suggests that emission potential can be made more accurate by assigning an emission potential to a road according to the value of the soil wind erodibility index through which the road passes. Also for vehicles other than TRAKER the emission potential will have to be scaled for the appropriate speed and weight parameters (Section 4.2).

4.5 Wind Tunnel Testing to Assess Surface Disturbance Effects on Dust Emissions

Dust particles of mineral origin are entrained and emitted from susceptible surfaces by the shearing action of the wind (Garland, 1983) and through impacts from saltating particles (Bagnold, 1941; Shao et al., 1993; Rice et al., 1996; Rice et al., 1997). Bagnold (1941) and more recently Shao et al. (1993) demonstrated that the interparticle forces are more easily disrupted by the impact of saltating grains than by aerodynamic forces. Shao et al. (1993) presented evidence that the emission of dust particles, and therefore the vertical flux of dust, is proportional to the friction velocity raised to the third power. Field and laboratory measurements have however found a great degree of variability in this relationship (e.g., Borrmann and Jaenicke, 1987; Nickling and Gillies, 1989; Nickling and Gillies, 1993). The variability in the emission rate of dust as a function of wind friction velocity has been linked to the textural qualities (% sand, silt, and clay) of the soil (Gillette and Walker, 1977; Nickling and Gillies, 1989). The variability is also influenced by supply limitations induced by inter-particle forces that can be augmented on surfaces depending on the degree of crusting (reducing supply) and on the level of disturbance (increasing supply).

The purpose of this component of the project was to assess the effects of military vehicular disturbance on dust emissions for off road surfaces. The empirical approach is to compare measured emissions from an undisturbed control plot with the emissions measured on the three plots disturbed by military vehicles. The non-disturbed plot serves as a reference point to compare with the disturbed plots. The disturbance plots were created using a HUMVEE, a 5-ton truck, and a Bradley Fighting Vehicle (BFV) (Fig. 4.23). Three levels of disturbance were created. The level of disturbance is solely a function of the number of vehicle passes allowed in a given area. The levels of surface disturbance can be characterized, for example, by measurements of soil integrity (degree of crusting), depth of disturbed layer, soil aggregate stability, etc.

Two series of tests were carried out for this component. The first emission measurements were done immediately after disturbance in 2001 and a second set two years later. During this time no further vehicle disturbance was allowed. The plots were exposed to the ambient meteorological conditions between the two measurement periods.

4.5.1 Site Description and Vehicle Impact Strategy

The test surface selected for establishing the disturbance plots is as area within the M88 Driver Training area at Ft. Bliss. According to anecdotal evidence this area has had only marginal (if any at all) disturbance in approximately the last 20 years. Prior to disturbance and as typified by the control plots, the surface soil was crusted and there is an established plant community of sparsely distributed annual grasses and small herbs/shrubs.

Four sub-areas within the selected test area were demarcated with nylon rope to define the different impact areas prior to the egress of the military vehicles. Each of these area was ~100 m long and ~10 m wide. One area was designated a control site where no vehicle disturbance was allowed. The control plot serves as a reference point to compare with the disturbed plots. Within each of the other three demarcated corridors three impact zones were delineated. The disturbance plots were created by having the vehicle drivers make a set number of passes over the surface in the strictly defined areas.

The first level of disturbance was a “one vehicle pass”. This entailed the vehicle making only one pass over the surface. However, to create a zone of impact wide enough to accommodate wind tunnel testing the drivers were instructed and guided to make side-by-side single passes until instructed to stop. In this way the wheels or tracks traversed the surface laterally, but going over the same track more than once was avoided. This defined the minimal impact plot. Having the vehicles make three additional passes per track on the second plot area created the second level of disturbance. Finally, on the third plot area the vehicles were instructed to make three more additional passes making a total of nine passes over the surface (covering the entire lateral extent of the plots). The vehicles were instructed to travel at ~25 km/hr over the plots.

4.5.2 The Portable Wind Tunnel

Measurements of dust flux and horizontal mass transport rate were made using the University of Guelph portable field wind tunnel (Fig. 3.4). The wind tunnel is a suction type, constructed of 7 collapsible aluminum and fiberglass sections that form a 0.75 m high with a 1.0 × 11.9 m open-floored working section. Six 25 cm adjustable wheels are mounted on the outside of the tunnel, which allows it to be raised and moved and transported from site to site without dismantling.

Air is drawn into the tunnel by a 0.96 m centrifugal fan powered by a 45 h.p. diesel engine. The fan is attached to the tunnel by a flexible 1 m diameter neoprene-impregnated canvas hose that allows the working section to be positioned relatively easily even in rather awkward locations.

Figure 4.23. The military vehicles used in the disturbance testing. Top to bottom: 5-ton truck, HUMVEE, and Bradley Fighting Vehicle.

Air enters the working section through a 1 m long two-dimensional, 2:1 contraction bell fitted with two fine screens at the entrance to the working section to straighten the airflow. In the natural environment, sand-sized particles passing over a given point are continually fed by sediment transported from an up-wind source. In the wind tunnel however, loose sand at the surface is often quickly removed and not replenished because of the closed system. In order to replicate more closely the natural system it is necessary to supply sand at the entrance of the working section using a hopper system. Pre-

screened and winnowed sand is poured into the hopper and fed into the tunnel by four 20 mm ID tubes that extend to approximately 10 cm above the surface. The rate of the feed into the tubes is controlled by a horizontal auger, which is attached to a variable speed electric motor. Sand is fed into the tunnel at a rate to maintain saturated flow conditions.

Wind Velocity Measurements

Wind velocities in the first year of testing were measured using a rake of 6 NPL Pitot tubes mounted through the ceiling of the wind tunnel at 2, 4, 6, 8, 12 and 17 cm above the surface. The Pitot tubes were connected to a scanning valve (Scani-valve Inc., model WS5-24) that allows the differential pressure from the Pitot tubes to be read sequentially by a single pressure calibrated differential pressure transducer (Viatran Inc., model 219-12). In FY03 a new system for measuring wind speed in the tunnel was used. In this system a single Pitot tube the position of which is controlled by a stepping motor system locates the tube at predetermined elevations above the surface where point wind speeds are taken. Typically, the first measurement height is 1.0 mm above the surface. The Pitot tube is connected by Tygon tubing to a calibrated pressure transducer. Differential pressures in each system were converted to point wind speeds by the relationship:

$$u = \left(\frac{2g\left(m_{H_2O}\right)\Delta P}{\rho_a} \right)^{0.5} \quad (1)$$

where g is acceleration due to gravity, ΔP is differential pressure from the transducer calibration and ρ_a is air density.

A PC running a custom designed Visual Basic program acquires the wind speed profile data and writes it to an EXCEL spreadsheet where the aerodynamic parameters of wind friction (u_*) speed and aerodynamic roughness length (z_o) are calculated from the time-averaged wind speed profile data using the "law of the wall".

PM_{10} Dust Concentration Measurements

PM_{10} dust concentrations during the wind-tunnel tests were measured at four heights above the surface using TSI DustTrak (DT) aerosol monitors (TSI Inc., model 8520) (Fig. 4.24). The DT uses a laser diode and optical backscatter principle to determine dust concentrations. The DT is calibrated using a zero checking mechanism provided by the manufacturer. In order to calibrate the instrument a zero filter is placed on the inlet orifice and the read concentration adjusted by a calibration potentiometer to 0 ± 0.001 mg/m^3. The manufacturer recommends a maximum concentration of 100 mg/m^3. The DT can read up to 350 mg/m^3. However, it is suggested that at this concentration, it only be used as a reference for order of magnitude.

The four DTs were positioned on top of the wind-tunnel and connected by Tygon™ tubing (1 m length, 8 mm ID) to 200 mm long, 8 mm ID stainless steel sampling nozzles positioned 5, 9, 16.5

Figure 4.24. The particulate flux measurement system installed in the wind tunnel.

and 30 cm above the surface (Fig. 4.24). The inlet nozzles were aligned into the flow and held in place by a support rod attached to the ceiling of the tunnel. The DT samplers were set to a logging interval of 1 s and concentration values were stored by internal memory in each instrument for the duration of each wind tunnel run.

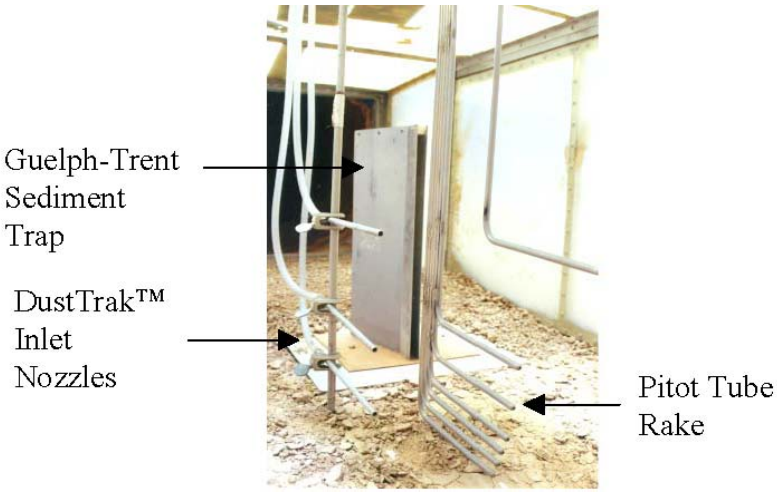

Measurement of Horizontal Mass Transport Rate

The horizontal mass transport rate was measured using the Guelph-Trent Sediment Trap (Fig. 4.24) as described by Nickling and McKenna Neuman (1997). The trap is wedge-shaped with a 20 × 300 mm rectangular orifice. The orifice extends in front of the wedge in order to maintain isokinetic flow conditions. The back of the trap is made of stainless steel mesh with 62.5 µm openings that allow air to flow through the trap while retaining sediment.

The cumulative weight of the sediment that enters the trap was measured on a Metler electronic balance (Metler Inc. model BD1201), which has an accuracy of ±0.001g. The balance was placed in a protective wooden box under the trap, positioned in the center of the tunnel. The weight on the balance was read on a 2 s interval by a computer through an A to D board.

4.5.3 Soil and Surface Characteristics of the Test Plots, 2001 - 2003

For each of the test plots soil and surface characteristics were measured for the 2001 and 2003 test periods. For each test plot the following tests were carried out: 1) digital images were taken of each individual wind tunnel test location through time (e.g., Fig. 4.25), 2) soil samples were taken from each test plot for particle size analysis (% sand silt and clay), percent organic matter, percent $CaCO_3$, pH, salt content (mg/kg). In 2002 digital images recording the state of the surface of each of the test plots were also recorded.

In situ measurements of the depth of the disturbed layer for each of the test plots were taken in April 2001. The mean depth of disturbance for the control plots was 0.30 cm (±0.51 cm). For the plots impacted by military vehicles the mean depth of disturbance were 4.92 cm (±2.05 cm),

Figure 4.25. Changes observed in the surfaces following the initial disturbance in April 2001. Top images are for the most disturbed 5-ton and the bottom images are from the most disturbed Bradley Fighting Vehicle plot.

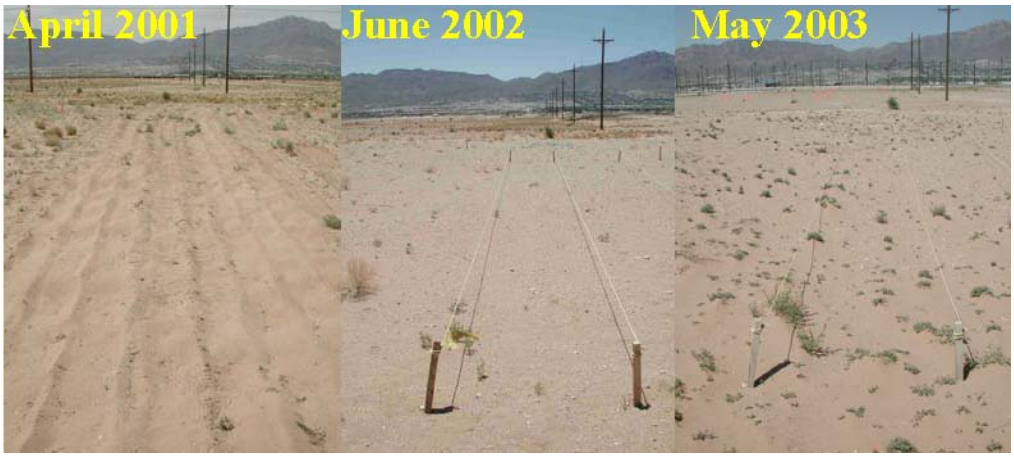

April 2

June 2

May 2

April 2

June 2

April 2

5.54 cm (±1.93 cm), and 4.95 (±1.41 cm) for the HUMVEE, Five-ton truck, and Bradley Fighting Vehicle, respectively. The depth of disturbance of all the impacted plots is an order of magnitude greater than the control plots. However, within the level of uncertainty there are no differences between the vehicle-impacted plots as a function of vehicle type or disturbance level. Although the depth to disturbance measurement is similar for the impacted sites there are distinct visual differences between the sites that are evident and documented in the digital photographs.

The HUMVEE plots and the Bradley Fighting Vehicle have much less surface relief as the impact of the wide tires of the HUMVEE and the tracks of the Bradley spread out the force of the vehicle over a wider area. However, the 5-ton truck creates deeper tracks in the loose material as it breaks up the soil. These deeper grooves and churning effect of the tires on the 5-ton creates a looser material that has a greater emission potential.

By 2002 the surface characteristics of the plots had changed markedly, and more so for the more heavily impacted plots (Fig. 4.26). The surfaces had lost any sign of imprints made by the wheels or tracks of the vehicles used to create the disturbance. Principally abiotic processes crusted the soil surface. The most likely crusting process was by clay bonding of loose particles following wetting by precipitation.

In 2003, a significant change in the test plot surfaces was observed with the establishment of a significant vegetation cover on many of the test plots (Fig. 4.27). The amount of vegetation on each of the test plots in 2003 are expressed as a percent cover in Table 4.8.

4.5.4 Wind Tunnel Testing Procedures

Prior to testing, sand from a local supplier was obtained. The sand was passed through a 1.0 m mesh screen in order to remove large particles and then winnowed twice to remove dust-size particles.

At each plot and for each disturbance level a paired set of test runs were carried out. The tests were performed over a range of wind velocities, from just above threshold to a maximum wind speed of approximately 22 m/s (equivalent 10 m wind speed). Every attempt was made to carry out all tests at a given site on the same day to try and maintain similar surface and atmospheric conditions. Each test consisted of 3 components of approximately 3 minutes each: a) determination of threshold shear velocity, b) measurement of PM_{10} dust emissions without sand feed, followed by c) measurement of PM_{10} dust emissions with sand feed. In order to obtain an airtight seal, heavy canvas sheets at the base of the tunnel wall were spread outward and buried. At the inlet bell, the surface was smoothed and moistened with a sprayer to prevent scouring. To measure the background PM_{10} concentration a fifth DT was mounted on a tripod at a height of 0.6 m, 1 m in front of the inlet bell. Once the Pitot tube rake, DT inlet nozzles, and the sediment trap were installed the fan was moved into place and connected to the working section by the canvas hose.

Figure 4.26. Image of the same disturbance plot (Humvee, least disturbed) showing that visual signs of disturbance from vehicle tires are not evident in two years passage of time.

Figure 4.27. Images of the plots showing the extensive growth of vegetation observed in 2003.

Control

Bradley

Humvee

5-t

Table 4.8. The percent cover of vegetation on the plots on 2003.

Site	Plot	Average % Cover	% Uncertainty
Control	csw1	13.4	3.5
"	cswo1	11.4	3.3
"	csw2	16.8	3.2
"	cswo2	13.3	2.5
"	csw3	1.0	
"	cswo3	5.9	2.6
Humvee	hmw1	13.1	3.0
"	hmwo1	9.0	3.2
"	hmw2	13.9	3.9
"	hmwo2	11.3	2.4
"	hmw3	4.3	3.5
"	hmwo3	3.5	2.7
5-ton	ftw1	16.6	3.1
"	ftwo1	14.6	3.1
"	ftw2	14.6	2.9
"	ftwo2	10.4	2.6
"	ftw3	4.5	1.5
"	ftwo3	6.0	1.9
Bradley F.V.	bvw1	8.4	2.0
"	bvwo1	12.6	3.4
"	bvw2	14.9	2.6
"	bvwo2	16.5	3.0
"	bvw3	13.2	2.3
"	bvwo3	10.2	2.1

In order to determine the threshold velocity for a given surface the fan was engaged at a very low speed and slowly increased until the onset of saltation and dust emission was visually apparent in the tunnel. The fan was then turned down slightly and run for 3 minutes during which time velocity measurements were taken. Following this, the fan speed was increased until a pre-selected free stream velocity was reached and velocity and PM_{10} measurements were recorded for 3 minutes. The hopper was then turned on, and the sand feed was adjusted using the variable speed motor so that small piles of sand just began to form under the inlet tubes in attempt to achieve a saturated flow condition for the given free stream velocity. Once the sand feed was adjusted wind speed, dust concentrations, and sand transport rate was monitored for 3 minutes. Following the run, the tunnel was raised by the screw jacks and wheeled to the next sampling location at the given site.

Between individual runs, as well as between the with- and with-out feed tests, the DT inlet nozzles were cleaned by blowing a jet of high-pressure air through the sampling

line. In addition the DTs were calibrated and the flow adjusted at the beginning and end of each day.

4.5.5 Wind Tunnel Test Results 2001

The initial tests performed without sand feed introduced at the front of the tunnel to represent an erosion system without an upwind sediment supply, which is common to many natural dust-emitting surfaces showed the PM_{10} concentrations measured at the four heights increased rapidly upon start up of the wind tunnel (Fig. 4.28). Following the initial peak in concentrations characteristically were observed to decline as a function of time. This was not always the case as there were instances when concentrations would increase dramatically during a test run and then begin to decline again. This is likely the result of small portions of the surface breaking free that instantaneously releases a pulse of dust. In addition, a new supply of saltation-sized particles can be liberated that increase the likelihood of more dust particles being raised into the airstream by abrasion and saltation impacts. For the second test condition sand is introduced via a hopper system into the upwind portion of the working section of the wind tunnel. The introduction of the sand simulates an increased availability of entrainable sediment for abrasion and bombardment that has been shown to increase dust emission and the breaking up of surface crusts and aggregates (Rice et al., 1997). Under these conditions the test surfaces were observed to emit dust more or less continually (Fig. 4.28).

Several metrics can be used to quantify the movement of sediment across the surface and the emission of dust. The flux of the sand-sized material moving in saltation was determined from the mass of sand collected in the 0.02 m wide × 0.30 m high vertically integrating, passive sediment transport trap described by Nickling and McKenna Neuman (1997). Laboratory testing of this wedge-shaped trap indicated that it is >90% efficient over a wide range of wind speeds (Nickling and McKenna Neuman, 1997). The saltation flux (q, g m^{-1} s^{-1}) is expressed as the mass of sand moving through a unit width in unit time.

The vertical flux of dust (F, mg m^{-2} s^{-1}) was calculated from:

$$F=-u_* \kappa \rho dC_z/dz \quad (2)$$

where u_* is the friction velocity, κ is von Karman's constant (~0.4), ρ is air density (kg m^{-3}), and C_z is the dust concentration at height z. The log-linear concentration gradient (dC_z/dz) was

Figure 4.28. Examples of the concentrations of dust as a function of height above the surface for tests without an added saltation component (top) and with added saltation (bottom). The data trace labeled dt1 is closest to the surface.

calculated through non-linear regression analysis using the four measured concentration values with height. The vertical flux represents the proportion of the total dust emitted from the surface that is transported vertically.

A second metric to measure the production of dust from the surface is the emission rate

(E, mg m^{-2} s^{-1}) (Shao et al., 1993; Houser and Nickling, 2001). This represents the mass of dust emitted from a surface of given area per unit time that can be expressed as:

$$E = \frac{1}{L}\int_{0}^{z} C u_z \, dz \qquad (3)$$

where L is the length of the wind tunnel over which dust is being emitted, C is the dust concentration and u is the wind speed at each measurement height (z) within the boundary layer.

The sediment transport data shows that the surfaces tested are highly variable in their emission characteristics. Generally, the data show only weak trends with respect to the theoretical relationships that have been developed and observed for ideal conditions. The variability observed is similar to what has been reported for other wind tunnel studies that have measured emissions on actual rather than laboratory-constructed surfaces (e.g., Nickling and Gillies, 1989; Houser and Nickling, 2001).

For most of the test plots the predicted relationship between saltation flux (q, g m^{-1} s^{-1}) and the wind friction velocity raised to the third power was not observed. This power function relationship (albeit rather weakly) between u_* and q, was observed for a few of the test surfaces (e.g., HUMVEE and 5-ton truck). However, in many of the test runs this relationship was not evident. The reason for this is because of the supply-limiting characteristics associated with the test surfaces. The surface characteristics that tend to reduce the expected transport rate include: trapping effects caused by the surface morphology (i.e., sediment becomes trapped in the tread-created depressions) and the presences of residual vegetation components. The plots were initially pruned after the vehicle-generated impacts to remove as much of the shrubs and grasses; however, there were still small patches of stems and exposed root-tops that effectively trapped the moving sand.

The range of vertical emission fluxes measured on the test plots are comparable to those measured with a portable wind tunnel by Nickling and Gillies (1989) for a range of surface types in Arizona and by Houser and Nickling (2001) for a disturbed clay-crusted playa also in Arizona. However, in several cases much greater emission fluxes were observed for the Ft. Bliss plots than have been previously reported in the literature. This suggests that the levels of disturbance are much greater than previous studies have encountered and/or the sediment texture of the Ft. Bliss plots results in greater emissions.

The vertical emission fluxes (F, µg m^{-2} s^{-1}) also were quite variable for most plots, similarly to the saltation flux, with few statistically significant relationships between F and friction velocity. For most of the test plots the predicted relationship between saltation flux (q, g m^{-1} s^{-1}) and the wind friction velocity raised to the third power was not observed. As noted by Shao (2000) different studies have observed that vertical dust flux (not necessarily the dust emission rate) is proportional to u_*^n with n varying between 2 and 5. This power function relationship (albeit rather weakly) between u_* and F, was observed for a few of the test surfaces (e.g., HUMVEE with and without added saltation,

BFV with added saltation).

The emission flux, E (mg m^{-2} s^{-1}), which describes the flux of dust emitted from surface, calculated for the Ft. Bliss test plots covers the same range as those measured on a crusted-playa by Houser and Nickling (2001). However, as was noted for the vertical fluxes, some of the emission fluxes measured on the Ft. Bliss test plots were much greater than any reported by Houser and Nickling (2001).

These data have shown that there is for all test plots a statistically significant relationship between the surface emission flux, E, and the horizontal saltation flux, q (Fig 4.29). The effect of the disturbance on the emissions is captured by the ratio of E to q. This ratio, with units of m^{-1}, provides an indication of how efficient a surface is in emitting a unit amount of dust for a unit amount of saltation. The wheeled vehicle impact plots (5-ton and HUMVEE) have average E/q values of ~2×10^{-5} m^{-1}, while the Bradley-impacted plots and the control plots have average values of 5×10^{-6} m^{-1} and 9×10^{-6} m^{-1}, respectively. The order of magnitude difference in the E/q ratio between the wheeled-vehicle impacted plots and the other plots suggests that for a given saltation flux the emissions of dust are much higher for this type of disturbance than for a surface impacted by a tracked vehicle.

4.5.6 Disturbance Effects on Dust Emissions, 2001

As discussed above the amount of dust emitted is critically linked with the amount of saltation, or sand transport occurring over a surface. This is also supported by theoretical considerations (Shao et al., 1993; Shao, 2001) and measurements from other studies (Houser and Nickling, 2001).

The variability in the observed flux measurements makes direct comparison of disturbance affects on dust emissions difficult. Several comparisons between the effects of disturbance and some simple indices of emission strength reveal several trends in the emissions as a function of disturbance. Two indices that illustrate the role of disturbance on emissions are the saltation flux, q, divided by the wind friction velocity, u_*, and the average dust concentration (from the four DustTraks) divided by the wind friction velocity. These simple measures quantify a unit amount of sediment in flux for a unit of wind energy.

The effect of disturbance on the unit flux of saltation as a function of wind friction velocity when the saltation is not limited by supply (i.e., sand is introduced at the front of the tunnel) is shown in Fig. 4.30a. The x-axis denotes disturbance level (defined by the number of vehicle passes, see Section 4.5.1) and the y-axis values have been normalized by the level-one disturbance values to allow comparison across vehicle types. A similar plot is shown in Fig. 4.30b, except these data are from the runs in which no sand was introduced into the tunnel during the tests. Figure 4.30 shows that as surface disturbance increased there was a concomitant increase in the amount of saltation flux for a given wind friction velocity. The effect is more dramatic when sand was not added through the hopper system. This is somewhat misleading because the absolute magnitude of the q/u_* index values for the without sand feed runs are lower than those of the with-sand-feed runs. In the runs with sand feed the emission system was more productive for dust on an absolute scale than the without sand feed tests. Based on the trends in the data shown in

Fig. 4.30 the increase in saltation flux per unit wind friction speed increases linearly with disturbance level. The degree of disturbance can be related to an increase in saltation flux per unit wind friction velocity between ~0.3 and ~2 times, depending on the limitation of the sand supply. Following the theory of dust emissions of Shao (2000) and Shao (2001), i.e., that saltation drives

Figure 4.29. The measured relationship between saltation flux and dust emissions on the disturbance plots in 2001.

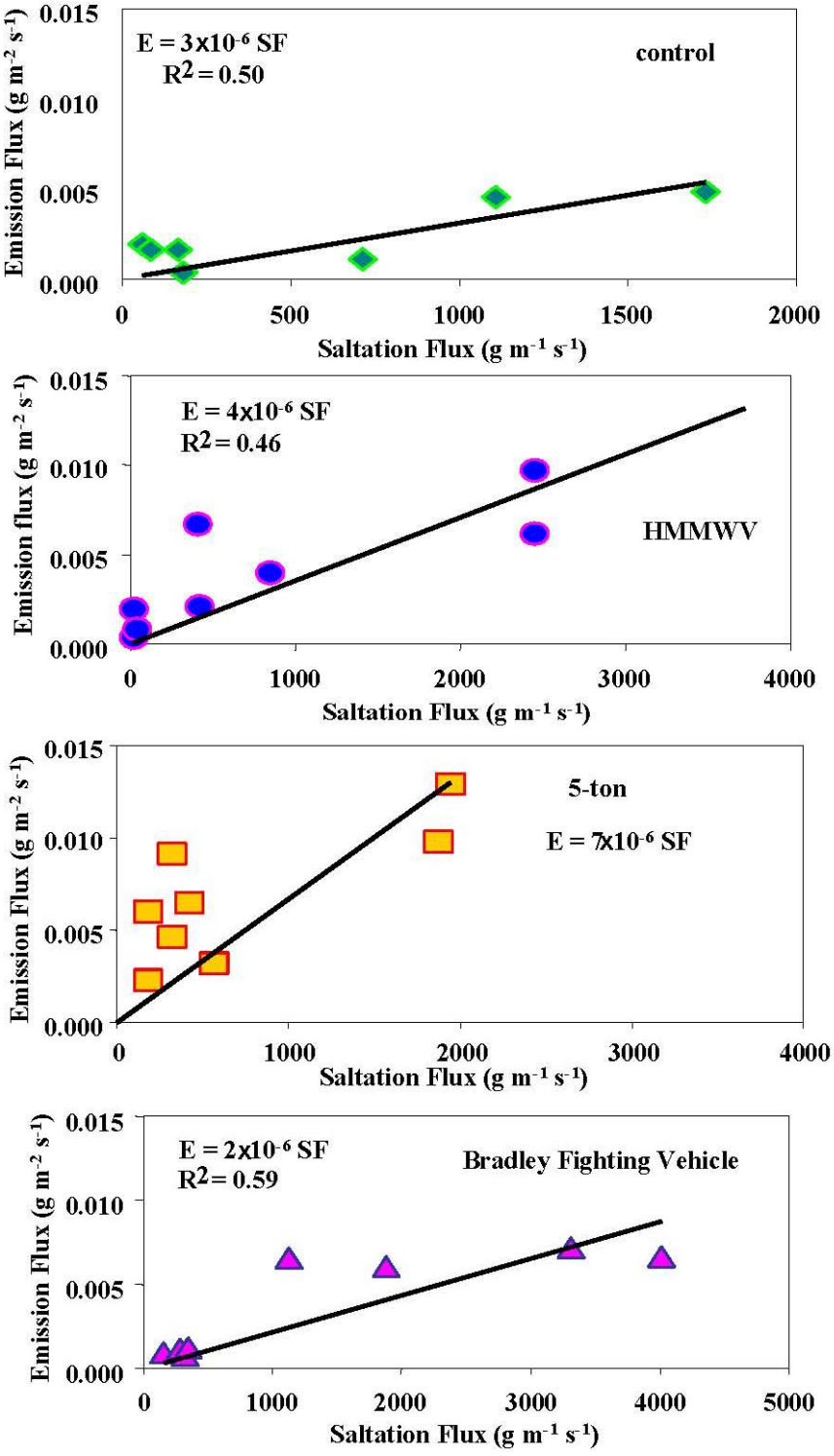

Figure 4.30. The observed relationship between disturbance level and the amount of

saltation flux per unit of wind friction speed for the test with sand feed (a) and without sand feed (b).

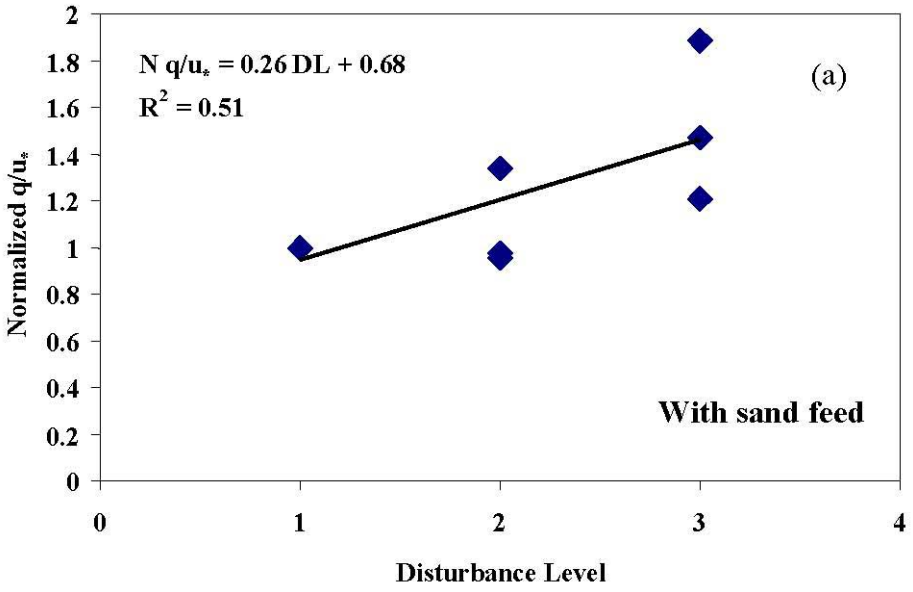

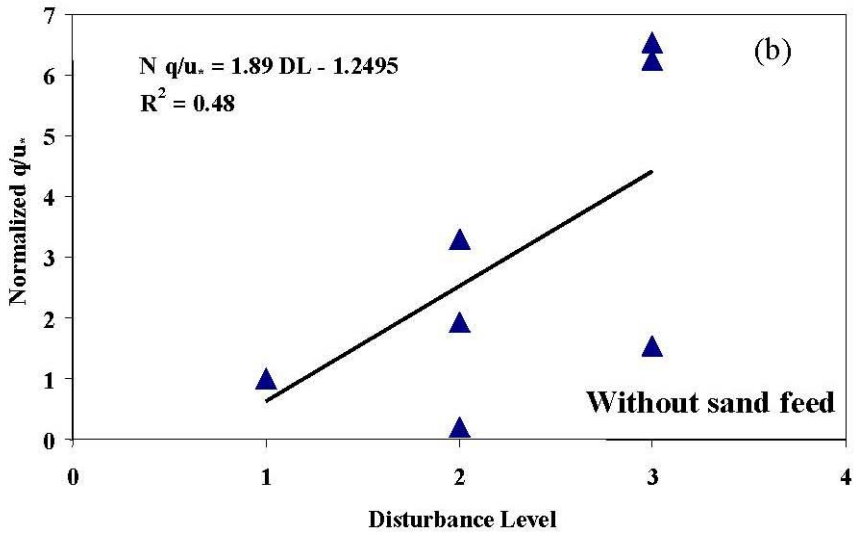

(b)

(a)

the dust emission process the relationships shown in Fig. 4.31 suggest that the emissions of dust would increase also as a function of disturbance. Although there is considerable scatter in the average dust concentration divided by wind friction speed index (Fig. 4.31) these data generally support the saltation index data trends (Fig. 4.30), i.e., the dust concentrations increase as a function of disturbance level at rates similar to those observed for the saltation (Fig. 4.30).

The disturbance experiments indicate that the physical process that has the greatest influence on dust emissions is the saltation flux. This result has been observed by numerous other studies (e.g., Gillette et al., 1997; Gillette et al., 1995; Lu and Shao, 1999; Shao et al., 1993). For the Ft. Bliss experiment the increase in dust emissions by wind on disturbed surfaces was observed to increase as a function of disturbance level, which appears to relate directly to the amount of sand that the disturbance makes available. Increased levels of disturbance increase the amount of sand that is potentially available for the wind to move. In effect the efficiency of the emission process is improved by disturbance, increasingly removing the limitations of a supply of particles for saltation, allows more efficient emissions of dust-sized particles.

4.5.7 Wind Tunnel Test Results 2003

The wind tunnel testing on the disturbed plots was repeated in April 2003. The wind tunnel was placed on the test plots in the exact locations of the 2001 testing. This was done to characterize how the dust emissions changed as a function of disturbance level with the passage of time. The most significant changes observed in the saltation and average dust concentration data for the wind tunnel tests were that the range of measured value decreased by two orders of magnitude for the saltation and one order of magnitude for the concentration, over the same range of wind friction velocities (Fig. 4.32). Within two years time following the vehicle disturbance, the potential for dust emissions from the disturbed areas has been dramatically reduced.

Examining the q/u_* relationship as a function of disturbance for the 2003 data, there is still evidence of some residual effects from disturbance (Fig. 4.33). As was shown in Fig 4.30 for the 2001 data, an increase in the saltation flux index as a function of disturbance is still evident in 2003. In 2003, however the relationship indicates that there is an effect of supply-limitation for the saltation system. Unlike the 2001 q/u_* relationships for the tests with and without added saltation material, which showed distinct differences between the two test situations, the 2003 shows no such distinction. This suggests that for either case there are supply limitations of the saltation component. This is likely a result of the influence of the vegetation that was present on the plots (Table 4.8) that restricted the saltation flux by sheltering and trapping effects, regardless of the input of sand via the hopper system into the wind tunnel. The difference in flux as a function of disturbance alone is also a bit misleading as the vegetation levels were less on the more disturbed sites (Table 4.8). Results from the Ft. Bliss experiments designed to assess the effect of vehicular disturbance levels on dust emissions by wind indicated that the emissions increase as a function of disturbance level. In the two years following disturbance, wind tunnel testing indicated that dust emissions were greatly reduced on all previously disturbed surfaces. The degree of recovery is greatly increased if favorable climatic conditions (i.e., rainfall) occur that promote crusting and plant growth. The disturbance effect that appears to relate directly to the observed increase in emissions is the amount of sand that the disturbance makes available.

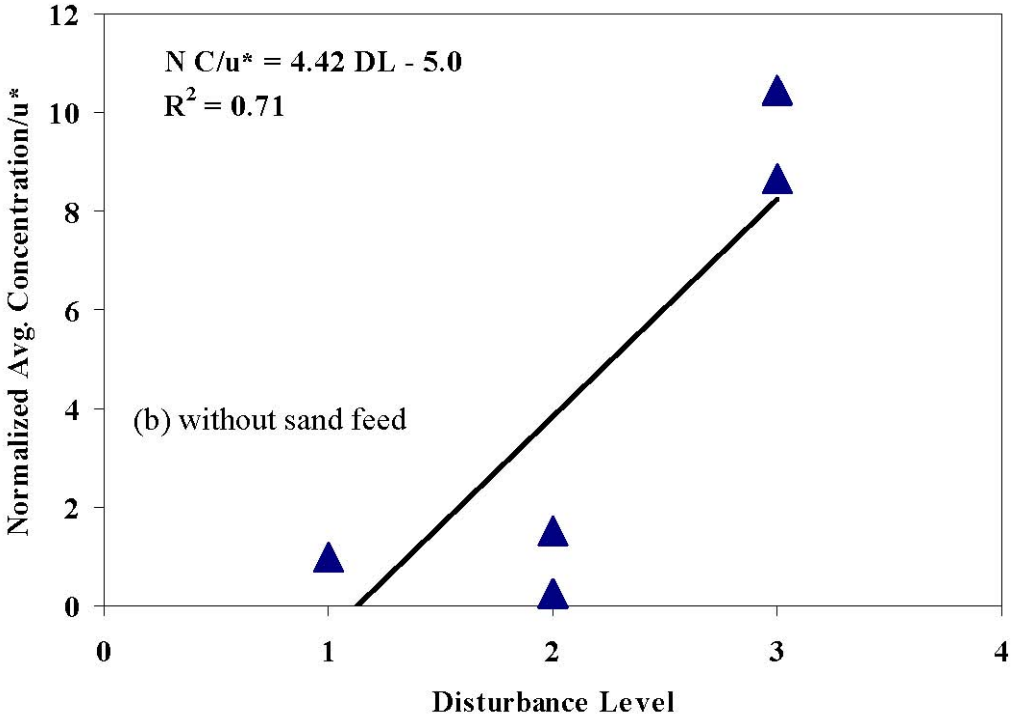
N C/u* = 4.42 DL - 5.0
R2 = 0.71
(b) without sand feed
Normalized Avg. Concentration/u*
Disturbance Level
0
2
4
6
8
10
12
0
1
2
3
4

Figure 4.31. The observed relationship between disturbance level and the average dust concentration in the wind tunnel per unit of wind friction speed for the test runs with sand feed (a) and without sand feed (b).

(b) without sand f

(a) with sand f

Figure 4.32. The observed range in saltation (top) and average dust concentration (bottom) as a function of wind friction speed in the wind tunnel comparing the 2001 tests at the time of disturbance and two years following the disturbance.

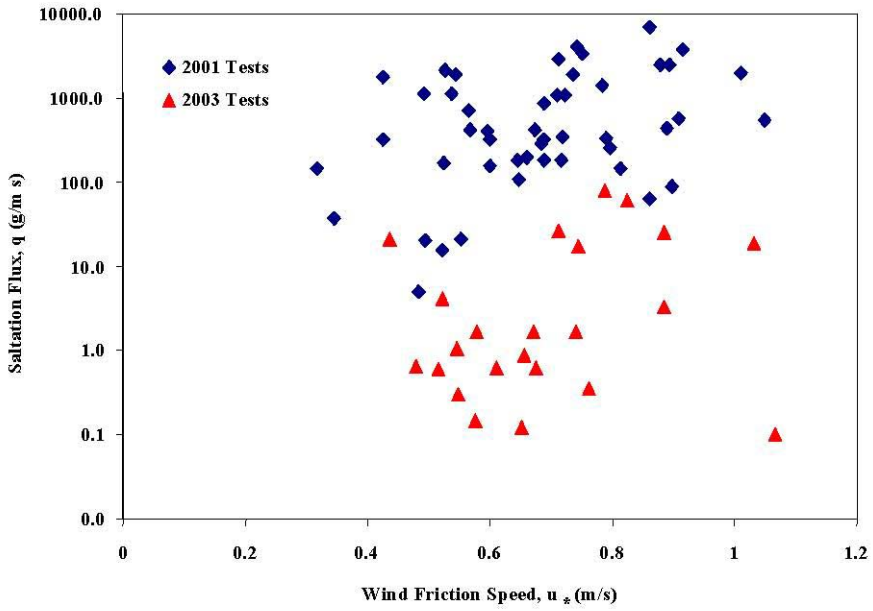
10000.0
1000.0
100.0
10.0
1.0
0.1
0.0
2001 Tests
2003 Tests
Saltation Flux, q (g/m s)
0
0.2
0.4
0.6
0.8
1
1.2
Wind Friction Speed, u * (m/s)

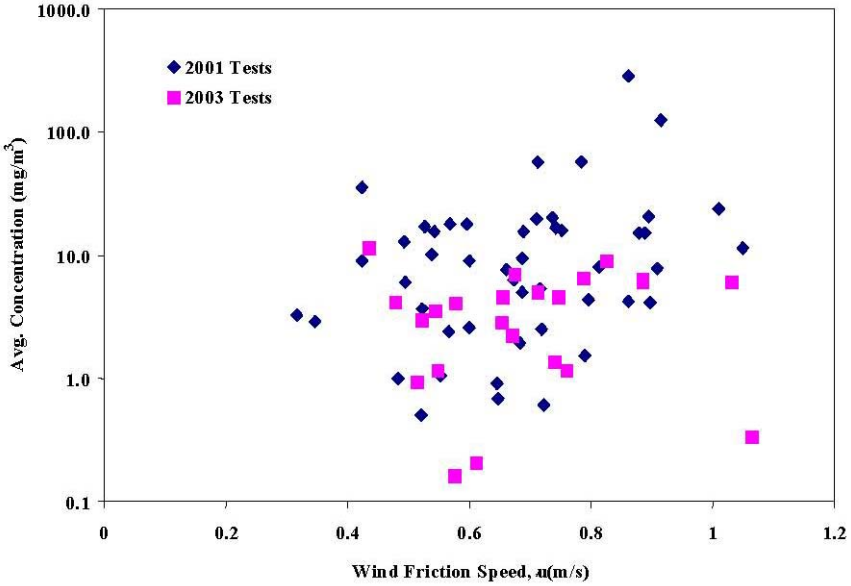
1000.0
100.0
10.0
1.0
0.1
2001 Tests
2003 Tests
Avg. Concentration (mg/m3)
0
0.2
0.4
0.6
0.8
1
1.2
Wind Friction Speed, u(m/s)

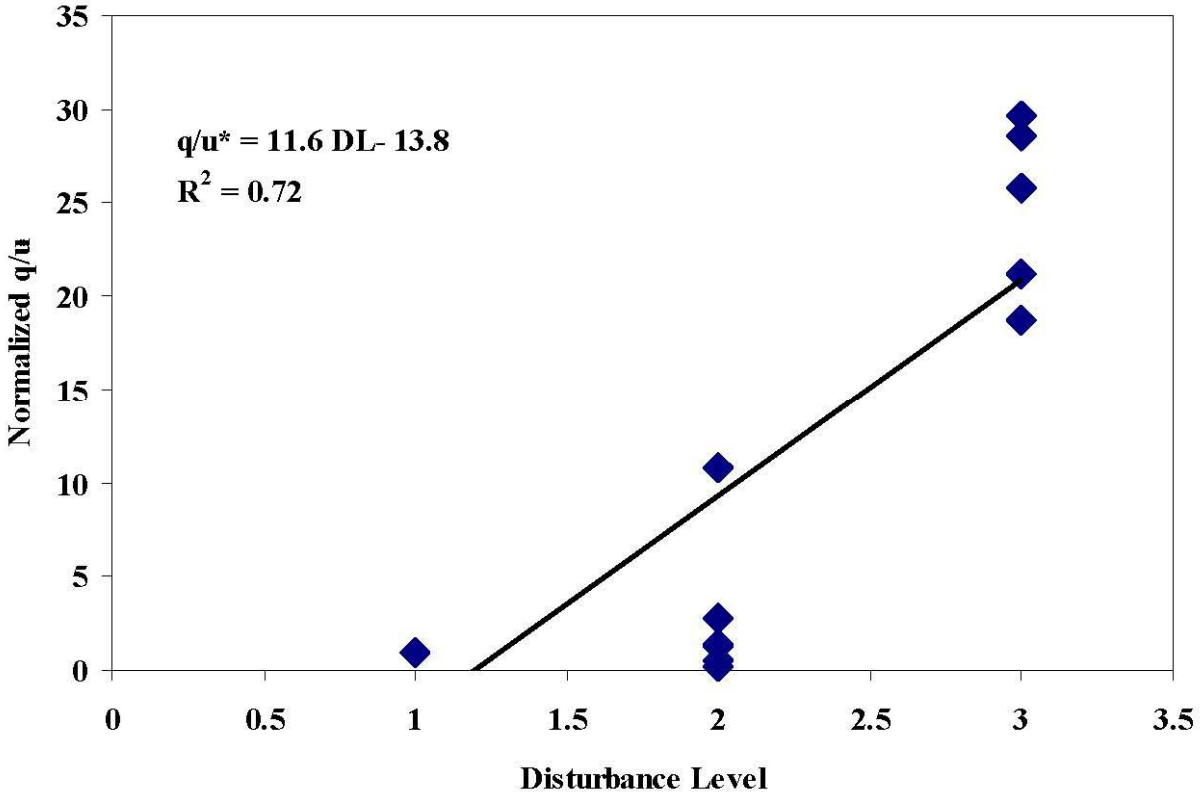
q/u* = 11.6 DL- 13.8
R2 = 0.72
Normalized q/u
Disturbance Level
35
30
25
20
15
10
5
0
0
0.5
1
1.5
2
2.5
3
3.5

Figure 4.33. The observed relationship between disturbance level and the amount of saltation flux per unit of wind friction speed on all the plots in 2003, data are normalized to the lowest disturbance level values.

For the wind tunnel testing carried out at Ft. Bliss we quantified disturbance simply by the number of passes a vehicle made over a designated area. Based on our analysis of the dust emission data and grain size distributions of the surface sediments an important metric to establish is the amount of loose sand created following the disturbance. For our test plots we observed that the texture (i.e., percent sand, silt, and clay) of the soil for the test plots was similar, but emissions were quite different depending on the amount of sand that was made available by the disturbance. In terms of a metric the amount of loose, available sand-sized material is critically important. This would currently have to be measured however with sufficient accumulation of data it may be that some generalization of disturbance level and degree of formation of loose material can be established. Secondary to information on the amount of loose sand available from disturbance effects would be a measure or evaluation from available data of the soil texture or another useful parameter such as the wind erodibility index of the USDA (2002), which is contained in available GIS databases.

4.6 Contributions to Regional Visibility Degradation.

Visibility and its degradation can be quantified by light extinction. This light extinction is due to both scattering extinction and light absorption by aerosols. While particles of any chemical composition contribute to light scattering, optical absorption is almost exclusively due to elemental carbon (EC) particles; products of the incomplete combustion of carbon based fuels. With the exception of wild fires, EC particles are always produced by human activities. Typical sources include combustion engines (especially diesel engines) and poorly controlled burning of biomass or fossil fuels. Therefore, the quantification of both optical extinction and its scattering and absorption component will allow us to distinguish between visibility degradation from combustion processes and from dust entrainment.

Optical measurements were carried out during the spring 2002 field season. These measurements were designed to characterize the light extinction and it's scattering and absorbing components and the total flux of extinction, scattering, and absorption cross sections from dust plumes entrained by vehicular activity.

4.6.1 In Situ Measurements

In situ measurements of the optical properties of the plume were carried out at a trailer located ~100 m downwind from the source road. The larger distance from the source makes the optical properties more representative of the particles undergoing long-range transport, as larger particles, which are subject to fast gravitational settling, have already settled out. The particle inlet was located at a height of ~5.5 m height above the instrument trailer. The aerosol-laden air was sampled and piped to a simple manifold distributing it to the five instruments: 1) an extinction meter, which folds several tens of kilometers of optical path into a one-meter length optical cavity and determines extinction by measuring the exponential decay of the optical power contained in the

cavity; 2) a commercial nephelometer measuring scattering extinction; 3) a newly-designed integrating sphere nephelometer; 4) two photoacoustic light absorption instruments operating at 512 and 1024 nm, which yields a real time *in situ* measurement of optical light absorption by utilizing resonant photoacoustic detection of light absorption. The use of an all-solid-state laser and an innovative acoustic design make this instrument much more compact and sensitive than its unpractical predecessors.

The Cavity Ring Down (CRD) Extinction Meter

Visibility can be characterized by measurement of optical extinction through the Koschmieder relationship. Atmospheric extinction can be as low as a few Mm-1, requiring large optical path lengths for its measurement. With the development of relatively inexpensive mirrors with ultra-low reflection losses, tens of kilometers of optical path length can be realized in practical, compact (1-m length) optical cavities. At the Desert Research Institute such cavities are being used for extinction measurements with sensitivities down to 0.1 Mm^{-1}.

Two pulsed laser techniques have been employed simultaneously to obtain highly sensitive extinction measurements with large dynamic range. The Cavity Ring Down (CRD) technique yields very sensitive detection, largely independent of laser power fluctuations, with a dynamic range from 0.1 Mm^{-1} to 1,000 Mm^{-1}. Cavity Enhanced Detection (CED) has a simpler experimental setup and data analysis algorithm than CRD, while yielding a dynamic range from 1 Mm^{-1} to about 5×10^{6} Mm^{-1}. The CED sensitivity limit is due to power fluctuations of the pulsed laser and could be further improved by measuring and accounting for these fluctuations. Capabilities of CRD and CED techniques including sensitivity, dynamic range, calibration, and complexity are currently being evaluated through examination of the Ft. Bliss dust plume and other available measurements.

The Integrating Sphere Integrating Nephelometer (ISIN)

The Integrating Sphere Integrating Nephelometer (ISIN) is a novel and unique reciprocal nephelometer that uses an integrating sphere with attached truncation-reduction tubes to contain the sample volume and to integrate the scattered light (Varma et al., 2003). Its main advantage over current integrating nephelometers is the seven-fold reduction in truncation angle to about 1^{0} that reduces errors in measuring scattering from large particles. Truncation losses of more than 25% occur for the ISIN at particle diameters of larger than 16 µm. Additional features include the improved ability to sample large particles and the well-defined operating wavelength.

Initial comparisons of the ISIN with two commercial nephelometers using sub-micron particles revealed excellent correlation and agreement within a few percent. Comparisons with one of the two commercial nephelometers showed good agreement for ambient fine particles (no entrainment) while the ISIN readings were up to four-times higher than those of the commercial instrument for freshly entrained coarse particulate matter. This large discrepancy is attributed to the reduced truncation error (up to a factor of two) and the improved large particle sampling of the DRI-ISIN.

Photoacoustic Light Absorption Instruments

Mineral dust aerosols can also cause significant light absorption, depending on the particle composition, size distribution, and the wavelength of interest. In contrast to black carbon (BC) from combustion, mineral dust light absorption has a strong wavelength dependence. The characterization of mineral dust light absorption has similar requirements as that of BC with the added need for wavelength dependent measurements and for the sampling of coarse particles.

Aerosol light absorption can be measured with filter techniques or with *in situ* techniques. Filter based methods concentrate aerosol particles on a filter substrate and measure light extinction through the loaded filter, either long after exposure in the laboratory (e.g., Lin et al., 1973) or in real time (Hansen et al., 1984; Bond et al., 1999). However, it is well known that the interaction of scattering from the concentrated aerosol and the filter medium can lead to errors on the order of a factor of two or three, as the filter instruments lack absolute calibration (Horvath, 1997; Bond et al., 1999). This situation can be improved by using correction methods utilizing the simultaneous measurement of aerosol scattering (Horvath, 1997; Moosmüller et al., 1998). However, an absolute calibration is still needed for filter methods. The photoacoustic technique (Petzold and Niessner, 1996; Arnott et al., 1999) is an *in situ* technique, which measures aerosol light absorption with the particles in their natural suspended state with an absolute calibration based on first principles.

An alternative to filter-based methods for light absorption measurement is to use a photoacoustic instrument (Petzold and Niessner, 1996; Arnott et al., 1999). No filters are used in these instruments, but instead, the sample air is continuously drawn through an acoustical resonator. A periodically modulated laser beam also passes through the resonator. Concomitant with light absorption by either gas or particles is heat transfer to the surrounding air. The resonator can be designed with an acoustic resonance frequency such that all of the heat from light absorption is transferred during the acoustic period. Upon receiving this heat, from light absorption, the surrounding air expands and this expansion contributes to the acoustic standing wave in the resonator. Measurement is made with a microphone. The microphone signal is linearly proportional to the aerosol light absorption coefficient. In practice, if one is seeking to measure particulate light absorption, the choice of laser wavelength is made to minimize influence of standard atmospheric gases. The typical wavelength that the Desert Research Institute (DRI) uses for the visible region is 532 nm, where high efficiency, frequency-doubled, compact ND-YAG lasers are available. In the near infrared (IR), 1047 nm lasers are used.

The photoacoustic measurement is a zero-based measurement in the sense that no light absorption corresponds to no microphone signal. By comparison, typical extinction measurements require careful monitoring of a reference level. The art to making the photoacoustic method viable in practice is to design the system so that the influence of ambient and pump acoustic noise are minimized (Arnott et al., 1999). The theoretical calibration of the DRI photoacoustic instrument has been thoroughly tested against light absorption measurements on absorbing gases – something that simply cannot be done with a filter based method (Arnott et al., 2000). The photoacoustic method has been touted as the desired way to obtain aerosol light absorption (Andreae, 2001).

Recent improvements have yielded a sensitivity corresponding to a light absorption lower

limit of B_{abs} = 0.15 Mm^{-1} (corresponding to an equivalent BC mass concentration of 30 ng m^{-3}) for the 1047 nm laser, laser power of 200 mW, and 2 minutes averaging time. This is a factor of 3 better than our previous efforts reported earlier (Arnott et al., 1999). The same instrument has been used to measure the real time BC content of diesel vehicle exhaust for heavy-duty diesel trucks on dynamometer test stands at loadings in excess of 30 mg m^{-3}, indicating an excellent dynamic range of 10^6, far exceeding that of filter-based instruments. We have also succeeded in making the photoacoustic instrument very insensitive to ambient noise as indicated by airborne operation in a small plane and ground-based operation only meters away from a fighter jet operating at 80% of maximum power.

So far the photoacoustic technique has been mainly used for the measurement of BC light absorption and the light absorption of ambient aerosols dominated by BC. The photoacoustic technique was used however to measure light absorption in the dust plumes during the 2002 field season. Photoacoustic measurements indicated that the light absorption measured here was several orders of magnitude smaller than the measured scattering, indicating an aerosol albedo extremely close to one. This preliminary result is a consequence of the white carbonate particles encountered at this location.

While BC particles are typically quite small with a typical mass mean diameter of about 100 nm, mineral dust can contain very large particles. This will make it necessary to characterize and possibly modify the sampling arrangement of the photoacoustic instrument for low-loss sampling of large particles.

4.6.2 Emission Factors for Visibility Impairment

Particulate emission factors quantify emissions of PM (particulate matter) mass emitted per unit activity such as vkt (vehicle-kilometers-traveled). Such emission factors are of direct use in conjunction with the U.S. EPA's mass-based $PM_{2.5}$ (PM with aerodynamic diameter smaller than 2.5 μm) and PM_{10} (PM with aerodynamic diameter smaller than 10 μm) standards used to minimize PM health effects. With PM mass emission factors and activity data, PM mass fluxes into a receptor volume can be calculated with dispersion models, yielding ambient PM concentration (i.e., PM mass per volume).

However, PM mass may be a poor surrogate for PM optical properties needed for visibility (Malm, 1999) and radiative transfer applications (Tegen *et al*., 1997; Quinn and Coffman, 1998). In particular, PM scattering is strongly dependent on particle size. For example, for small particles (small compared to the wavelength of the scattered radiation), the mass scattering efficiency is proportional to the third power of the particle diameter (Moosmüller and Arnott, submitted). Therefore, if optical properties of the atmosphere are of concern, it may be advantageous to measure emission factors of optical cross sections directly.

In addition to health-based ambient air quality standards that regulate PM mass concentrations, the U.S. EPA's 1999 Regional Haze Rule sets the stage for a 65-year effort to return visibility, as quantified by the extinction coefficient, to its natural state at 156 national parks and wilderness areas (Watson, 2002; Chow *et al*., 2002). Visibility impairment is primarily caused by light scattering from suspended particles, with

important contributions from both fine (e.g., sulfate, carbonaceous particles) and coarse size fractions (e.g., entrained mineral dust). If PM scattering cross section emission factors are measured, their fluxes into a receptor volume can be calculated. This can in turn provide an estimate of ambient PM scattering coefficients with dimension of inverse distance, which are scattering cross section concentrations, i.e., PM scattering cross sections (dimension of area) per volume.

For visibility and radiative transfer applications, we therefore propose a new paradigm that directly quantifies the flux of visibility impairment by PM into the atmosphere or into a specific airshed with optical cross section emission factors. Such emission factors can be used most directly for non-hygroscopic, inert particles available for long-range transport, where the scattering cross section is largely conserved during mixing and transport. A similar paradigm for the flux of PM absorption cross section has been discussed previously (Bond et al., 1998).

Scattering cross section emission factors were measured for mineral dust entrained by vehicles traveling on an unpaved road. Most unpaved roads consist of a graded and compacted roadbed usually created from the parent soil-material. The rolling wheels of the vehicles impart a force to the surface that pulverizes the roadbed material and ejects particles from the shearing force as well as by the turbulent vehicle wakes (Nicholson *et al*., 1989; Moosmüller *et al*., 1998). Studies have found that dust emission rates depend on the fine particle content of the road (Cowherd et al., 1990), soil moisture content, vehicle speed (U.S. EPA, 2003), and vehicle weight.

To determine scattering coefficients in vehicle dust plumes downwind of an unpaved road, a novel nephelometer operating in the green spectral region at 532 nm with an enhanced capability for accurately measuring scattering from large particles was used (Varma *et al*., 2003). Fluxes and emission factors for scattering cross section were calculated from these data in conjunction with vertical plume and wind velocity profiles. The resulting scattering cross section emission factors were analyzed with respect to their dependence on vehicle weight and speed.

4.6.2.1 Setup of Visibility Impairment Experiment

This work was a part of the CP-1191 study on PM_{10} emissions from military vehicles traveling on unpaved roads. Field experiments were conducted from April 11 through April 24, 2002 on a spur road south of Loyalty Lane at Ft. Bliss, a military base near El Paso, TX (Gillies *et al*., in press; Etyemezian *et al*., 2004).

During the study period, brief rain occurred, but the soil surface dried rapidly due to springtime wind and sun. For all tests reported here, the unpaved road was dry and the soil moisture content for at least the top several centimeters was near zero (Etyemezian *et al*., 2004). The surroundings of the unpaved road are arid with a sparse vegetation cover and most of the surface has previously been disturbed by various military activities. The prevailing winds were from the west, approximately perpendicular to the north-south road. Three towers were set up collinearly and perpendicular to a 1,000-m section of the road in the open range of Ft. Bliss. The three towers were downwind (i.e., east) of the road at distances of 7 m, 50 m, and 100 m from the road. Two integrating nephelometers (DRI ISIN and RR M903), the DRI PA, and a TSI DT were set up in a trailer near tower

3, 100 meters downwind of the road. The sampling inlet for these instruments was located at a height of 5.7 m to match the height of a DT mounted on tower 3. On tower 3, mass concentrations and wind velocity were measured with DTs and anemometers deployed with approximately logarithmic vertical spacing at 1.25 m, 2.6 m, 5.7 m, and 12.2 m above ground level (AGL) with an additional DT mass concentration measurement at 0.4 m AGL. A schematic of the setup is shown in Fig. 4.34.

Vehicles used for dust entrainment during this study include standard commercial vehicles and common military vehicles with vehicle types and relevant specifications listed in Table 4.9.

4.6.2.2 Visibility Impairment Instrument Descriptions

In this study, the recently developed DRI Integrating Sphere Integrating Nephelometer (ISIN) was used for measuring the light scattering coefficient (B_{sca}) and a photoacoustic instrument was used to measure the light absorption coefficient (B_{abs}).

The DRI ISIN is a cell-reciprocal nephelometer specifically designed to accurately measure the light scattering coefficient from large particles, such as the ones contained in freshly entrained road dust (Varma *et al*., 2003). Commercially available integrating nephelometers have two major shortcomings for this application: poor sampling of large particles and poor detection of near forward scattering, which constitutes about half of the total scattering for large particles (Moosmüller and Arnott, 2003). The DRI ISIN addresses these imperfections through reducing sampling losses by employing a straight vertical flow path and an appropriate flow velocity, and by using an integrating sphere design with forward and backward truncation angles of 1°, compared to 7° to 10° truncation angles found in commercial designs. For example, for a truncation angle of 7°, 25% of scattered light is not detected (i.e., truncated) for particles of 2.3 µm diameter, greater losses are encountered for larger particles. For the DRI ISIN's truncation angle of 1°, 25% loss occurs at a much larger diameter of 16µm (Varma *et a*l., 2003). The low ISIN truncation angles are achieved through truncation reduction tubes attached on the inlet and outlet of the integrating sphere. The DRI ISIN operates in the green spectral region at 532 nm and has a large dynamic range for scattering coefficient measurements with an upper measurement limit larger than 50,000 Mm^{-1}.

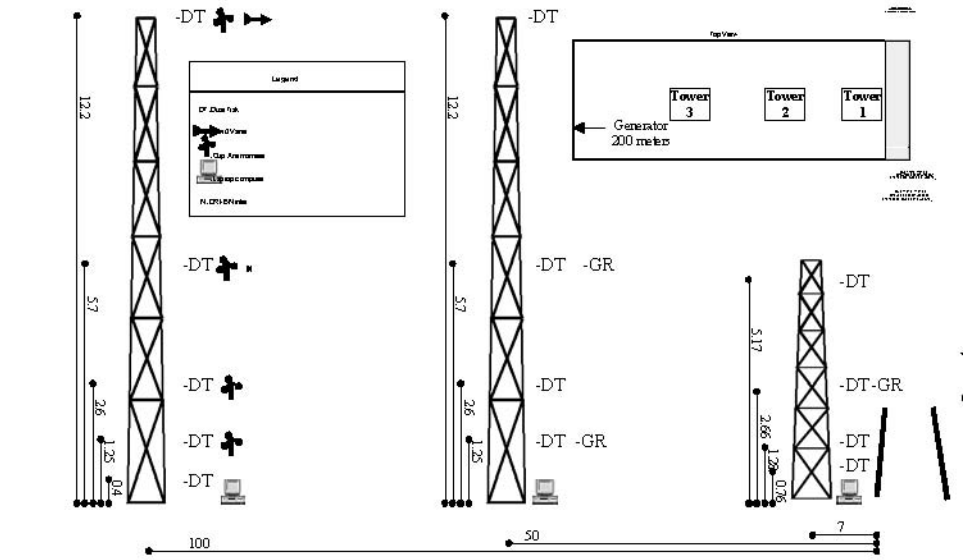

Figure 4.34. Experimental setup for the fugitive dust study at Ft. Bliss near El Paso, TX. The road is to the right of the 5 m tower and the prevailing wind was from right to left (westerly).

Table 4.9. Test vehicles and some of their specifications used in the visibility impairment study.

Vehicle Type (units)	**Model Year**	**Mass (kg)**	**Length (m)**	**Width (m)**	**Height (m)**	**Under-Carriage Area (m^2)**	**Number of Wheels**
Dodge Neon	2002	1176	4.34	1.71	1.42	7.43	4
Ford Taurus	2002	1516	5.08	1.83	1.41	9.30	4
Dodge Caravan	2002	1759	5.09	1.83	1.76	9.31	4
HMMWV	n/a	2445	4.57	2.16	1.83	9.87	4
G20 Van	1979	3100	5.10	1.85	2.00	9.44	4
M1078 LMTV	n/a	8060	6.43	2.44	2.69	15.69	4
M915A4 Freightliner	n/a	8982	14.73	2.44	n/a	35.92	22
M923A2 (5-ton)	n/a	14318	8.74	2.44	3.07	21.32	6
M977 HEMTT	n/a	17727	9.96	2.44	2.85	24.29	8
n/a: data not available							

wind
direction

For comparison, we also employed the commercially available Radiance Research (RR) M903 integrating nephelometer. The RR M903 integrating nephelometer operates at a nominal wavelength of 530 nm and has a forward truncation angle of about 10°. The RR M903 nephelometer has a measurement range with an upper limit of about 1000 Mm^{-1} (Operation manual, Radiance Research). For measurement of gaseous and ambient fine particle scattering (no dust entrainment), the RR M903 and DRI ISIN show excellent agreement while the DRI-ISIN readings were up to four-times higher than those of the RR M903 for freshly entrained coarse particulate matter. This large discrepancy is attributed to the improved angular response, including a reduction of the truncation error by up to a factor of two, and the improved large particle sampling of the DRI ISIN compared to the RR M903 (Varma *et a*l., 2003). Therefore, only DRI ISIN scattering coefficients were used in the following.

The Photoacoustic (PA) Spectrometer, developed at the DRI (Arnott *et al*., 1999, 2000, 2003), directly measures the optical absorption by atmospheric gases and particles at a wavelength of 532 nm. Light absorption by PM converts light energy to an acoustic

pressure wave in the DRI PA instrument. A microphone detects the acoustic signal, and hence a measure of light absorption is produced. The DRI PA does not use any filters for absorption measurements and has a lower detection limit of 0.5 Mm^{-1}. Absorption coefficients of vehicle-entrained dust, measured with the DRI PA, were negligible for the experiments described here.

The TSI DUSTTRAK Aerosol Monitor (DT) is a portable, battery-operated, laser-photometer that measures 90° light scattering and reports it as PM mass concentration. The reported PM mass concentration is factory-calibrated using the respirable fraction of an Arizona Road Dust standard (ISO 12103-1, A1). The ISO 12103–1, A1 standard consists of primarily silica particles (70%) that are provided with some particle size specifications. By volume, the standard consists of 1–3% particles with diameter less than 1 µm, 36–44% with diameter less than 4 µm, 83–88% with diameter less than 7 µm, and 97–100% with diameter less than 10 µm. A pump draws the sample aerosol through a PM_{10} inlet into an optical chamber where it is measured. A sheath air system isolates the aerosol in the chamber to keep the optics clean. The DT measurements were made at several vertical levels as explained below.

Besides the DT, four anemometers, one wind vane, and one temperature probe were mounted on the tower in order to characterize the local meteorological conditions. The meteorological data were averaged and stored in 5-minute intervals.

4.6.2.3 Calculation of Scattering Cross Section Emission Factors

Visibility relevant emissions can be characterized by the emitted cross-sections σ for scattering σ_{sca}, absorption σ_{abs}, and extinction σ_{ext}, with $\sigma_{ext} = \sigma_{sca} + \sigma_{abs}$. In this study, $\sigma_{abs} \approx 0$ (as measured with the photoacoustic instrument) for vehicle entrained dust and therefore $\sigma_{ext} = \sigma_{sca}$. For a vehicle traveling on a homogeneous road, we are interested in measuring a PM cross section emission factor EF_{scat} giving the emitted scattering cross-section σ_{sca} per distance d traveled (in units of vkt = vehicle-km-traveled). We can write this emission factor as:

$$EF_{sca} = \frac{\sigma_{sca}}{d} = \frac{\sum_i \sigma_{sca\_i}}{vt} \quad (4)$$

where t is the time it takes to travel the distance d at the vehicle speed v and the emitted scattering cross section σ_{sca} can be expressed as the sum of the scattering cross sections σ_{sca_i} of all individual emitted particles.

Monitoring the scattering coefficient B_{sca} at a distance d_0 downwind from the road, we can approximate the road as a homogeneous line source if $d >> d_0$ and we may write the emission factor EF_{scat} as:

$$EF_{sca} = \frac{\sigma_{sca}}{d} = \frac{\int B_{sca}\, dV}{d} = \int B_{sca}\, dA = \int \left(\int v_{\perp} B_{sca}\, dt \right) dh \quad (5)$$

where v is the wind velocity component perpendicular to the road, the integral of B_{sca} over time t is our primary measurement, and the integral over height h takes the vertical extent of the plume into account. For the sparsely vegetated site, deposition between the road and measurement site can be neglected (Etyemezian *et al.*, 2004).

Both wind velocity v and scattering coefficient B_{sca} vary with height and time. The wind velocity is measured continuously at several heights on tower 3 and generally follows a logarithmic profile averaged over the dust plumes (Moosmüller et al., 1998). The scattering coefficient B_{sca} is measured with the DRI ISIN at 5.7 m inlet height. The DT measurements at several heights on tower 3 are normalized with the ISIN measurement at 5.7 m height to yield a vertical profile of B_{sca} over the plume under the assumption that the proportionality factor between ISIN and DT measurement is independent of plume height.

The unpaved road on which experiments were performed runs in a North-South direction; therefore the optimum wind direction for emission factor measurements is westerly, which is also the dominant wind direction. In this case, the wind direction is along the tower line and perpendicular to the road resulting in a maximum mass flux density along the tower line. To limit systematic measurement errors due to inhomogeneity of the road surface along its length and random errors due to insufficient plume density, only vehicle passes with the wind direction within 70º of westerly are used for analysis.

4.6.2.4 Scattering Cross Section Emission Factors Results and Discussion

Scattering cross section emission factors EF_{sca} were measured for 9 different vehicles (Table 4.9) with vehicle masses ranging from 1176 kg (Dodge Neon) to 17727 kg (M977 HEMTT) at speeds ranging from about 8 km/h to about 80 km/h. For each vehicle and speed, dust emissions for between 2 and 16 vehicle passes were measured and used to calculate scattering cross section emission factors EF_{sca} with Eq 5. The resulting emission factors EF_{sca} range from 12.5 ± 2.1 m^2/vkt (Neon at 16 km/h) to 3724 ± 873 m^2/vkt (HEMTT at 64 km/h) and generally increase with both vehicle speed and mass. These emission factors are shown in Fig. 4.36 as function of vehicle speed, where error bars denote the standard deviation of the mean derived from repeated vehicle passes. These error bars are indicative of variations between vehicle passes, but do not give an absolute measurement of accuracy. Also note that for some vehicles (i.e., Neon and HMMWV) only data from 2 passes for each speed were available. Emission factors EF_{sca} for individual vehicles can be approximated as linear function of vehicle speed as:

$$EF_{sca} = EF_{sca/sp} \quad (6)$$

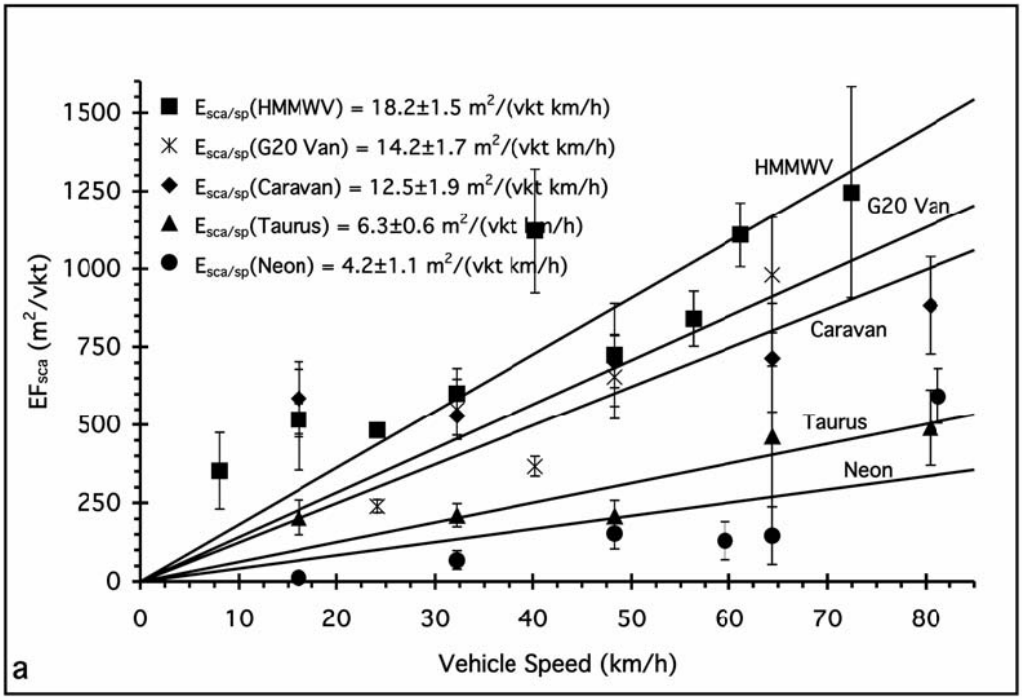
$E_{sca/sp}$(HMMWV) = 18.2±1.5 m²/(vkt km/h)
$E_{sca/sp}$(G20 Van) = 14.2±1.7 m²/(vkt km/h)
$E_{sca/sp}$(Caravan) = 12.5±1.9 m²/(vkt km/h)
$E_{sca/sp}$(Taurus) = 6.3±0.6 m²/(vkt km/h)
$E_{sca/sp}$(Neon) = 4.2±1.1 m²/(vkt km/h)
HMMWV
G20 Van
Caravan
Taurus
Neon
EFsca (m²/vkt)
Vehicle Speed (km/h)
0
250
500
750
1000
1250
1500
0
10
20
30
40
50
60
70
80
a

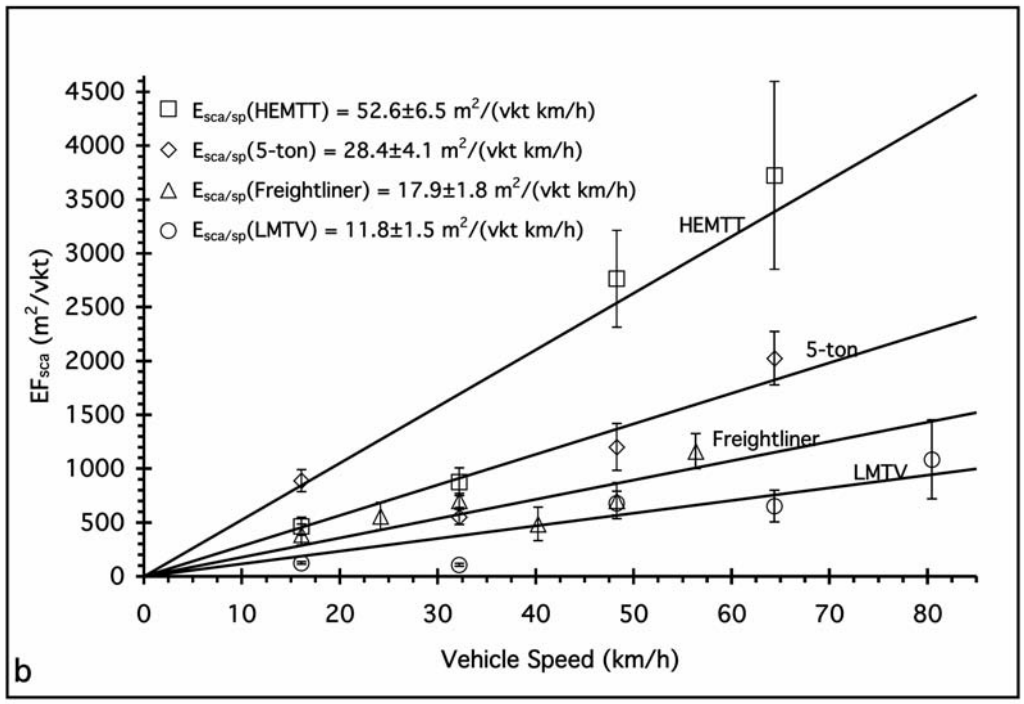

Figure 4.35. Scattering coefficient emissions factors EF_{sca} as function of vehicle speed for light (a) and heavy (b) vehicles. Solid lines show a linear regression (forced through zero) for each vehicle with the slope being the scattering coefficient emissions factors per vehicle speed $EF_{sca/sp}$.

where $EF_{sca/sp}$ is obtained as the slope of a linear regression of emission factors EF_{sca} versus vehicle speed v (Fig. 4.35). Numerical values of the scattering cross section emission factor per speed $EF_{sca/sp}$ and their standard errors are given in Table 4.10 and Fig. 4.36 for all 9 vehicles with emission factors $EF_{sca/sp}$ ranging from 4.2 m^2/(vkt km/h) for the Neon to 53 m^2/(vkt km/h) for the HEMTT with a fractional uncertainty between 8% and 15% for most vehicles.

A linear regression approximating the relationship between the scattering cross section emission factor per speed $EF_{sca/sp}$ and the vehicle mass m may be written as:

$$EF_{sca/sp} = EF_{sca/(spm)} \quad (7)$$

where the scattering cross section emission factor per vehicle speed and mass $EF_{sca/(sp\ m)}$ is obtained as the slope of the linear regression of emission factors $EF_{sca/sp}$ versus vehicle mass m (Fig. 4.37). A regression for all vehicles yields $EF_{sca/(sp\ m)}$ as:

$$EF_{sca/(spm)} = 0.0025 \pm 0.0003 \, m^2/(vkt(km/h)kg) \quad \text{(for all vehicles)} \quad (8)$$

However, it is obvious from Fig. 4.36 that the 9 vehicles should be separated into two categories; 5 light vehicles (vehicle mass $m \leq 3100$ kg) and 4 heavy vehicles (vehicle mass $m > 8000$ kg). Individual linear regressions for these two vehicle categories yield $EF_{sca/(sp\ m)}$ as:

$$EF_{sca/(spm)} = 0.0056 \pm 0.0007 \, m^2/(vkt(km/h)kg) \quad \text{(for light vehicles)} \quad (9)$$

$$EF_{sca/(spm)} = 0.0024 \pm 0.0003 \, m^2/(vkt(km/h)kg) \quad \text{(for heavy vehicles)} \quad (10)$$

The emission factor for heavy vehicles is, within its uncertainty, identical to that for all vehicles while the emission factor for light vehicles is more than a factor of two larger. This difference may be due to different dust entrainment mechanisms as a function of vehicle mass and possibly also due to other correlated parameters such as vehicle size and tire pressure.

In this study, the light vehicles emit significantly more scattering cross section per vehicle speed and mass than the heavy vehicles, which may be due to increased PM mass emissions and/or due to an increased scattering mass efficiency of the emitted PM mass. To investigate these possibilities, the results presented here are compared with previously published results on PM_{10} mass emissions measured during the same study (Gillies *et al.*, in press). This previous work approximates the PM_{10} mass emissions per vehicle speed as a single linear function of vehicle mass showing no obvious differences between the light and heavy vehicles. Table 4.10 lists, in addition to the scattering cross section emission factors $EF_{sca/sp}$, PM_{10} mass emission factors $EF_{mass/sp}$. The PM_{10} mass scattering

efficiency E_{sca} can be calculated from these two sets of emission factors, under the assumption that most or all of the measured scattering is due to PM_{10}, as

$$E_{sca} = \frac{EF_{sca/sp}}{EF_{mass/sp}} \quad (11)$$

and the resulting mass scattering efficiencies are listed in Table 4.9. These mass scattering efficiencies range from 0.6 m^2/g to 2.0 m^2/g with the exception of one outlier for the Neon with E_{sca} = 5.1 m^2/g. This outlier is caused by the fact that the PM_{10} mass emission factors $EF_{mass/sp}$ is drastically smaller than those of the somewhat larger vehicles while the scattering cross section emission factors $EF_{sca/sp}$ is only somewhat smaller. The outlier may also be related to the

Table 4.10. Scattering cross section emission factor per speed $EF_{sca/sp}$, mass emission factor per speed $EF_{mass/sp}$, and resulting mass scattering efficiency E_{sca} for all vehicles.

Vehicle Type (units)	**$EF_{sca/sp}$ (m^2/(vkt km/h))**	**$EF_{mass/sp}$ (g-PM_{10}/(vkt km/h)**	**E_{sca} (m^2/g)**
Dodge Neon	4.2 ± 1.1	0.83 ± 0.09	5.1 ± 1.8
Ford Taurus	6.3 ± 0.6	6.0 ± 0.5	1.0 ± 0.2
Dodge Caravan	12.5 ± 1.9	9.6 ± 0.8	1.3 ± 0.3
HMMWV	18.2 ± 1.5	9.2 ± 0.7	2.0 ± 0.3
G20 Van	14.2 ± 1.7	9.0 ± 0.9	1.6 ± 0.4
M1078 LMTV	11.8 ± 1.5	18.5 ± 2.2	0.6 ± 0.2
M915A4 Freightliner	17.9 ± 1.8	23.9 ± 1.3	0.8 ± 0.1
M923A2 (5-ton)	28.4 ± 4.1	47.4 ± 7.0	0.6 ± 0.2
M977 HEMTT	52.6 ± 6.5	48.3 ± 3.7	1.1 ± 0.2

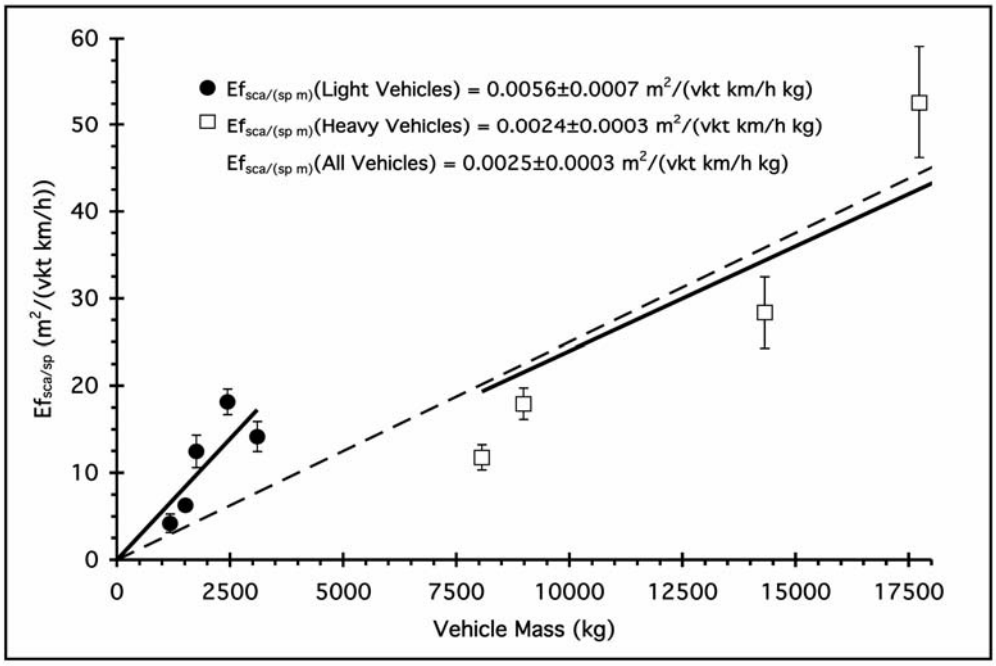

Figure 4.36. Scattering coefficient emissions factors per vehicle speed $EF_{sca/sp}$ as function of vehicle mass. Lines show linear regressions (forced through zero) for all vehicles (dashed line), heavy vehicles, and light vehicles with the slopes being the scattering coefficient emissions factors per vehicle speed and mass $EF_{sca/(sp\ m)}$.

extremely small number of vehicle passes used to derive the emission factors for the Neon and therefore will not be considered in the following discussion of the mass scattering efficiencies. Neglecting the outlier, the average mass scattering efficiency for the lighter vehicles is E_{sca_light} = 1.5±0.4 m^2/g and that for the heavy vehicles is E_{sca_heavy} = 0.8±0.2 m^2/g. This indicates that most of the difference in scattering cross section per vehicle speed and mass between light and heavy vehicles is due to the increased scattering mass efficiency of the emitted PM mass for light vehicles. This difference in scattering mass efficiency may be explained with Mie theory by heavy vehicles emitting larger-diameter PM than light vehicles. The mass scattering efficiencies obtained here are significantly larger than the value of 0.4 m^2/g, previously used for PM entrainment from an unpaved shoulders along a paved road (Moosmüller *et al*., 1998). However, entrainment from unpaved shoulders is due to aerodynamic shear stress from the vehicles wake, while entrainment from unpaved roads is largely facilitated by tire – road surface interactions. In interpreting the mass scattering efficiencies presented here, it must be

considered that the PM_{10} mass emissions given by Gillies *et al*. (in press) were measured with a light scattering instrument (TSI DustTrak) and may not be exactly equivalent to true mass measurements.

4.6.2.5 Scattering Cross Section Emission Factors Conclusions

For vehicles traveling on an unpaved road, scattering cross section emission factors have been determined and parameterized as function of vehicle speed and mass. In addition, comparison with mass emission factors resulted in mass scattering efficiencies.

Further work is needed to improve our understanding of the parameterization in terms of physical processes leading to entrainment of different PM sizes as function of entrainment parameters. For example, is vehicle mass really a primary parameter controlling entrainment or would it be more useful to replace it with a combination of tire pressure and vehicle mass? This question could be studied with a single vehicle by varying its mass and tire pressure. Also, the influence of vehicle generated turbulence on PM entrainment and injection into the atmosphere needs to be further studied (Gillies *et al*. in press).

4.6.3 Optical Remote Sensing

While the *in situ* instruments yield well-calibrated quantitative measurements of light extinction and its scattering and absorption components, they do not provide any information about the three-dimensional distribution of optical properties. In an attempt to gain understanding of the optical properties of the dust plumes in three dimensions we deployed a Light Detection and Ranging system operated by NASA personnel and a sun photometer operated by University of Arizona personnel under the direction of Utah State University collaborators on this project.

4.6.3.1 Holographic Airborne Rotating Lidar Instrument (HARLIE)

The main objective for the HARLIE measurements during the Fort Bliss field campaign was to enhance the value of the *in situ* measurements by extending them in space horizontally and vertically, and providing measurements upwind into ambient air. HARLIE was located on the edge of a small bluff approximately 2 km due east of the DRI mobile lab and the three towers supporting the *in situ* instruments. This bluff is part of the local sanitary landfill that has been capped and is a few meters higher in elevation than the base of the monitoring towers. The entire landfill compound is devoid of vegetation and there is active dumping taking place a few hundred meters west of HARLIE that often raised significant windblown dust plumes, which were then transported and dispersed by the prevailing westerlies over the test range. In addition, occasional army troop training activities would take place in the space between HARLIE and the vehicle test area raising additional dust plumes. Since HARLIE remotely sensed aerosol measurements over this region continuous in space and time, it was believed that it would be possible to identify fugitive emission plumes created by non-participants that contaminated the planned experiment tests.

HARLIE backscatter signals in principal should be useful in raw form for locating and defining the spatial extent of aerosol plumes, but they are only relative measures of aerosol density. In order to relate HARLIE backscatter signals to aerosol number or mass density and optical extinction measurements, the HARLIE data must be calibrated against

coincident measurements of absolute backscatter and extinction coefficients taken with a nephlometer and an extinction meter and should have a range dependent extinction correction applied. These instruments were located at the base of the tower farthest from the road used for the test vehicles, in a laboratory trailer. Once data from these instruments were available, it should be possible to process the HARLIE data to absolute calibration.

NASA-GSFC unfortunately found during post processing of the backscatter data that the LIDAR instrument had fatal technical problems that in the end precluded any meaningful analysis of these data. The principal problem with HARLIE appears to have been a malfunctioning temperature control valve in the laser cooling system. It was thought that a correction algorithm could be constructed, but this was in the end not possible and the corruption in the data was too severe to allow corrections to be applied with any confidence. Unfortunately, this component of CP-1191 was not successful in its objective. The use of LIDAR techniques still holds great potential for providing insight into dust plume behavior over distances that are not achievable with *in situ* monitoring. The application and refinement of this technique should be further pursued, as there is substantial opportunity to provide insights into the mechanics of dust emission, transport, and deposition with this measurement method.

4.6.3.2 Solar Radiometric Measurements: The Sun Photometer

The Remote Sensing Group (RSG) of the University of Arizona, Tucson, collected data in support of CP-1191 at Fort Bliss April 8-24, 2002 during the period when dust emissions from wheeled vehicles were being carried out. What follows is a description of the approach used for the data collection and a summary of the results from this work. Weather conditions for the collections were monitored using a handheld portable barometer and thermometer and cloud conditions were monitored visually. The equipment used for the atmospheric measurements in all cases was an automated 10-band solar radiometer. The solar radiometer was relatively calibrated immediately prior to the field campaign and this calibration was verified after the campaign as well. In both cases, the radiometer was also cross-compared to two other similar instruments used by the RSG and shown to be in agreement to better than 1% in output giving agreement to better than 0.01 in spectral optical depth.

The solar radiometer data are used in a Langley method retrieval scheme to determine spectral atmospheric optical depths. The optical depth results are used as part of a simple power-law inversion scheme to determine ozone optical depth and an Angstrom turbidity coefficient (or equivalently a Junge distribution). The advantage to such a distribution is that it requires only one number to define the aerosol size distribution, the so-called Junge Parameter. Columnar water vapor is derived from the solar extinction data using a modified-Langley approach. The nominal uncertainties for these results are the 0.01 for the aerosol retrieval, 0.3 in Junge parameter, 10% in water vapor, and 20% in ozone. Precision of the instrument however is typically a factor of 10 better than this. The uncertainties in all quantities are primarily a function of the accuracy of the calibration of the solar radiometer. An additional source of error is that the aerosols may not follow a Junge law (especially true of newly created dust in the atmosphere). Data were collected and processed for a total of 12 dates (April 8, 10, 11, 12, 14, 15, 16, 18, 19, 22, 23, and 24).

The dates for which there are sufficient confidence to compute background aerosol size distributions are April 8, 11, 15, and 16, 2002. On all of these dates were periods for which there were low wind conditions, clear skies, and successful solar radiometer data collections. The range of Junge parameter for these dates was quite small with values from 2.8 to 3.1 and excluding values on the 16th give an even smaller range with values from 3.0 to 3.1. The lower values were seen on April 16 and could possibly be due to sub-visual clouds in front of the sun since there were thin clouds noted in other portions of the sky.

While many of the dates included measurements with visible dust clouds, the short period of many of these clouds or contamination from clouds limits the analysis of these data. Thus, the best data set to evaluate is the period on April 16, 2002 from 2000 to 2200 UTC. The 550 nm optical depth derived from the power law retrieval with the average 550 nm optical depth value from the early morning period prior to the vehicular tests. The average optical depth found during this early morning period was 0.0639 with a 1-σ standard deviation of 0.002. The Junge parameter is found by subtracting the background size distribution from the values determined during the vehicular test. The background Junge parameter was found to be 2.80 with a 1-σ standard deviation of 0.03.

Several key results emerged from the sun-photometer measurements. The first is that the residual Junge parameter is relatively constant during the entire test period. The average value is 1.98 with a 1-σ standard deviation of 0.04. This value of Junge parameter indicates particle sizes such that there is close to no spectral effects of the scattering by the raised dust particles. The near constancy of the residual Junge parameter is indicated by the fact that the standard deviation is nearly the same value as found during the early morning background period.

A second interesting result is that the residual Junge parameter that is found does not appear to be strongly correlated to the optical thickness due to the dust. Thus, while the optical depth changes from 0.04 to 0.10 the sizes of the particles do not change. This is interesting because it indicates that over a period of two hours, the transport, creation, and gravitational settling of the particulates is insufficient to alter the relative sizes of the particles and only the concentration changes. This is also corroborated by the analysis of the particle size data collected with the GRIMM 1.108 (see section 4.3 and Etyemezian et al., 2004), which showed very little deposition of particles <20 μm over the 100 m travel distance from source to receptor.

Averaging the optical depth due to the raised dust gives a value of 0.070 with a standard deviation of 0.015. Again, this is the average value due to the inferred dust loading only since the background dust has been subtracted. Considering that the average optical depth for the background aerosols is found to be 0.0064 with a standard deviation of 0.002, it is remarkable that the dust nearly doubles this optical thickness. Crudely speaking, the dust raised from the vehicular traffic is larger in most cases then the entire amount of dust throughout the atmosphere prior to the movement of the vehicles. In addition, the confidence that this extra aerosol loading is not due to a change in background atmospheric condition is inferred from the high standard deviation of the vehicular dust. This indicates the transient nature of the aerosols measured in this time period. Of course, this could be due to water/ice clouds, but the comments made by

visual observation make no mention of visible clouds near the sun during this period and aerosols of this optical depth magnitude would be easily visible. The final observation is that during the time period around 2120 UTC (04-16-02), there does appear to be a correlation between the optical depth and the Junge parameter. However, this trend is the opposite of what would be expected if there were a correlation. That is, if the optical depth decreases, one would attribute this to a loss of aerosols with larger particles settling sooner than smaller particulates. This would lead to a larger Junge parameter. This fact, coupled with the fact that no similar correlation is seen around 2030 UTC indicates that the "correlation" is most likely coincidental.

Ideally, a greater number of clearly recognizable dust cases would allow the results from April 16 to be verified. Unfortunately, the limitation of the solar radiometer approach is that it requires a clear understanding of a stable and well-characterized background aerosol. Thus, when measurements of a transient dust cloud occur, the transient aerosol can be separated from the background allowing an inference of the nature of the transient case. Combinations of cloudy conditions and lack of known transient dust conditions limits the results shown here to a two-hour period on one day of the entire campaign. This is unfortunate, and it is hoped that future data sets or other independent data sets from the same campaign can verify the results found from the solar radiometer data.

The two critical results found here were:

1) the windborne dust seen at Ft. Bliss is of a size and composition that leads to a spectrally invariant extinction coefficient,

2) the size distribution does not depend on the concentration of the windborne dust.

Several questions still remain unanswered after these collections and they are:

1) How long do the dust particles remain airborne?

2) Are the results from April 16 indicative of typical dust behavior?

3) If the extinction is spectrally neutral why does the dust appear brown?

The first of these questions could realistically have been answered with a data collection on the 17th of April but clouds prevented this from happening. The data from April 18 and 19 are also cloud contaminated and thus it is not until the 22nd when there are sufficient data to indicate a background aerosol. At this point, the atmospheric optical depths approach those on the 16th and prior dates, but it is likely that the background conditions were present prior to the 22nd. The second two questions can only be answered with subsequent collections or with other measurement sets. Overall, the results of these collections are encouraging in terms of using solar radiometry to assess aerosol conditions due to windborne dust. The ability to reconfigure the instrumentation to operate at 1-s time intervals improved significantly the data set collected here. For future work, the following are recommended:

1) documentation of sky conditions using digital or film camera systems,

2) development of simple two-band radiometers with wavelengths at 400 and 780 nm that can be deployed at alternate locations to examine the spatial variability of the dust,

3) better documentation of vehicular passes to allow correlation of measurements

4) operation of the solar radiometer whenever clear skies permit to ascertain a better understanding of the background conditions.

Implementing these ideas would greatly enhance the understanding of data sets similar to the one discussed here. Even without these suggestions, there is still reasonable confidence in the results produced here though further verification is still needed.

4.7 Development of Emission Components for the DUSTRAN GIS-based emission model.

As part of CP-1191 objectives the information on dust emission factors was converted into algorithms to be used within the CP-1195 DUSTRAN model. The DUSTRAN graphical interface allows the user to graphically identify the locations of training activities on a map and allows for specifying the types, speeds, and number of vehicles active during an exercise. The active-emission component of the dust module represents dust emissions as the product of an empirically formulated emission factor and the vehicle activity, the latter taken as the total vehicle distance traveled (summed if there are multiple vehicles) in a given period of interest. The emission factor is an estimate of the amount of PM emissions that result from incremental levels of a certain activity and, in the case of road dust, is expressed as the mass of particles in a given size range emitted as a result of a unit of vehicle travel (e.g., grams per vehicle kilometers traveled or g/vkt). Through the interface, the user specifies the time of the training exercise, duration of the exercise, size of modeling domain (depends on whether interest is in near-field or far-field impacts), duration of the simulation, and source of meteorological data. After execution of the dispersion model, the ground-level dust air concentrations and deposition fields are displayed graphically within the GIS.

4.8 Conclusions

CP-1191 had considerable success in meeting its target objectives (see Section 1). It was determined that for the most part dust emissions attributable to Ft. Bliss were a significant contribution to ambient PM_{10} when there were high winds that caused wind blown dust to be generated within the installation. It was not possible to resolve with current measurement techniques the dust that was raised by testing and training activities within Ft. Bliss beyond the post boundaries. The quantifying contributions from testing and training can best be served with a more thorough understanding of the strength of the source contributions (i.e., emission factors) and also improved modeling of the transport and fate of the particulate matter as it disperses from the source area and interacts with the surface over which it travels.

This project was very successful in developing emission factors for military vehicle from unpaved roads producing specific emission factors for 5 military vehicles, but more importantly it was determined that the strength of emission were well explained by the product of vehicle weight and speed. This provides an important general relationship that can be used for any vehicle type. The emission factor information was also linked to the TRAKER on-vehicle measurement system emission potential. The TRAKER can be used to map dust emission potential and the quantity then adjusted to reflect other

vehicles based on knowledge of their mass and speed. An open area of inquiry in this research area is to further develop understanding the relative roles of the aerodynamic and mechanical forces that cause the emission of dust from the surface. This is also an open question for tracked vehicles and aircraft as well.

It was observed that at Ft. Bliss under the climatic conditions that prevailed and the sparsely vegetated desert community the transport of the dust from the unpaved road surface was not diminished over the travel distances measured (~100m). An attempt was made to model the transportable fraction of the dust emitted, but this remains one of the most highly uncertain aspects of the work. The measurements by CP-1191 made at Ft. Bliss are very different to the data published by Veranth et al. (2003) that shows deposition of PM_{10} over ~100 m of travel to exceed 85% under stable atmospheric conditions and in the presence of large roughness elements. Resolving the processes that affect dust deposition and accounting for their effect on the transportable fraction of dust remains a critical area of research.

The role of surface disturbance and its effect on dust emissions by wind were addressed in this research. The principle finding was that the amount of loose sand created by the disturbance was a major control on the surface's subsequent ability to emit dust when acted upon by wind. Quantifying disturbance levels and their effect on wind driven dust emissions needs to take this aspect of the disturbance into account. Further research on the relationship between the textural qualities of the disturbed soil (i.e., %sand, silt and clay) would be useful to extend the results of CP-1191 to other areas.

New and innovative instrumentation was used in this research to characterize the visibility degrading properties of the emitted dust. The data from the DRI-ISIN was used to develop a new type of emission factor that quantifies directly the amount of light scattering associated with the fresh dust emissions. This work would be enhanced through a quantification of the visibility degrading potential of the particles that are available for long-distance transport, which also links with the recognition that modeling the mass fraction of the emissions available for long distance transport remains uncertain.

CP-1191 provided data and relationships that were integrated into the GIS-based Complex Terrain Model for Atmospheric Dust Dispersion developed by CP-1195 developed by the research team lead by Dr. Jerry Allwine, Pacific Northwest National Laboratory. It will be important to maintain and further develop the DUSTRAN model and bring it to a level that is usable for DOD personnel. It should also remain flexible for receiving new information on dust emissions as it becomes available from follow on SERDP-supported research and from other information sources as well.

The information developed as part of this project was disseminated through peer-reviewed publications, conference presentations, quarterly and annual reports, as well as this Final Report. The CP-1191 team hopes that this information will provide a valuable resource for the DOD and its installation personnel and an aid to addressing the environmental impacts of dust emissions from testing and training activities at DOD installations.

5. REFERENCES

Andreae, M. O., 2001. The dark side of aerosols. *Nature*, **409**: 671-672.

Arnott, W. P., Moosmüller, H., Rogers, C. F., Jin, T., and Bruch R., 1999. Photoacoustic spectrometer for measuring light absorption by aerosol: instrument description. *Atmos. Environ.* **33**: 2845-2852.

Arnott, W. P., Moosmüller, H., Sheridan, P. J., Ogren, J. A., Raspet, R., Slaton, W. V., Hand, J. L., Kreidenweis, S. M., J. L., and Collett, J., 2003. Photoacoustic and filter-based ambient aerosol light absorption measurements: instrument comparison and the role of relative humidity, *J. Geophys. Res.*, **108**: 4034-4044, doi: 10.1029/2002JD002165.

Arnott, W. P., Moosmüller, H., and Walker, J. W., 2000. Nitrogen dioxide and kerosene-flame soot calibration of photoacoustic instruments for measurement of light absorption by aerosols, *Rev. Sci. Instrum.*, **71**: 4545-4552.

Bagnold, R.A., 1941. *The Physics of Blown Sand and Desert Dunes*. Chapman and Hall, London, 265 pp.

Bond, T. C., Anderson, T. L., and Campbell, D., 1999. Calibration and intercomparison of filter-based measurements of visible light absorption by aerosols. *Aerosol Sci. & Tech*. **30**: 582-600.

Bond, T. C., Charlson, R. J., Heintzenberg, J., 1998. Quantifying the emission of light-absorbing particles: measurements tailored to climate studies, *Geophys. Res. Lett.*, **25**: 337-340.

Borrmann, S. and Jaenicke, R., 1987. Wind tunnel experiments on the resuspension of sub-micrometer particles from a sand surface. *Atmos. Environ.*, **21** (9): 1891-1898.

Chow, J. C., Bachman, J. D., Wierman, S. S. G., Mathai, C. V., Malm, W. C., White, W. H., Mueller, P. K., Kumar, N., and Watson, J. G., 2002. Critical review discussion -- visibility: science and regulation, *J. Air & Waste Manage. Assoc.*, **52**: 973-999.

Chow, J.C. and Watson, J.G., 1999. Ion chromatography in elemental analysis of airborne particle. In: S. Landsberger and M. Creatchman (Editors), *Elemental Analysis of Airborne Particles*. Gordon and Breach Science, Amsterdam, pp. 97-137.

Chow, J.C., Watson, J.G., Ashbaugh, L.L., and Magliano, K.L., 2003. Similarities and differences in PM10 chemical source profiles for geological dust from the San Joaquin Valley, California. *Atmos. Environ.*, **37** (9-10): 1317-1340.

Chow, J.C., Watson, J.G., Crow, D., Lowenthal, D.H., and Merrifield, T., 2001. Comparison of IMPROVE and NIOSH carbon measurements, *Aerosol Sci. & Tech*., **34** (1): 23-34.

Chow, J.C., Watson, J.G., Houck, J.E., and Pritchett, L.C., 1994. A laboratory resuspension chamber to measure fugitive dust size distributions and chemical compositions, *Atmos. Environ.*, **28** (21): 3463-3481.

Chow, J.C., Watson, J.G., Lowenthal, D.H., Solomon, P.A., and Magliano, K.L., 1992. PM10 source apportionment in California's San Joaquin Valley, *Atmos. Environ.* **26A** (18): 3335-3354.

Chow, J.C., Watson, J.G., Pritchett, L.C., Pierson, W.R., Frazier, C.A., and Purcell, R.G.,

1993. The DRI Thermal/Optical Reflectance carbon analysis system: description, evaluation, and applications in U.S. air quality studies, *Atmos. Environ.*, **27A** (8): 1185-1201.

Countess, R., 2001. *Methodology for Estimating Fugitive Windblown and Mechanically Resuspended Road Dust Emissions Applicable for Regional Scale Air Quality Modeling*, Countess Environmental Prepared for the Western Governors Association, Westlake Village, CA.

Cowherd, C., 1999. Profiling Data for Open Fugitive Dust Sources, Midwest Research Institute, Kansas City, MO.

Cowherd, C., Englehart, P., Muleski, G. E., Kinsey, J. S., and Rosbury, K. D., 1990. *Control of Fugitive and Hazardous Dusts*; Noyes Data Corp., Park Ridge, NJ.

Etyemezian, V., Gillies, J.A., Kuhns, H., Gillette, D., Ahonen, S., Nikolic, D., and Veranth, J., 2004. Deposition and removal of fugitive dust in the arid southwestern United States: measurements and model results, *Journal of the Air and Waste Management Association* **54**: 1099-1111.

Etyemezian, V., Gillies, J.A., Kuhns, H., Nikolic, D., Gillette, D., Sheshardi, G., and Veranth, J., 2003c. Estimating near-field removal of fugitive dust: the regionally-transportable fraction of PM_{10} emissions from unpaved roads. In *Proceedings of the A&WMA 96th Annual Meeting and Exhibition*, San Diego, CA, 22-26 June 2003, paper # 69531.

Etyemezian, V., Gillies, J.A., Kuhns, H., Nikolic, D., Veranth, J., Laban, R., Seshadri, G., and Gillette, D., 2003d. *Field Testing and Evaluation of Dust Deposition and Removal Mechanisms*. Prepared for The WESTAR Council, Lake Oswego, OR, 97035 (in print).

Etyemezian, V., Kuhns, H., Gillies, J.A., Green, M., Pitchford, M., and Watson, J., 2003a. Vehicle based road dust emissions measurement (I): methods and calibration, *Atmos. Environ.*, **37**: 4559–4571.

Etyemezian, V., Kuhns, H., Gillies, J.A., Chow, J., Green, M., Hendrickson, K., McGowan, M., and Pitchford, M., 2003b. Vehicle based road dust emissions measurement (III): effect of speed, traffic volume, location, and season on PM_{10} road dust emissions, *Atmos. Environ.* **37**: 4583–4593.

Fujita, E. et al., 1988. *Northern Front Range Air Quality Study: Volume C: Source Apportionment and Simulation Methods and Evaluation*, Report Prepared by Desert Research Institute for Colorado State University, Cooperative Institute for Research in the Atmosphere, Foothills Campus, Fort Collins, CO 80523, Reno.

Fung, K.K., Chow, J.C., and Watson, J.G., 2002. Evaluation of OC/EC speciation by thermal manganese dioxide oxidation and the IMPROVE method, *Journal of the Air and Waste Management Association*, **52** (11): 1333-1341.

Garland, J.A., 1983. Some recent studies of the resuspension of deposited material from soil and grass, in *Precipitation Scavenging, Dry Deposition and Resuspension*, Elsevier, Amsterdam, pp. 1087-1097.

Gertler, A.W., Coulombe, W.G., Watson, J.G., Bowen, J.L., and Marsh, S., 1993. Comparison of PM10 concentrations in high- and medium-volume samplers in a desert environment, *Environmental Monitoring and Assessment*, **24**: 13-25.

Gillette, D.A. Fryear, D.W., Gill, T.E., Levy, T., Cahill, T.A., and Gearhart, E.A., 1997. Relation of vertical flux of particles smaller than 10µm to total aeolian horizontal mass flux at Owens Lake, *J. Geophys. Res.*, **102**: 26009-26015.

Gillette, D.A., Fryrear, D.W., and Ley, T., 1995. Ratio of vertical mass flux of PM10 to total horizontal mass flux of airborne particles by wind erosion, Air & Waste Management Association 88th Annual Meeting and Exhibition, San Antonio, TX, pp. 95-TA38.02, 1-16.

Gillette, D.A. and Walker, T.R., 1977. Characteristics of airborne particles produced by wind erosion of sandy soil, High Plains of West Texas, *Soil Science*, **123**: 97-110.

Gillies, J.A., Arnott, W.P., Etyemezian, V., Gillette, D.A., Kuhns, H., McDonald, E., Moosmüller, H., Nickling, W. G., Schwemmer, G., and Wilkerson, T., 2001. *Characterizing and Quantifying Local and Regional Particulate Matter Emissions from Department of Defense Installations: Annual Report 2001*, Desert Research Institute Prepared for Strategic Environmental Research and Development (SERDP), Arlington, VA, 22203-1821, Reno, NV.

Gillies, J.A., Arnott, W.P., Etyemezian, V., Gillette, D.A., Kuhns, H., McDonald, E., Moosmüller, H., Nickling, W. G., Schwemmer, G., and Wilkerson, T., 2002. *Characterizing and Quantifying Local and Regional Particulate Matter Emissions from Department of Defense Installations: Annual Report 2002*, Desert Research Institute Prepared for Strategic Environmental Research and Development (SERDP), Arlington, VA, 22203-1821, Reno, NV.

Gillies, J.A., Arnott, W.P., Etyemezian, V., Gillette, D.A., Kuhns, H., McDonald, E., Moosmüller, H., Nickling, W. G., Schwemmer, G., and Wilkerson, T., 2003b. *Characterizing and Quantifying Local and Regional Particulate Matter Emissions from Department of Defense Installations: Annual Report 2003*, Desert Research Institute Prepared for Strategic Environmental Research and Development (SERDP), Arlington, VA, 22203-1821, Reno, NV.

Gillies, J.A., Etyemezian, V., Kuhns, H., Nikolic, D., and Gillette, D.A., 2003. Effect of vehicle characteristics on unpaved road dust emissions, in: R. Joumard (Editor), 12th International Symposium "Transport and Air Pollution", INRETS, Avignon, France, pp. 51-58.

Gillies, J.A., Etyemezian, V., Kuhns, H., Nikolic, D., and Gillette, D.A., 2005. Effect of vehicle characteristics on unpaved road dust emissions, *Atmos. Environ.* (in press).

Gillies, J.A., Watson, J.G., Rogers, C.F., DuBois, D., and Chow, J.C., 1999a. Long-term efficiencies of dust suppressants to reduce PM10 emissions from unpaved roads, *Journal of the Air & Waste Management Association*, **49**: 3-16.

Hansen, A.D.A., Rosen, H., and Novakov, T., 1984. The Aethalometer - an instrument for the real-time measurement of optical absorption by aerosol particles, *Sci. Total*

Environ., **36**: 191-196.

Horvath, H., 1997. Experimental calibration for aerosol light absorption measurements using the integrating plate method - summary of the data, *J. Aerosol Sci.*, **28**: 1149-1161.

Houser, C.A. and Nickling, W.G., 2001. The emission and vertical flux of particulate matter <10 μm from a disturbed clay-crusted surface, *Sedimentology*, **48**: 255-267.

Kuhns, H. Etyemezian, V., Landwehr, D., MacDougall, C., Pitchford, M., and Green, M., 2001. Testing Re-entrained Aerosol Kinetic Emissions from Roads (TRAKER): a new approach to infer silt loading on roadways, *Atmos. Environ.*, **35**: 2815-2825.

Kuhns, H., Etyemezian, V., Gillies, J.A., Ahonen, S., Durham, C., and Nikolic, D., 2005. Spatial variability of unpaved road dust emissions factors near El Paso, Texas, *Journal of the Air and Waste Management Association* **55**: 3-12.

Labban, R., Veranth, J.M., Chow, J.C., Engelbrecht, J., and Watson, J.G., 2003. Size and geographical variation in PM_1, $PM_{2.5}$, and PM_{10} source profiles from soils in the western United States, *Water, Air and Soil Pollution*, **157**: 13-31.

Lowenthal, D.H. et al., 1992. The effects of collinearity on the ability to determine aerosol contributions from diesel- and gasoline-powered vehicles using the chemical mass balance model, *Atmos. Environ.*, **26A** (13): 2341-2351.

Lin, C.I., Baker, M.B., and Charlson, R.J., 1973. Absorption coefficient of atmospheric aerosols: a method for measurement, *Appl. Opt.*, **12**: 1356-1363.

Lu, H. and Shao, Y., 1999. A new model for dust emission by saltation bombardment, *J. Geophys. Res.*, **104** (D14): 16827-16842.

Malm, W. C., 1999. *Introduction to Visibility*; Cooperative Institute for Research in the Atmosphere (CIRA), NPS Visibility Program, Colorado State University: Fort Collins, CO.

Moosmüller, H. and Arnott, W. P., 2003. Angular truncation errors in integrating nephelometry, *Rev. Sci. Instrum.*, **74**: 3492-3501.

Moosmüller, H. and Arnott, W. P., submitted. Light scattering by particles in the Rayleigh regime, *Aerosol Sci. Tech.*

Moosmüller, H., Gillies, J. A., Rogers, C. F., DuBois, D. W., Chow, J. C., Watson, J. G., and Langston, R., 1998. Particulate emission rates for unpaved shoulders along a paved road, *J. Air & Waste Manage. Assoc.*, **48**: 398-407.

Moosmüller, H., Arnott, W.P., Rogers, C.F., Chow, J.C., Frazier, C.A., Sherman, L.E., and Dietrich, D. L., 1998. Photoacoustic and filter measurements related to aerosol light absorption during the Northern Front Range Air Quality Study (Colorado 1996/1997), *J. Geophys. Res.* **103**: 28149-28157.

MRI, 2001. Revisions to AP-42 Section 13.2.2 "Unpaved Roads", Midwest Research Institute, Kansas City, MO.

Nicholson, K.W., Branson, J.R., Geiss, P., and Cannell, R.J., 1989. The effects of vehicle

activity on particle resuspension, *Journal of Aerosol Science*, **20**: 1425-1428.

Nickling, W.G. and Gillies, J.A., 1989. Emission of fine-grained particulate from desert soils, in: M. Leinen and M. Sarnthein (Editors), *Paleoclimatology and Paleometeorology: Modern and Past Patterns of Global Atmospheric Transport*. Kluwer Academic Publishers, pp. 133-165.

Nickling, W.G. and Gillies, J.A., 1993. Dust emission and transport in Mali, West Africa, *Sedimentology*, **40**: 859-868.

Nickling, W.G. and McKenna Neuman, C., 1997. Wind tunnel evaluation of a wedge-shaped aeolian transport trap, *Geomorphology*, **18**: 333-345.

National Research Council, 1993. *Protecting Visibility in National Parks and Wilderness Areas*. National Academy Press, Washington, DC, 446 p.

Pace, T.G. and Watson, J.G., 1987. Protocol for Applying and Validating the CMB Model. EPA 450/4-87-010, U.S. EPA, RTP, NC.

Petzold, A. and Niessner, R., 1996. Photoacoustic soot sensor for *in-situ* black carbon monitoring, *Appl. Phys.* B, **63**: 191-197.

Quinn, P. K. and Coffman, D. J., 1998. Local closure during the first Aerosol Characterization Experiment (ACE 1): aerosol mass concentration and scattering and backscattering coefficients, *J. Geophys. Res.*, **103**: 16575-16596.

Rice, M.A., Mullins, C.E. and McEwan, I.K., 1997. An analysis of soil crust strength in relation to potential erosion by saltating particles, *Earth Surface Processes and Landforms*, **22** (9): 859-884.

Rice, M.A., Willetts, B.B. and McEwan, I.K., 1996. Observations of collisions of saltating grains with a granular bed from high-speed cine film, *Sedimentology*, **43** (1): 21-32.

Shao, Y., 2000. *Physics and Modelling of Wind Erosion*. Kluwer Academic Publishers, Dordrecht, 393 pp.

Shao, Y., 2001. A model for mineral dust emission, *J. Geophys. Res.*, **106** (D17): 20239-20254.

Shao, Y., Raupach, M.R., and Findlater, P.A., 1993. Effect of saltation bombardment on the entrainment of dust by wind, *J. Geophys. Res.*, **98**: 12719-12726.

Tegen, I., Hollrig, P., Chin, M. Fung, I., Jacob, D., and Penner, J., 1997. Contribution of different aerosol species to the global aerosol extinction optical thickness: estimates from model results, *J. Geophys. Res.*, **102**: 23895-23915.

U.S.D.A., 2002. Soil Survey Geographic (SSURGO) database of the Ft. Bliss Military Reservation, New Mexico and Texas - NM719, U.S. Department of Agriculture, Natural Resources Conservation Service, Ft. Worth, TX.

U.S. Environmental Protection Agency, 1995. User's Guide for the Industrial Source Complex (ISC3) Dispersion Models Volume II: Description of Model Algorithms. US Environmental Protection Agency, Office of Air Quality Planning and Standards: Emissions, Monitoring, and Analysis Division, RTP,

NC.

U.S. Environmental Protection Agency, 1996. Compilation of Air Pollutant Emission Factors. Vol. 1: Stationary Point and Area Sources, U.S. EPA Office of Air and Radiation, Office of Air Quality Planning and Standards, RTP, NC.

U.S. Environmental Protection Agency, 1999. Compilation of Air Pollutant Emission Factors - Vol. 1, Stationary Point and Area Sources. AP-42, U.S. EPA, RTP, NC.

U.S. Environmental Protection Agency, 2003. Miscellaneous Sources, in *AP-42 5th Edition, Vol. 1, Chapter 13*: Research Triangle Park, NC (http://www.epa.gov/ttn/chief/ap42/ch13/final/c13s0202.pdf) .

Varma R., Moosmüller, H., and Arnott, W. P., 2003. Towards an ideal integrating nephelometer, *Optical Letters*, **28** (12): 1007-1009.

Veranth, J.M., Seshadri, G., and Pardyjak, E., 2003. Vehicle-generated fugitive dust transport: analytic models and field study, *Atmos. Environ.*, **37** (16): 2295-2303.

Watson, J. G., 2002. Critical review -- visibility: science and regulation, *J. Air & Waste Manage. Assoc.*, **52**: 626-713

Watson, J.G. and Chow, J.C., 1994. Particle and gas measurements on filters, in: B. Markert (Editor), *Sampling of Environmental Materials for Trace Analysis*. VCH-Publisher, Weinheim, New York, pp. 83-175.

Watson, J.G. and Chow, J.C., 2000. Reconciling Urban Fugitive Dust Emissions Inventory and Ambient Source Contribution Estimates: Summary of Current Knowledge and Needed Research, DRI Document No. 6110.4F Prepared for the U.S. Environmental Protection Agency, Reno, NV.

Watson, J.G. and Chow, J.C., 2001. Source characterization of major emission sources on the Imperial and Mexicali valleys along the U.S./Mexico border, *Science of the Total Environment*, **276** (1-3): 33-47.

Watson, J.G., Chow, J.C., and Frazier, C.A., 1999. X-ray fluorescence analysis of ambient air samples, in: S. Landsberger and M. Creatchman (Editors), *Elemental Analysis of Airborne Particles*. Gordon and Breach, Amsterdam, pp. 67-96.

Watson, J.G., Chow, J.C., and Pace, T.G., 1991. Chemical mass balance, in: P.K. Hopke (Editor), *Receptor Modeling for Air Quality Management*. Elsevier Press, New York, pp. 83-116.

Watson, J.G., Cooper, J.A., and Huntzicker, J.J., 1984. The effective variance weighting for least squares calculations applied to the mass balance receptor mode, *Atmos. Environ.*, **18** (7): 1347-1355.

Watson, J.G., Robinson, N.F., Chow, J.C., Henry, R.C., Kim, B.M., Pace, T.G., Meyer, E.L., and Nguyen, Q., 1990. The U.S. EPA/DRI chemical mass balance receptor model, CMB 7.0, *Environmental Software*, **5** (1): 38-49.

Appendix I: List of Technical Publications

1. Peer Reviewed Journal Articles

Varma R., H. Moosmüller, and W. P. Arnott (2003). Towards an ideal integrating nephelometer. *Optical Letters* **28** (12): 1007-1009.

Etyemezian, V., H. Kuhns, J.A. Gillies, M. Green, M. Pitchford, and J. Watson (2003). Vehicle based road dust emissions measurement (I): methods and calibration. *Atmospheric Environment* **37**: 4559–4571.

Etyemezian, V., H. Kuhns, J.A. Gillies, J. Chow, M. Green, K. Hendrickson, M. McGowan, and M. Pitchford. (2003). Vehicle based road dust emissions measurement (III): effect of speed, traffic volume, location, and season on PM_{10} road dust emissions. *Atmospheric Environment* **37**: 4583–4593.

Etyemezian, V., J.A. Gillies, H. Kuhns, D. Gillette, S. Ahonen, D. Nikolic, and J. Veranth (2004). Deposition and removal of fugitive dust in the arid southwestern United States: measurements and model results. *Journal of the Air and Waste Management Association* **54**: 1099-1111.

Gillies, J.A., V. Etyemezian, H. Kuhns, D. Nickolic, and D.A. Gillette (2005). Effect of vehicle characteristics on unpaved road dust emissions. *Atmospheric Environment* (in press).

Kuhns, H., V. Etyemezian, J.A. Gillies, S. Ahonen, C. Durham, and D. Nikolic (2005). Spatial variability of unpaved road dust emissions factors near El Paso, Texas. *Journal of the Air and Waste Management Association* **55**: 3-12.

Moosmüller, H., R. Varma, and W. P. Arnott (2005). Cavity ring-down and cavity-enhanced detection techniques for the measurement of aerosol extinction. *Aerosol Sci. Tech.*, **39**: 30-39.

Moosmüller, H., R. Varma, W.P. Arnott, H.D. Kuhns, V. Etyemezian, and J.A. Gillies (2005). Scattering cross section emission factors for visibility and radiative transfer applications: military vehicles traveling on unpaved roads. *Journal of the Air and Waste Management Association* (submitted).

2. Technical Reports

Gillies, J.A., P. Arnott, V. Etyemezian, D.A. Gillette, H. Kuhns, E. McDonald, H. Moosmüller, W. G. Nickling, G. Schwemmer, and T. Wilkerson (2001). *Characterizing and Quantifying Local and Regional Particulate Matter Emissions from Department of Defense Installations: Annual Report 2001*. Prepared for Strategic Environmental Research and Development (SERDP), Arlington, VA, 22203-1821.

Gillies, J.A., P. Arnott, V. Etyemezian, D.A. Gillette, H. Kuhns, E. McDonald, H. Moosmüller, W. G. Nickling, G. Schwemmer, and T. Wilkerson (2002). *Characterizing and Quantifying Local and Regional Particulate Matter Emissions from Department of Defense Installations: Annual Report 2002*. Prepared for Strategic Environmental Research and Development (SERDP), Arlington, VA, 22203-1821.

Gillies, J.A., P. Arnott, V. Etyemezian, D.A. Gillette, H. Kuhns, E. McDonald, H. Moosmüller, W. G. Nickling, G. Schwemmer, and T. Wilkerson (2003). *Characterizing and Quantifying Local and Regional Particulate Matter Emissions from Department of Defense Installations: Annual Report 2003*. Prepared for Strategic Environmental Research and Development (SERDP), Arlington, VA, 22203-1821, Dec. 2003.

Gillies, J.A., P. Arnott, V. Etyemezian, D.A. Gillette, H. Kuhns, E. McDonald, H. Moosmüller, W. G. Nickling, G. Schwemmer, and T. Wilkerson (2004). *Characterizing and Quantifying Local and Regional Particulate Matter Emissions from Department of Defense Installations: Final Report*. Prepared for Strategic Environmental Research and Development (SERDP), Arlington, VA, 22203-1821, Dec. 2004.

Etyemezian, V., J.A. Gillies, H. Kuhns, D. Nikolic, J. Veranth, R. Laban, G. Seshadri, and D. Gillette (2003). *Field Testing and Evaluation of Dust Deposition and Removal Mechanisms*. Prepared for The WESTAR Council, Lake Oswego, OR, 97035 (in print).

3. Conference/Symposium Proceedings and/or Papers

Gillies, J.A., V. Etyemezian, H. Kuhns, D. Nikolic, and D.A. Gillette (2003). Effect of vehicle characteristics on unpaved road dust emissions. In *Proceedings of the 12th Symposium "Transport and Air Pollution"*, R. Joumard (ed.), INRETS-LTE, Avignon, France, 16-18 June 2003, pp. 51-58.

Gillies, J.A., V. Etyemezian, H. Kuhns, D. Nikolic, and D.A. Gillette (2003). Unpaved road dust emissions: effect of vehicle characteristics. In *Proceedings of the A&WMA 96th Annual Meeting and Exhibition*, San Diego, CA, 22-26 June 2003, paper # 69658.

Kuhns, H., V. Etyemezian, J.A. Gillies, D. Nikolic, S. Ahonen, and C. Durham (2003). Spatial variability of unpaved road dust emissions near El Paso, TX. In *Proceedings of the A&WMA 96th Annual Meeting and Exhibition*, San Diego, CA, 22-26 June 2003, paper # 65014.

Etyemezian, V., J.A. Gillies, H. Kuhns, D. Nikolic, D. Gillette, G. Sheshardi, and J. Veranth (2003). Estimating near-field removal of fugitive dust: the regionally-transportable fraction of PM_{10} emissions from unpaved roads. In *Proceedings of the A&WMA 96th Annual Meeting and Exhibition*, San Diego, CA, 22-26 June 2003, paper # 69531.

Gillies, J.A. (2000). Characterizing dust emissions from Department of Defense installations. Paper presented, *Partners in Environmental Technology, Technical Symposium and Workshop*, Crystal City, Arlington, VA, 28-30 Nov. 2000.

Gillies, J.A., W.P. Arnott, V. Eteymezian, D.A. Gillette, H. Kuhns, E. McDonald, H. Moosmüller, W.G. Nickling, G. Schwemmer, and T. Wilkerson (2001). Characterizing and quantifying local and regional particulate matter emissions from Department of Defense installations. Poster presented, *Partners in*

Environmental Technology Technical Symposium and Workshop, Washington, D.C., 27-29 Nov. 2001.

Kuhns, H., V. Etyemezian, J.A. Gillies, M. Green, and M. Pitchford (2002). Spatially-resolved, direct measurement of road dust emission from vehicles. Paper presented, *Real World Clean Air Symposium*, San Diego, CA, 21–23 May 2002.

Etyemezian, V., H. Kuhns, J.A. Gillies, M. Green, and M. Pitchford (2002). Temporally and spatially-resolved road dust emissions from vehicles. Paper presented, *7th International Highway and Urban Pollution Symposium*, Barcelona, Spain, 20–23 May 2002.

Varma, R., W.P. Arnott, H. Moosmüller, J.A. Gillies, H. Kuhns, and V. Etyemezian (2002). A new integrating nephelometer for aerosol light scattering studies. Paper presented, *21st Annual Conference of the American Association for Aerosol Research*, Charlotte, NC, 7-11 Oct. 2002.

Gillies, J.A., W.P. Arnott, V. Etyemezian, D.A. Gillette, H. Kuhns, E. McDonald, H. Moosmüller, W.G. Nickling, G. Schwemmer, and T. Wilkerson (2002). Characterizing and quantifying local and regional particulate matter emissions from Department of Defense installations. Paper and Poster presented, *Partners in Environmental Technology Technical Symposium and Workshop*, Washington, D.C., 3-6 Dec. 2002.

Etyemezian, V., D. Gillette, J.A. Gillies, H. Kuhns, D. Nikolic, G. Seshadri, J. Veranth, and J. Watson (2003). PM_{10} emissions from unpaved roads: correction for near-field deposition. Poster presented, *American Association for Aerosol Research Particulate Matter: Atmospheric Sciences, Exposure and the Fourth Colloquium on PM and Human Health* (AAAR PM), Pittsburgh, PA, 31 March- 4 April 2003.

Etyemezian, V., J.A. Gillies, H. Kuhns, D. Nikolic, and John Vernath (2003). Reconciling fugitive dust emissions with ambient measurement: along the unpaved road. Paper presented, *12th Annual Symposium on Emission Inventories, USEPA, Office of Air Quality Planning and Standards, Emission Factor and Inventory Group, and the Emission Inventory Improvement Program (EIIP). "Emission Inventories -Applying New Technologies"*, San Diego, CA, 28 April – 1 May 2003.

Etyemezian, V., D. Nikolic, J.A. Gillies, H. Kuhns, G. Seshadri, J. Veranth (2003). Estimating near-field removal of fugitive dust: the regionally-transportable fraction of PM_{10} emissions from unpaved Roads. Paper presented, *96th Annual Meeting, Air & Waste Management Association*, San Diego, CA, 22-26 June 2003.

Gillies, J.A., V. Etyemezian, H. Kuhns, D. Nikolic, and D.A. Gillette (2003). Effect of vehicle characteristics on unpaved road dust emissions. Paper presented, *96th Annual Meeting, Air & Waste Management Association*, San Diego, CA, 22-26 June 2003.

Gillies, J.A., V. Etyemezian, H. Kuhns, D. Nikolic, and D.A. Gillette (2003). Effect of vehicle characteristics on unpaved road dust emissions. Paper presented at *12th Symposium "Transport and Air Pollution"*, Avignon, France, 16-18 June 2003.

Gillies, J.A., H. Kuhns, V. Etyemezian, D. Nikolic, H. Moosmüller, and W.P. Arnott (2003). Tower based real time monitoring system for quantifying fugitive emissions. Paper presented, *NARSTO Emission Inventory Workshop: Innovative Methods for Emission Inventory Development and Evaluation*, Austin, TX, 14-17 Oct. 2003.

Moosmüller, H., R. Varma, W. P. Arnott, J. Walker, H. D. Kuhns, V. Etyemezian, and J.A. Gillies (2003). Emission factors for visibility impairment from fugitive dust emissions. Paper presented, *NARSTO Emission Inventory Workshop: Innovative Methods for Emission Inventory Development and Evaluation*, Austin, TX, 14-17 Oct. 2003.

Kuhns, H., V. Etyemezian, J.A. Gillies, D. Nikolic, S. Ahonen (2003). Spatially-resolved, direct measurement of road dust emissions from vehicles. Paper presented, *NARSTO Emission Inventory Workshop: Innovative Methods for Emission Inventory Development and Evaluation*, Austin, TX, 14-17 Oct. 2003.

Gillies, J.A., W.P. Arnott, V. Etyemezian, D.A. Gillette, H. Kuhns, H. Moosmüller, W.G. Nickling (2003). Characterizing and quantifying local and regional particulate matter emissions from Department of Defense installations. Poster presented, *Partners in Environmental Technology Technical Symposium and Workshop*, Washington, D.C., 2-5 Dec. 2003.

Gillies, J.A., V. Etyemezian, H. Kuhns, G. Nikolich, and S. Ahonen (2004). Near-field transport and deposition of fugitive dust emissions from an unpaved Road. Paper presented *Western Pacific Geophysical Meeting*, Honolulu, HI, 19-24 August 2004.

Gillies, J.A. (2004). Characterizing and quantifying fugitive dust emissions from Department of Defense sources including unique military activities. Invited Paper Presented, *2nd Surficial Processes on Military Lands Workshop*, Zyzzx, CA, 18-22, September 2004.

Nikolic, D., H. D. Kuhns, H. Moosmüller, J. Xu, J. A. Gillies. S. Ahonen, V. Etyemezian, and M. Pitchford (2004). PI-SWERL: a novel method for quantifying windblown dust emissions. *23rd Annual Conference of the American Association for Aerosol Research*, Atlanta, GA, October 4-8, 2004.

Varma, R., H. Moosmüller, W. P. Arnott, J. Walker, H. D. Kuhns, V. Etyemezian, and J. A. Gillies (2004). Emission factors of scattering cross section for visibility impairment from fugitive dust sources. *Regional and Global Perspectives on Haze: Causes, Consequences, and Controversies (Visibility Specialty Conference)*, Asheville, NC, October 25-29, 2004.

Moosmüller, H., W. P. Arnott, and R. Varma (2004). Measurement of atmospheric extinction with cavity ring down and cavity enhanced detection. *Regional and Global Perspectives on Haze: Causes, Consequences, and Controversies*

(Visibility Specialty Conference), Asheville, NC, October 25-29, 2004.

Moosmüller, H., W. P. Arnott, and R. Varma (2004). A new integrating nephelometer with reduced truncation losses. *Regional and Global Perspectives on Haze: Causes, Consequences, and Controversies (Visibility Specialty Conference)*, Asheville, NC, October 25-29, 2004.

Varma, R., H. Moosmüller, W. P. Arnott, J. Walker, H. D. Kuhns, V. Etyemezian, and J. A. Gillies (2004). Emission factors of scattering cross section for visibility impairment from fugitive dust sources. *Proceedings of the Visibility Specialty Conference: Regional and Global Perspectives on Haze: Causes, Consequences, and Controversies*, Air & Waste Management Association, Pittsburgh, PA, 13 pp.

Moosmüller, H., W. P. Arnott, and R. Varma (2004). Measurement of atmospheric extinction with cavity ring down and cavity enhanced detection. *Proceedings of the Visibility Specialty Conference: Regional and Global Perspectives on Haze: Causes, Consequences, and Controversies*, Air & Waste Management Association, Pittsburgh, PA, 6 pp.

Moosmüller, H., W. P. Arnott, and R. Varma (2004). A new integrating nephelometer with reduced truncation losses. *Proceedings of the Visibility Specialty Conference: Regional and Global Perspectives on Haze: Causes, Consequences, and Controversies*, Air & Waste Management Association, Pittsburgh, PA, 5 pp.

Gillies, J.A. (2004). Characterizing and quantifying fugitive dust emissions from Department of Defense sources including unique military activities. Invited paper presented, *Partners in Environmental Technology Technical Symposium and Workshop*, Washington, D.C., 29 Nov. - 2 Dec. 2004.

Gillies, J.A., W.P Arnott, E. Etyemezian, D.A. Gillette, H. Kuhns, H. Moosmüller, W.G. Nickling, J. Allwine, and R. Hashmonay (2004). Characterizing and quantifying fugitive dust emissions from Department of Defense sources including unique military activities. Poster presented, *Partners in Environmental Technology Technical Symposium and Workshop*, Washington, D.C., 29 Nov. - 2 Dec. 2004.

4. Published Technical Abstracts

Gillies, J.A. (2000). Characterizing dust emissions from Department of Defense installations. *Partners in Environmental Technology, Technical Symposium and Workshop*, Crystal City, Arlington, VA, 28-30 Nov. 2000, Abstract Volume, p. 63.

Gillies, J.A., W.P. Arnott, V. Eteymezian, D.A. Gillette, H. Kuhns, E. McDonald, H. Moosmüller, W.G. Nickling, G. Schwemmer, and T. Wilkerson (2001). Characterizing and quantifying local and regional particulate matter emissions from Department of Defense installations. *Partners in Environmental Technology Technical Symposium and Workshop*, Washington, D.C., 27-29 Nov. 2001, Abstract Volume, p. 114.

Gillies, J.A., W.P. Arnott, V. Eteymezian, D.A. Gillette, H. Kuhns, E. McDonald, H. Moosmüller, W.G. Nickling, G. Schwemmer, and T. Wilkerson (2002). Characterizing and quantifying local and regional particulate matter emissions

from Department of Defense installations. *Partners in Environmental Technology Technical Symposium and Workshop*, Washington, D.C., 3-6 Dec. 2002, Abstract Volume, p. 128.

Eteymezian, D.A. Gillette, J.A. Gillies, H. Kuhns, D. Nikolic, G. Seshadri, J. Veranth, and J. Watson (2003). PM_{10} emissions from unpaved roads: correction for near-field deposition. *American Association for Aerosol Research Particulate Matter: Atmospheric Sciences, Exposure and the Fourth Colloquium on PM and Human Health* (AAAR PM), Pittsburgh, PA, 31 March- 4 April 2003 (Abstract Volume on CD).

Moosmüller, H., W.P. Arnott, and R. Varma (2003). New Integrating Nephelometer for Visibility Studies. *American Association for Aerosol Research Particulate Matter: Atmospheric Sciences, Exposure and the Fourth Colloquium on PM and Human Health* (AAAR PM), Pittsburgh, PA, 31 March- 4 April 2003, Abstract Volume (Abstract Volume on CD).

Moosmüller, H., W.P. Arnott, and R. Varma (2003). Measurement of Atmospheric Visibility with a High-Quality Cavity. *American Association for Aerosol Research Particulate Matter: Atmospheric Sciences, Exposure and the Fourth Colloquium on PM and Human Health* (AAAR PM), Pittsburgh, PA, 31 March- 4 April 2003 (Abstract Volume on CD).

Eteymezian, J.A. Gillies, H. Kuhns, D. Nikolic, and J. Veranth (2003). Reconciling fugitive dust emissions with ambient measurement: along the unpaved road. *12th Annual Symposium on Emission Inventories, USEPA, Office of Air Quality Planning and Standards, Emission Factor and Inventory Group, and the Emission Inventory Improvement Program (EIIP). "Emission Inventories -Applying New Technologies"*, San Diego, CA, 28 April – 1 May 2003 (Abstract Volume on CD).

Eteymezian, D. Nikolic, J.A. Gillies, H. Kuhns, G. Seshadri, and J. Veranth (2003). Estimating near-field removal of fugitive dust: the regionally-transportable fraction of PM_{10} emissions from unpaved roads. *96th Annual Meeting, Air & Waste Management Association*, San Diego, CA, 22-26 June 2003 (Abstract Volume on CD).

Gillies, J.A., V. Etyemezian, H. Kuhns, D. Nikolic, and D.A. Gillette (2003). Effect of vehicle characteristics on unpaved road dust emissions. *96th Annual Meeting, Air & Waste Management Association*, San Diego, CA, 22-26 June 2003 (Abstract Volume on CD).

Moosmüller, H., W.P Arnott, and R. Varma (2003). A new integrating nephelometer for the measurement of mineral dust light scattering coefficients. *Second International Workshop on Mineral Dust*, Paris, France, September 10-12, 2003, Conference Abstracts Volume.

Moosmüller, H. and W.P Arnott (2003). Capabilities of the photoacoustic techniques for the measurement of light absorption by mineral dust. *Second International Workshop on Mineral Dust*, Paris, France, September 10-12, 2003, Conference

Abstracts Volume.

Gillies, J.A., H. Kuhns, V. Etyemezian, D. Nikolic, H. Moosmüller, and W.P. Arnott (2003). Tower based real time monitoring system for quantifying fugitive emissions. Paper presented, *NARSTO Emission Inventory Workshop: Innovative Methods for Emission Inventory Development and Evaluation,* Austin, TX, 14-17 Oct. 2003, Abstract Volume, p. 68.

Moosmüller, H., R. Varma, W. P. Arnott, J. Walker, H. D. Kuhns, V. Etyemezian, and J.A. Gillies (2003). Emission factors for visibility impairment from fugitive dust emissions. Paper presented, *NARSTO Emission Inventory Workshop: Innovative Methods for Emission Inventory Development and Evaluation,* Austin, TX, 14-17 Oct. 2003, Abstract Volume, p. 69.

Kuhns, H., V. Etyemezian, J.A. Gillies, D. Nikolic, S. Ahonen (2003). Spatially-resolved, direct measurement of road dust emissions from vehicles. Paper presented, *NARSTO Emission Inventory Workshop: Innovative Methods for Emission Inventory Development and Evaluation,* Austin, TX, 14-17 Oct. 2003, Abstract Volume, p.75.

Gillies, J.A., W.P. Arnott, V. Eteymezian, D.A. Gillette, H. Kuhns, E. McDonald, H. Moosmüller, W.G. Nickling, G. Schwemmer, and T. Wilkerson (2003). Characterizing and quantifying local and regional particulate matter emissions from Department of Defense installations. *Partners in Environmental Technology Technical Symposium and Workshop,* Washington, D.C., 2-5 Dec. 2003, Abstract Volume, p. 22.

Gillies, J.A., W.P Arnott, E. Etyemezian, D.A. Gillette, H. Kuhns, H. Moosmüller, W.G. Nickling, J. Allwine, and R. Hashmonay (2004). Characterizing and quantifying fugitive dust emissions from Department of Defense sources including unique military activities. Poster presented, *Partners in Environmental Technology Technical Symposium and Workshop*, Washington, D.C., 29 Nov. - 2 Dec. 2004, Abstract Volume, p. 122.